Design of joints for laterally loaded UHPC columns

by

Rakesh Srinivas Murthy

A thesis submitted to the graduate faculty

in partial fulfillment of the requirements for the degree of

MASTER OF SCIENCE

Major: Civil Engineering (Structural Engineering)

Program of Study Committee:
Sri Sritharan, Major Professor
Terry J. Wipf
Lester W. Schmerr

Iowa State University

Ames, Iowa

2009

TABLE OF CONTENTS

LIST OF FIGURES

LIST OF TABLES

ACKNOWLEDGEMENTS

I would like to take this opportunity to express my gratitude to those who have helped me with various aspects of research and writing of this thesis. First and foremost, I would like to thank Dr. Sritharan for his guidance, patience and support throughout this project, especially during writing of this thesis. His insights, constructive criticism and encouragement inspired me to extend my research study and take up graduate program with thesis option.

The Post-tensioning steel was donated by Dywidag System International, UHPC donated by Lafarge North America and UHPC casted by Iowa Prestress Concrete, Inc. which is greatly acknowledged.

I would specially like to thank Sriram Aaleti for his guidance throughout my graduate study and valuable support in finishing the thesis.

Additionally, I would like to thank Dough Wood, Dustin, Andrew and Matthew Goliber for helping me in the laboratory during testing.

Finally, I would like to thank my friends, Ujwala, Pooja, Purnima, Amanpreet, Pavana, Atul, Richard and all my roommates for their friendship and support throughout my graduate study at Iowa State University.

ABSTRACT

This study focuses on the use of Ultra-High Performance Concrete (UHPC) on seismic applications. As part of this effort, UHPC members have been tested for the first time under non-emulative connections for resisting seismic type lateral loads. Due to the limited compression strain of UHPC, identifying a suitable soft interface material at the member end was the main objective in order to accommodate large compression strain demand so that the UHPC members can be subjected to large lateral displacements.

Three precast unbounded post-tensioned UHPC columns were experimentally and analytically investigated using three different interface materials. They were Hydrostone, steel fiber grout and glass fiber epoxy pad along with easily replaceable external steel angles as energy dissipaters. Through this investigation, it was intended to establish a precast UHPC column connection with replaceable external energy dissipater and adequately deformable member end interface as these features enable the UHPC columns to be used in seismic applications. Before testing, a finite element model was developed to predict the lateral load behavior of the test columns, using all known UHPC properties and assumed interface material properties. To study the influence of the pad on the system, the UHPC columns were first tested for few cycles only with the pad. In addition to repeating these cycles, they were tested under large lateral displacements after the external energy dissipaters had been added. As the tests were conducted, samples from the interface materials were collected and tested separately for obtaining compressive stress-strain envelopes, which were later used in the finite element model to improve the analysis results.

Based on the research results, it was found that the Glass fiber epoxy performed better than other interface materials and the analytically calculated load versus displacement responses closely matched with the responses of all the experimental results. It was also found from the analysis that use of hollow UHPC columns may be adequate as this would lead to cost-effective design.

CHAPTER – 1 INTRODUCTION

Adequately detailed structural connections between members play an important role in the performance of structures designed to withstand extreme loads such as that due to earthquakes. Earthquakes can impart significant amount of energy into a building or bridge structure, causing the structure to experience large lateral forces and deformations. In order to withstand such displacement and force demands safely and cost effectively, the structures are designed with adequate strength and ductility. The traditional cast-in-place reinforced concrete structures experience large amount of damage when subjected to moderate to large earthquakes due to formation of plastic hinges that make the structure ductile. With the advancement of precast concrete and post-tensioning technology, various precast concrete connections have been developed for applications in the seismic regions. In past two decades research also has shown that the recently developed connections for precast concrete members using unbonded post-tensioning can enable such structures to sustain lateral loads and undergo large lateral displacements without experiencing any significant damage to the structures. In this type of structures, the energy is provided through external means rather than by the yielding of embedded reinforcement in concrete members. This type of connections designed with unbonded post-tensioning is known as dry or non-emulative connections.

There has been significant amount of research conducted to understand and characterize the lateral load behavior of non-emulative connections for precast concrete members and structural steel members. However, there are no studies available in the

literature on the usage of non-emulative connections suitable for prefabricated ultra high performance concrete (UHPC) members such that UHPC can be used for seismic application. A unique difference between the normal concrete and UHPC is the strain capacity. The strain capacity of normal concrete is approximated to 0.004, which can be increased by an order of magnitude through confinement. For UHPC, the strain capacity is approximately limited to 0.003, which cannot be increased to a larger value through confinement due to its dense matrix and not using large aggregates. Given the large deformation demands for structure in high seismic regions, it may not be feasible for the structure with precast UHPC members to undergo large deformations due to the limited strain capacity. What is exported in the research presented in this report is increasing deformation capacity of UHPC flexural members through accommodating a soft interface layer with in connections. Presented in the reminder of the chapter one is benefits of UHPC concrete, common precast connections used in the seismic regions, scope of current research and report layout.

1.2 Ultra High Performance Concrete (UHPC)

Ultra High Performance Concrete is a special concrete with superior characteristics compared to the normal concrete, which was developed by better understanding of the concrete material in micro level. UHPC is a advance higher technology product that integrates best features of different concrete types such as normal concrete, shingle concrete, flowable concrete, self compacting concrete and high strength concrete, which were developed for specific purposes. It also possesses some special properties which are different

from normal concrete and high performance concrete. Some of the common benefits and drawbacks of using UHPC compared to the normal concrete are as follows:

1.2.1 Benefits of Using UHPC

- High compressive strength - Up to 26 ksi can be achieved almost ten times that of normal concrete [1].
- High shear and tensile strength- Tensile strength up to 1 ksi can be achieved, thereby eliminating shear and tensile reinforcement [1].
- Low creep and shrinkage- Low in creep compared to normal concrete and negligible shrinkage can be achieved by heat treatment.
- High impermeability- With improved microstructure and reduction of pores makes the concrete highly impermeable.
- High durability- Require less maintenance cost.
- Self placing capability- The fluidity nature of the concrete mix makes it suitable for self placing and no vibration is necessary [1].
- Elimination of mild steel reinforcement - Due to its high compressive and shear strength compared to normal concrete mild steel and the labor cost for placing the reinforcement is eliminated.

UHPC with all the above mentioned benefits and the requirements for heat treatment is very well suited for precast construction. The UHPC also provides constructability benefits and they are as follows:

- Because of the high compressive strength and dependable tensile strength, UHPC usage will result in reduction in sizes of many required members and thus producing a lighter section. The light weight members can be transported and erected easily compared to normal concrete members with large sections.
- Rapid strength development and high early strength capability allows post-tensioning to be applied at an early stage and thus decreasing the time of construction. The high compressive strength of UHPC also allows the structural member to be prestressed to a higher value than a traditional concrete section.

1.2.2 Drawbacks of Using UHPC

- High material cost- since no coarse aggregate is used in the concrete mix.
- Mixing time- Time required to batch a mix is longer, and the entire concrete quantity to be placed for a member must be produced before placement is ready [2].
- The High energy mixing required could damage the mixer [2].
- Cleaning- Time required for cleaning is longer due to use of large amount of sand and fibers [2].
- Curing- Longer setting and curing time requires the precasting beds for longer time.
- Heat treatment- Adds as additional cost.

1.3 Connections

Commonly used connection types practiced in seismic design which is required for understanding the connection types used in this research study with corresponding code standards are discussed in the following section.

1.3.1 Monolithic Connections

In monolithic connections, the beam to column or the column to foundation connection is established monolithically with mild steel reinforcement running continuously from one member to the other member. Extensive research has been conducted to understand the lateral load behavior of members or structures with monolithic connections. The research findings have been incorporated into design standards such as the current ACI-318 building design code [3]. In structures designed with monolithic connections in high seismic regions, seismic energy imparted to it is dissipated through formation of plastic hinges and yielding of the longitudinal reinforcement in the critical regions. This leads to development of large residual displacements and increased cost of repair for a structure after it experienced a major earthquake event. With monolithic connections, structures can be designed to posses' high ductility.

1.3.2 Precast Concrete Connections

Commonly used precast concrete moment resistant connections can be classified into two types: emulative connections and non-emulative connections [4]. In emulative connections, the connections are designed such that the precast members provide performance similar to monolithic members. The energy dissipation concept used in precast systems with monolithic connections is similar to that of monolithic members. Requiring emulative connections is one

of the means, by which the UBC (1997), IBC (2000), and ACI-318 (2004) give approval for use of precast concrete members in the seismic region.

In non-emulative connections, the connections are designed to be weaker than the adjoining precast member, forcing the inelastic actions to occur within the connections. The flexural cracking of member in this case is largely concentrated at the precast connection interface, thus protecting the main structural member from experiencing significant damage. Within this type of connections, the energy dissipation is provided by external means through the use of special connectors placed at the precast interface. A recent trend that has become popular for tying precast members together in this type of connections is the use of unbonded post-tensioning. According to the ACI-318 building code, non-emulative connections designed for precast members fall into the alternative design category. Prior to usage in the field, the code requires that systems with these connections must undergo an experimental and analytical verification to ensure their satisfactory performance under simulated earthquake loading.

1.4 Scope of Research

The primary objective of the research presented in the, thesis is to establish a connection for precast UHPC columns that may be used in seismic regions. Recognizing the limited compressive strain capacity of UHPC, this connection is to be established using a soft interface between the column and foundation and connecting the column to the foundation using unbonded post-tensioning and energy dissipating elements. Within this context, the interface material needs to be resilient in nature, highly deformable while protecting the

UHPC edges from any damage when transferring the column edges from any damage when transferring the column load to the foundation. The study examines the possibility of using three different interface materials, namely Hydrostone, Steel Fiber Reinforced Grout and Glass Fiber Reinforced Epoxy.

Given the high strength of UHPC and the ability to easily attach short embedment plates to the sides of the columns, a pair of steel angles is used as energy dissipating element. In addition to examine the lateral load behavior of the UHPC column with three interface materials, the possibility of using steel angles as energy dissipating devices is examined in two of these cases. In each case, the UHPC columns behavior is examined through laboratory testing and 2D finite element analysis using ANSYS.

1.5 Report Layout

This report is organized into five chapters including the introduction to the UHPC material and non-emulative precast connections in this introductory chapter. In Chapter 2, a summary of recent literature on UHPC, focusing on material and engineering properties, and non-emulative connections, focusing on the post experimental and analytical studies, is presented. The experimental study of three UHPC columns with different interface materials tested with and without including the energy dissipaters is presented in Chapter-3 along with test results. Chapter-4 presents a 2-D finite element model developed in ANSYS for analytical investigation of the test specimens as well as the validation of the finite element model through comparison between the analytical and experimental results. The possibility of using hollow UHPC columns is also examined through the analysis model in this chapter.

Finally, conclusions drawn from the study and recommendations for the future study are presented in Chapter 5.

CHAPTER – 2 LITERATURE REVIEW

2.1 Introduction

A brief summary of previous research conducted on UHPC material properties and precast concrete connections for seismic regions is presented in this chapter. For UHPC, significant amount of research has been done in recent years on material behavior to structural applications, therefore a significant number of research publications is available for reference, but for precast concrete connections, exclusively with external energy dissipaters, limited research has been conducted different successful concepts, and therefore the main focus of the literature review on this topic is somewhat limited.

2.2 UHPC

This section focuses on published literature on UHPC materials and properties

2.2.1 Types of UHPC

There are several types of UHPC developed by different manufactures in different countries. Among them, the three main types are Compact reinforced composite (CRC), multi scale cement composite (MSCC), and reactive powder concrete (RPC), with the main difference between them being the type and amount of fibers used. (CRC) and (MSCC) both use high amount of fibers and use different fiber sizes than those used in RPC(Rossi 2005)[5]. RPC is one of the leading types of UHPC and one such product is marketed under the name DUCTAL® by the French companies Lafarge, Bouygues, and Rhodia. Since RPC is

the most commonly available types of UHPC, this was used for the laboratory experiments in the current study.

2.2.2 Strength Principles

UHPC is a new generation cement material with a number of perfect properties. It is an outcome from systematically eliminating typical defects found in normal concrete such as micro cracks and interconnected capillary pores, and improving the mechanical properties. Following are some of the basic principles used for enhancing strength of UHPC:

- Enhance the homogeneity of concrete by eliminating coarse aggregate. It is well known that the transition zone between the coarse aggregate and matrix is often the source for micro cracks in the concrete. Normal concrete and High performance Concrete (HPC) suffer from mismatch in the physical and mechanical properties between the matrix and the aggregates, and thus they are eliminated in UHPC by selecting constitutes material with similar elastic moduli (Gao et al. 2006)[6]. The aggregates in normal concrete form a rigid skeleton and transfer forces through the contacts between the aggregates. When compressive forces are applied, shear and tensile stresses develop at the interfaces between the aggregates, forming small cracks approximately proportional in size to the maximum aggregate size (600μm) [7]. In UHPC, the aggregates are small in size as they are used in crushed form and are part of a continuous matrix, and hence

the stresses is transmitted by both aggregates and the surrounding matrix forming a more uniform distribution as shown in Figure 2.1 .

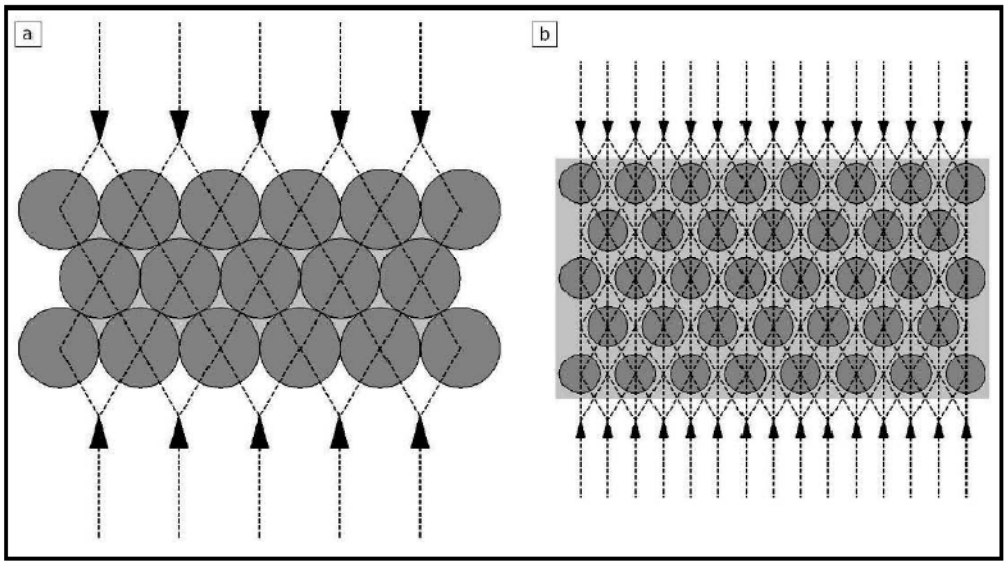

Figure 2.1 Force transfer mechanism in (a) normal concrete and (b) UHPC (after Walraven 2002)[8].

- Improve the properties of the matrix by addition of silica fumes, which produce concrete modifying filler effect in voids among cement or other particles after a pozzolanic reaction with $Ca(OH)_2$. In concrete mix with normal Portland cement, 18% by weight of silica fumes is enough for total consumption of $Ca(OH)_2$ released during hydration. However, in UHPC considering the filler effect, the content of silica fumes is increased to 25-30% [9].
- Improve the properties of the matrix by reducing water to binder ratio. The aim is not to minimize water content but to maximize relative density. The variation of water/binder ratio (w/b) with respect to relative density is shown in the Figure 2.2. The minimum w/b ratio for a workable mixture is 0.08 and the peak relative

density occurs at around 0.13 [10]. Beyond this point addition of water decreases the density of the concrete. (w/c) ratio of 0.14 is considered as optimum for UHPC.

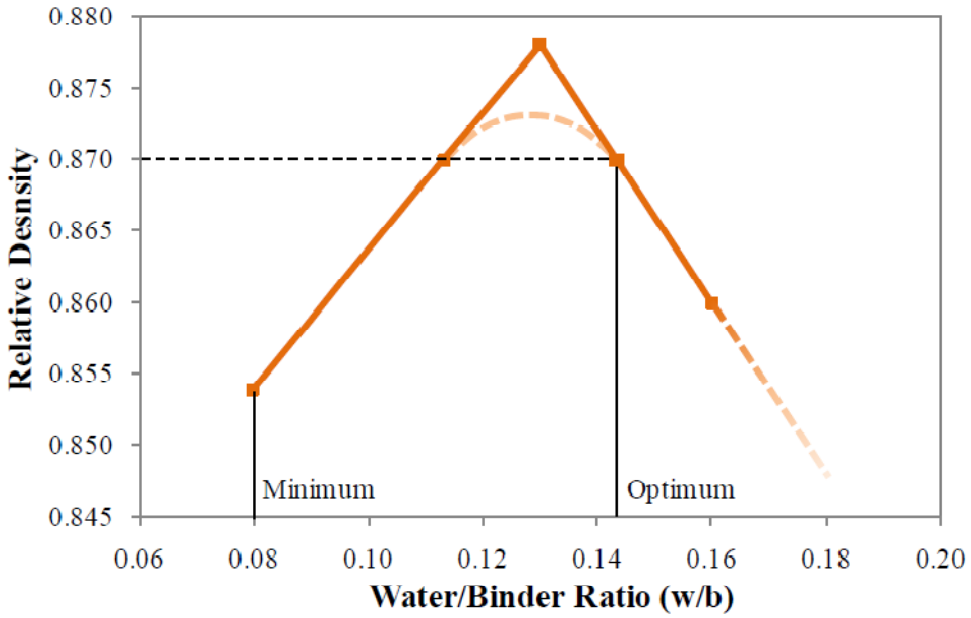

Figure 2.2 Variation of Water/binder ratio with respect to Relative Density [10].

- Enhancing of the packing density by using optimization of the granular mixture through a wide distribution of powder size classes. The mix is also proportioned in such a way that the fine aggregates will be set of movable particles rather than a rigid skeleton. Hence, the wide distributions of granular classes not only maximize density and create uniform stress distribution it also contributes to flowability of mixture. The smaller grains serve as lubricant, allowing sand particles of same size to move past each other with minimum interference [10].
- Enhancing of the microstructure by post-set heat-treatment. Heat treatment enhances the hydration reaction in concrete to further reduce the porosity of

UHPC and enhancing durability properties. Durability of the concrete is intrinsically dependent on porosity and superior durability properties are achieved by low and disconnected pores (Perry 2001) [11].

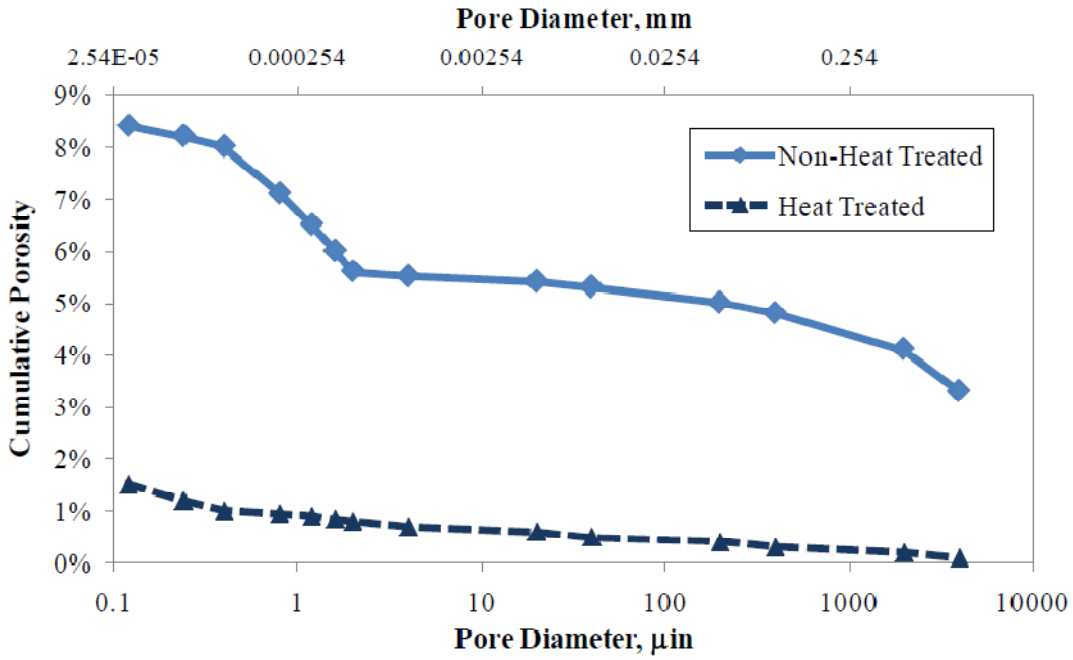

Figure 2.3 Comparison of porosity in Heat treated and Non Heat treated UHPC [10].

- Enhancing of ductility by using small steel fibers. Application of all the described principles without fibers leads to a concrete with high compressive strength without any improvement in ductility. The addition of steel fiber helps to improve ductility and tensile strength of the concrete [5].

2.2.3 Composition of UHPC

A typical UHPC mix contains sand, cement, silica fume, crushed quartz, fibers, superplasticizers, and water in the proportion (volume fraction) shown in the Figure 2.1. Table 2.1 shows a typical UHPC mix components in terms of weight per unit volume, mass ratio relative to cement, and volume as a percentage of total volume.

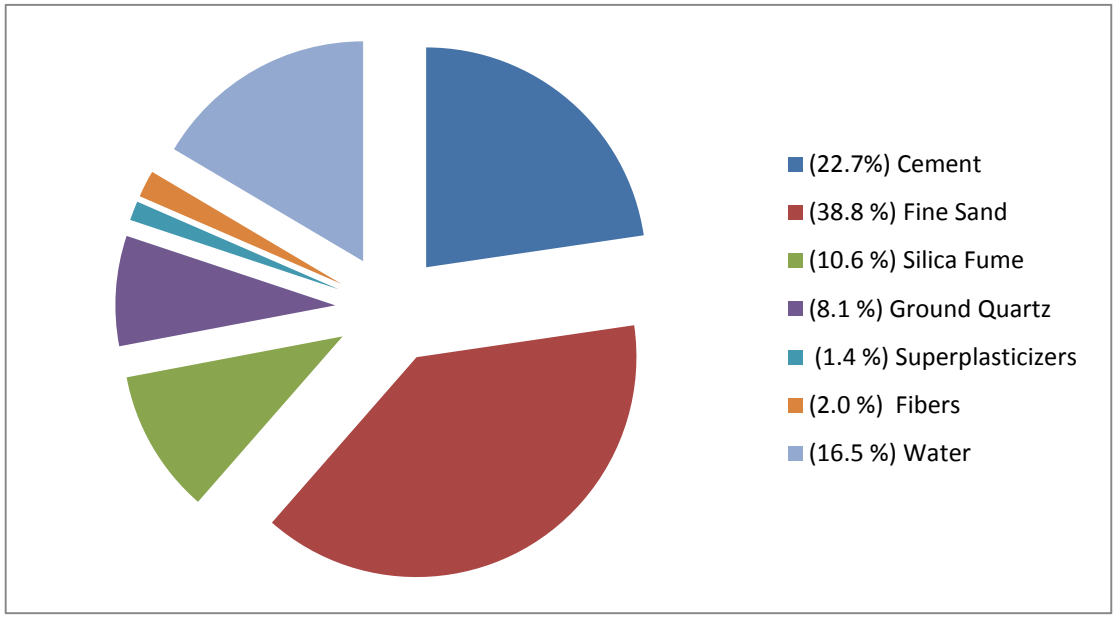

Figure 2.4 UHPC material components based on volume fraction.

Table 2.1. Typical UHPC mix components [7].

Components	Weight per Cubic Foot	Mass Ratio /Cement	Volume Fraction
Sand	61.9 lb	1.430	38.8%
Cement	42.3 lb	1.000	22.7%
Silica fumes	14.0 lb	0.325	10.6%
Crushed Quartz/Fly ash	13.0 lb	0.3	8.1%
Fibers	9.4 lb	0.218	2.0%
Superplasticizers*	0.90 lb	0.021	1.4%
water	9.9 lb	0.229	16.5%

*Superplasticizers are expressed as the weight of solid fraction; the liquid fraction is included in the water weight.

The functions of various components in a UHPC mix can be summarized as follows.

Sand- Sand plays the role of confining the cement matrix to add strength, as explained before in the strength principles. A variety of quartz sand is usually used, which is not chemically active in the cement hydration reaction at room temperature [7].

Cement- Typical Portland cement can be used in UHPC. Only a part of the used cement becomes hydrated in UHPC and acts as a bonding agent; the un-hydrated potion of the cement grains can act as high elastic modulus reinforcing (17,400 ksi) in the matrix [12].

Crushed Quartz- Since only part of the cement is hydrated, some of it can be replaced by crushed quartz. Replacing quartz not only reduces the cement requirement, but it also increases flow ability [9].

Fly Ash or Blast Furnace Slag - This can be used as an alternative to using crushed quartz for cement replacement, especially where, using small quartz particles may pose respiratory problems. It provides the same lubricating effect, making UHPC more flow able and self compacting (Walraven 2002) [8].

Silica Fume – This component provides following three important functions in UHPC: filling the voids in the next larger granular class (cement); enhancing lubrication due to its perfect sphericity, and production of secondary hydrates by pozzolanic reaction with the products from primary hydration [10].

Fibers – Steel fibers are considered for applications where high tensile capacity and ductility demand is required. Without fibers, UHPC is a strong and brittle material. Fibers are included to increase tensile capacity and improve ductility [10]. Organic fibers are also used with UHPC but it reduces the performance of the structure when compared to steel fiber structures [7].

Superplasticizers – These are high range water reducers composed of powerful water polymers, which are used to disperse cement particles and silica fume, effectively improving

the flowability of UHPC mixes. Superplasticizers can allow water/cement ratio and lower water/binder ratio without sacrificing workability [7].

Water – As with any concrete, water is required for hydration in concrete mix and the water/cement ratio has typically been used as an indicator of compressive strength. Compressive strength of UHPC cannot be characterized by w/c ratio since it affects the porosity. The final porosity is the better indicator of strength for UHPC [7].

2.2.4 Mechanical Properties

Tensile Strength

Normal Portland cement concrete typically has low tensile strength ranging from 300 to 700 psi, and hence its tensile strength contribution is ignored while designing for most of the structural application. HPC with additional strengthening ingredients to normal concrete develops tensile strength in range of 800 to 900 psi. UHPC develops higher tensile strength compared to HPC. According to the tests by Graybeal [13] on mortar briquettes, it was found that the first cracking of UHPC should be expected at around 1220 psi with the ultimate tensile strength of about 1350 psi. The post-cracking strength is provided by the fibers holding the cracks together. The tensile stress-strain curve assumed for this project is shown in Figure 4.9a, in which the maximum tensile strength is assumed to be 1700 psi.

Tensile flexural strength

Flexural tensile stress versus deflection curve of a UHPC beam is compared to that of a comparable normal concrete beam and the ultimate flexure strength of UHPC is about 5 times as shown In Figure 2.2. Typically, the UHPC tension curve can be divided into three phases as shown. The first being the linear phase with elastic behavior until the cracking of the material occurs, next is the non-linear strain hardening phase which take the material behavior until the maximum load is reached, and then the curve gradually falls indicating the strain softening phase.

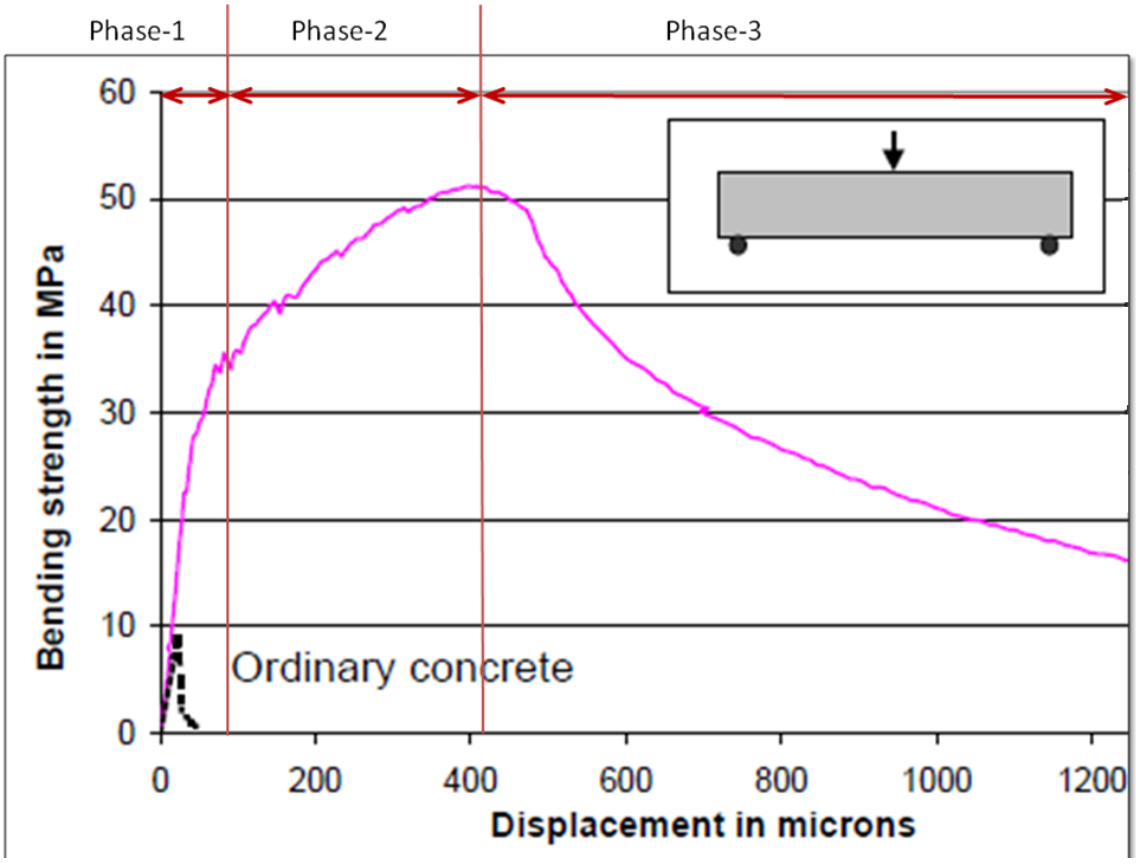

Figure 2.5 Force verses displacement curve of UHPC in bending [1].

Strain limits

According to Graybeal [13] the compressive stress-strain response of heat-treated UHPC deviates from linearity by 5 percent before the peak stress is reached and this occurs at a strain of 3620 x 10^{-6} compared to the strain of 4100 x 10^{-6} , and for untreated UHPC the strain at peak compressive stress is 3500 x 10^{-6} which is lower than that of heat treated UHPC. According to Sritharan et al. [14] the linear elastic behavior of heat treated UHPC occurs essentially up to failure, which corresponds to a strain of 3200 x 10^{-6}. This strain value of 3200 x 10^{-6} is also agreed by Dugat et al [15].

Shrinkage and Creep

UHPC has a very low creep value compared to the normal concrete, with creep factor ranging from 0.15 – 0.3. Shrinkage also is very low. Shrinkage can be completely eliminated by heat treatment. The overall shrinkage of untreated UHPC at the end of 90 days is 930 x 10^{-6} according to Graybeal (2006) [13].

2.2.5 UHPC Applications

UHPC has already been utilized in many special construction projects around the world for wide range of applications and some of the applications are presented below.

- Because of its high compressive and bending strengths compared to normal concrete makes it excellent material for bridge superstructures, especially for long span or wide and thin deck bridges, bridge. The first UHPC structure in the world was a

pedestrian bridge in sherbrooke, cannada, completed in 1997 is shown in Figure 2.6. Also The first vehicular bridge in North America is the Wapello County Mars Hill Bridge in Iowa, United States shown in Figure 2.7.

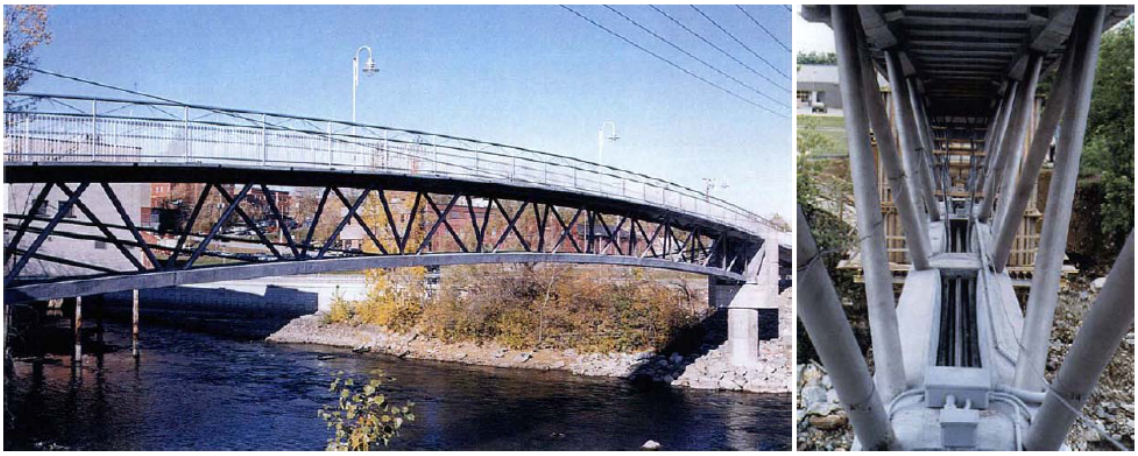

Figure 2.6 Views of Completed Sherbrooke pedestrian bridge (Blais and couture 1999)[16].

Figure 2.7 View of completed Mars Hill Bridge [7].

- Because of its ability to be cast into thin high strength components. UHPC has been used for roof structures as it will reduce the load of super structure on the foundations. Figure 2.8 shows the most famous UHPC structure in the world, the Shawnessy LRT station in Calgary, Cannada.

Figure 2.8 View of Shwnessy LRT station with UHPC canopies (Perry 2006) [11].

- UHPC is being considered for nuclear waste containers for storing radioactive waste due to its ability to resist impacts without losing integrity.[7]

- Anti-fire product of UHPC with a 0.6% volume of polypropylene fibers can be used for buildings and structures were fire proofing is required [Schmidt et al. 2003].The fibers melts at 338°F (170°C) taking up the heat of the fire [1] [16].

2.3 Connections for Prefabricated Members

This section focuses on published literature on suitable connections investigated for use of precast members in seismic regions.

2.3.1 Post-tensioned Hybrid Coupled Wall Subassemblages

Kurama et al. (2006) conducted an experimental program to investigate the behavior of post-tensioned hybrid coupled wall subassemblages at the University of Notre Dame. The main focus of the study was to understand the influence of unbonded post-tension coupling beam connecting two shear walls with a pair of externally connected angles for energy dissipation. A total of eleven tests at half-scale were conducted to investigate the nonlinear reverse cyclic behavior of the beam-to- wall connections. An analytical investigation was also performed to validate the test results. The testing, modeling of walls and subassemblages with results are published in three separate publications and is summarized below.

2.3.1.2 Coupling Beam Connection Details

An elevation view of the proto type, eight story coupled wall system and the unbonded post-tensioned beam wall hybrid connection details is shown in the Figure 2.9. The post-tensioning was provided by multi strand tendons on either side of the beam web as shown in the section view of Figure 2.9c. Inside the walls, the tendons were placed in oversize un-grouted ducts and anchored only at the outer ends of the wall. The beam to wall connection consisted of top and seat angles connecting the beam flanges and the steel plate embedded into the walls. Spiral transverse reinforcements were used for confining the steel plates embedded into the walls as shown in Figure 2.10 Cover plates were welded onto the flanges for stabilizing and strengthening the flanges and to prevent or delay the yielding of the

flanges in compression. The function of the angles are to serve as energy dissipaters during earthquake loads, provide resistance to moments, prevent sliding of the beams against the wall and provide beam support during construction.

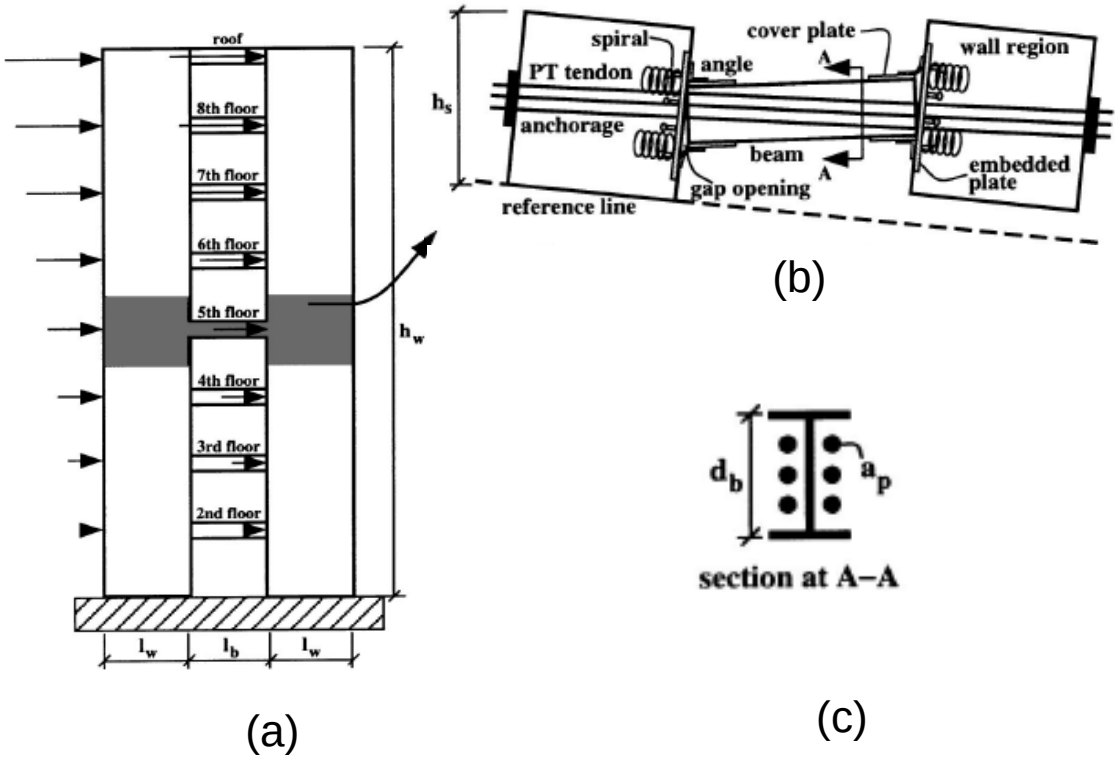

Figure 2.9 Coupled wall system with sub-assemblage connection details investigated by Kurama and Shen [17].

A closer view of the connection details with all the parts labeled is shown in Figure 2.10. In the beam to wall connection region, the reaction block and the loading block consist of embedment plates and spiral reinforcements. The embedment plates have shear studs which are flushed into the concrete block during casting, help in distribute contact stresses

and the spiral reinforcement used behind the plates help resist and distribute stresses without excessive deformation. One leg of the external angles is connected to the embedment plate of the wall using two or four unbonded post-tensioning strands and the other end of the angle is connected to the beam with bolted connection using two 22.2 mm diameter slip critical bolts. To protect the beam flange from yielding and any permanent deformation shim plates were welded on to the beam flanges and the embedment plates.

Gap opening takes place at the connection where angle leg is connected to the wall embedment plate, and the post-tension strands connecting the angle and the embedment plate pass through a 1 in. duct and anchored at the far end of the wall using wedge/barrel anchorage system as shown in Figure 2.10b. Post-tensioning strands were used for the connection to prevent yielding of the angle. Bolted or welded angle connection was not considered to avoid development of large tensile stresses in the concrete.

Typical beam wall connection is shown in Figure 2.9b, showing the expected exaggerated deformed shape of the beam-to-wall connections when the lateral load acted upon the walls from left to right direction. The nonlinear displacements occur primarily as gap opening at the beam ends. In a properly designed connection, the desired behavior is yielding of the angles, with little yielding and damage to the beam and walls.

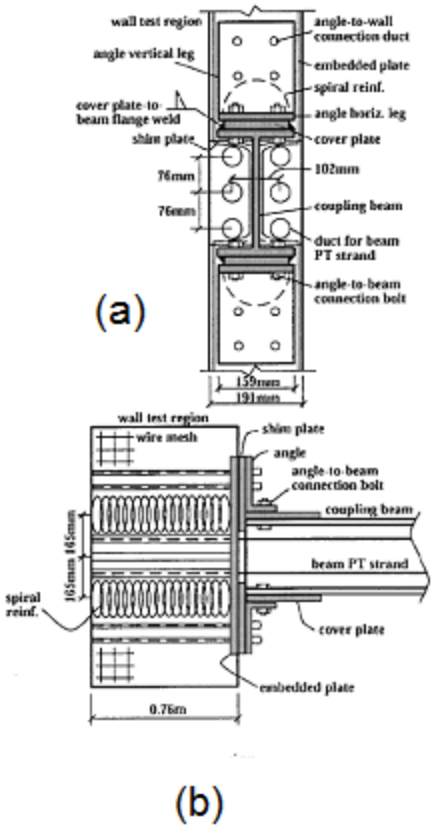

Figure 2.10 Connection detail materials at (a) beam end view and (b) beam-to-wall connection region [18].

2.3.1.3 Experimental Test Setup

An elevation view of the test setup is shown in Figure 2.11. The coupling beam is connected to a reaction block on the south end and to loading block on the north end side. The reaction block is in turn connected to two actuators as shown in the Figure 2.11. The actuators were operated in displacement control to move the loading block. Inner steel bracing frame assembly (not shown in figure) was used to prevent out of plane bending of beam and the loading block.

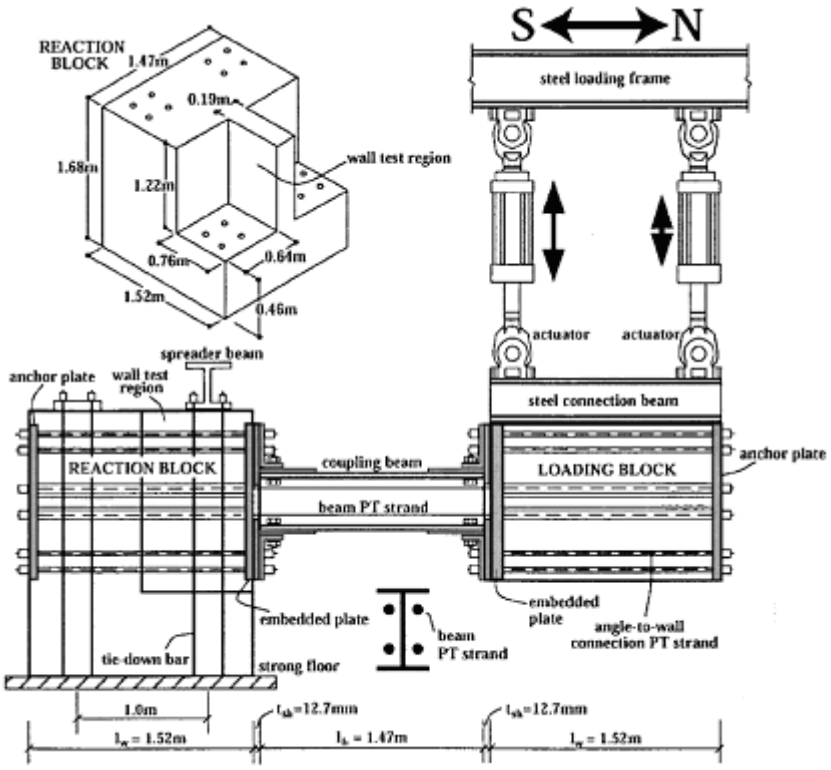

Figure 2.11 Elevation view of the test setup [18].

2.3.1.4 Experimental tests

Eleven different tests were conducted with the previously described test setup. The tests can be broadly grouped into the following categories based on the design parameters investigated

1. Loading type - cyclic or monotonic.
2. Beam size - to study the effect of coupling beam with varying sizes of the beams.
3. With, without angles and change in thickness - to study the effect of angles as well as the effect of angle thickness.

4. With, without cover plate and change in thickness- to study the effect of cover plate and also the effect of increase in plate thickness.
5. With, without post-tensioning steel and change in area - to study the effect of post tensioning force and change in steel area.

The responses of the first three cyclic tests are shown below in Figure 2.12

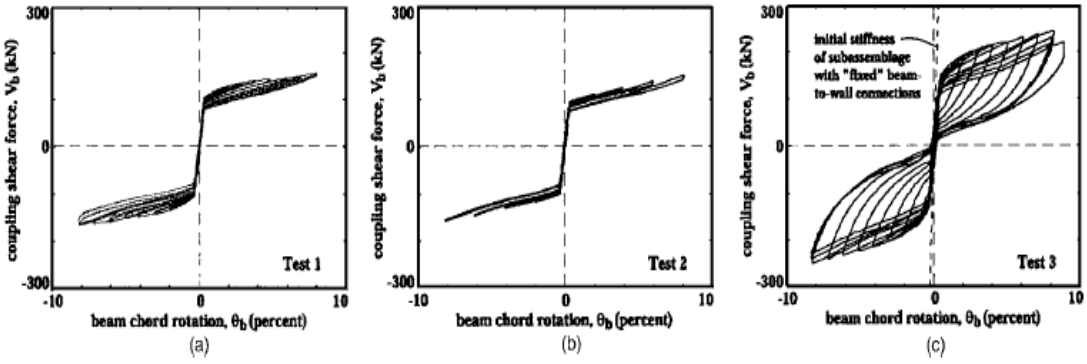

Figure. 2.12 Measured coupling shear forces versus chord rotation (V_b -θ_b) behaviors: (a) Test-1, (b) Test-2 and (c) Test-3 [18].

In the first two tests, angles were not used for the beam to wall connection and tested only with the post-tensioning to study the behavior of the sub-assemblages and to verify the analytical model without the angles. Hence, there is not much energy dissipation observed in the first two test responses with the lateral load reaching around 150 kN (33.7 kips) as shown in Figures 2.12a and b. For Test-3, the top and bottom seat angles were used for the beam to wall connection and energy dissipation was clearly visible, with the lateral load reaching more than 200 kN (45 kips) for around 8-9 % chord rotation as shown in Figure 2.12c.

Based on all the eleven test results the connection was evaluated as follows:

- Inclusion of cover plates reduced coupling beam flange strains.
- Increase in the connection angle thickness improved coupling resistance and energy dissipation of the connection.
- Increase in post-tensioning steel area/force increased, but still small levels of damage in the coupling beam and wall concrete.
- Increased in beam size resulted in large gaps at the ends of deep beam increasing the elongation of the post-tensioning strands which led to premature failure of the strands close to the anchorage at very early stage.

2.3.1.5 Analytical Modeling

Analytical models for the multi-story unbonded post-tensioned hybrid coupled joined together by coupling beam sub assemblages at roof and floor level was first developed for Shen and Kurama (2002) and later improved based on the experimental tests conducted in 2006. Figure 2.9 shows the model developed in 2002 using the program DRAIN-2DX (Prakash et al.) as the analytical platform.

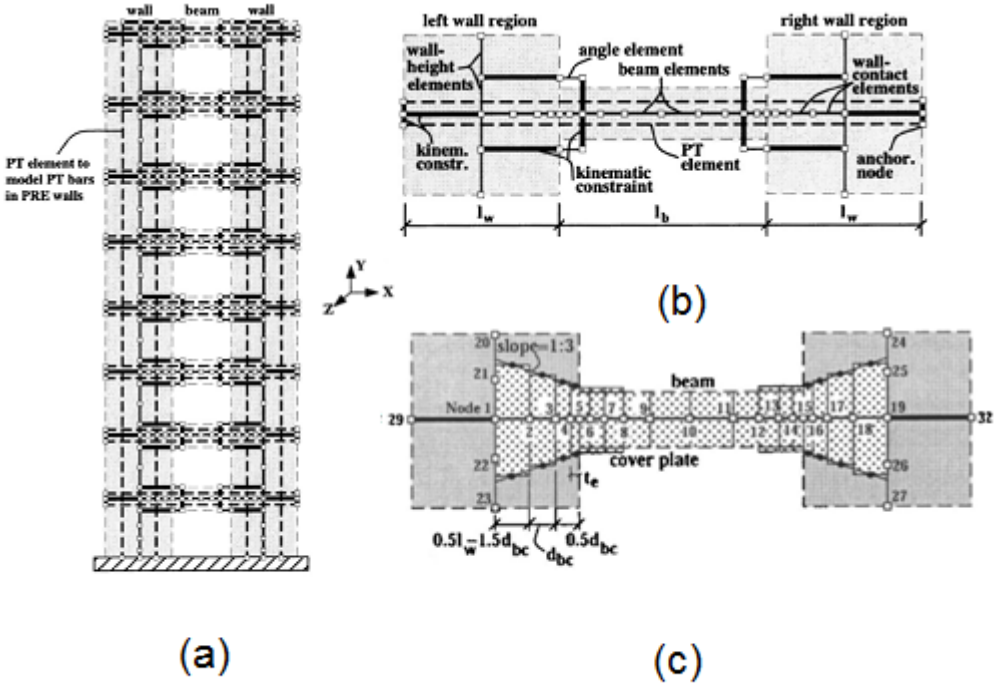

Figure 2.13 Analytical model of (a) multistory wall (b) subassemblages and (c) wall-contact elements and beam contact elements (adapted from Shen and Kurama 2002)[17][19].

The concrete wall region is modeled using two types of elements; the first element type was wall height element in the vertical direction, for modeling the axial flexure and shear behavior of the wall along the height while the second element was wall-contact element in horizontal direction, for modeling the local behavior of the wall contact region at the ends of the coupling beam. The truss element was used for modeling the post-tensioning tendon and fiber beam-column element for the coupling beams. The wall and beam regions are modeled concrete and/or steel fibers along the length of the elements. Each fiber has a location in the cross section and defined by cross section area, multi- linear stress-strain relationship. The end nodes of the beam 5 and 15 are constrained for translation in Y-axis only and the fibers

near the interface of beam to wall interface is modeled using zero tensile strength and zero stiffness to allow and capture gap opening.

Based on the experiments results presented in Kurama et al (2006), following modifications were made to the model:

1. Post-tension element was modeled using three truss elements instead of one for modeling the kinking effect.
2. Two zero length spring were elements used to model the angle instead of 1 fiber element and horizontal shear force was also modeled. To capture the non linear failure of the angle by formation of plastic hinges.
3. Shim plates were introduced at the beam to wall interface. The test results showed that shim plates have significantly affected the overall behavior by reducing the contact depth between the wall and the beam. Introduction of shim plate also led to changes of the contact elements depth and slope as shown in Figure 2.14 b.

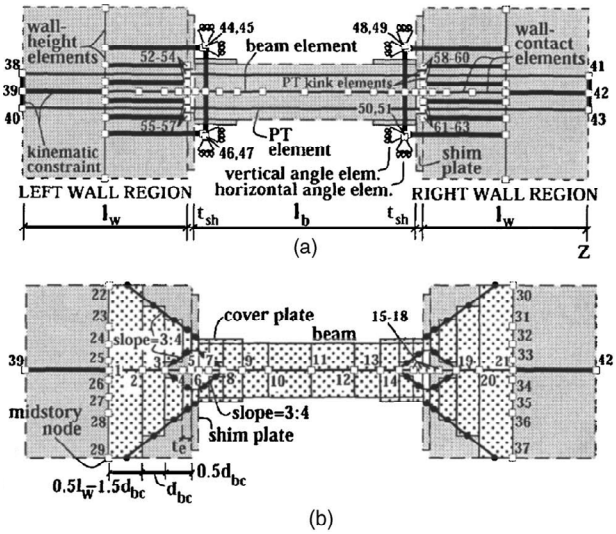

Figure 2.14 Revised analytical model [19].

For verifying the model, various parameters were compared between calculated analytical results from the improved model and the experimental results. Figure 2.15 presents the comparison of horizontal displacement of the loading block with respect to chord rotation for Test 3, 9 and 10. Test 3 was tested without cover plates for angles, while Test-9 examined the effect of increasing the post-tensioning steel area and Test-10 with increase in beam depth. In all three cases the calculated displacement value was over predicted by the analytical model when compared to the experimental value at large rotations. This also implies that the model is over-estimating the post-tensioning strand elongation and the post-tensioning force.

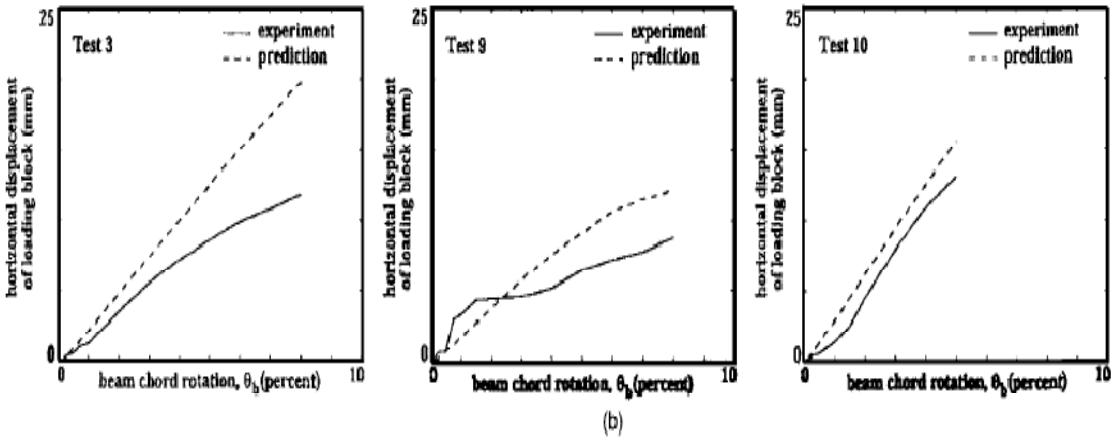

Figure 2.15 Analytical and experimental displacement comparison with respect to beam chord rotation [19].

2.3.2 Post-tensioned Precast CFT Segmental Bridge Columns with Unbonded Stands

Chou et al. conducted two reversed cyclic loading tests on ungrouted post-tensioned, precast concrete-filled tube (CFT) segmental bridge columns to investigate their seismic performance. One of the test units was tested with an external energy dissipating device, while the other was done without any external energy dissipation. The main objectives of the tests were to study the behavior of the two unbonded post-tensioned columns under cyclic lateral loading and to examine the effect of the proposed external energy dissipating device on the hysteretic energy.

2.3.2.2 Test Specimen

Each column specimen consists of four concrete segments with a PVC post-tension duct at the centre and confined outside by a steel tube. The segments were post-tensioned to the concrete foundation using Grade 270 low-relaxation prestressing strands as shown in the Figure 2.16.

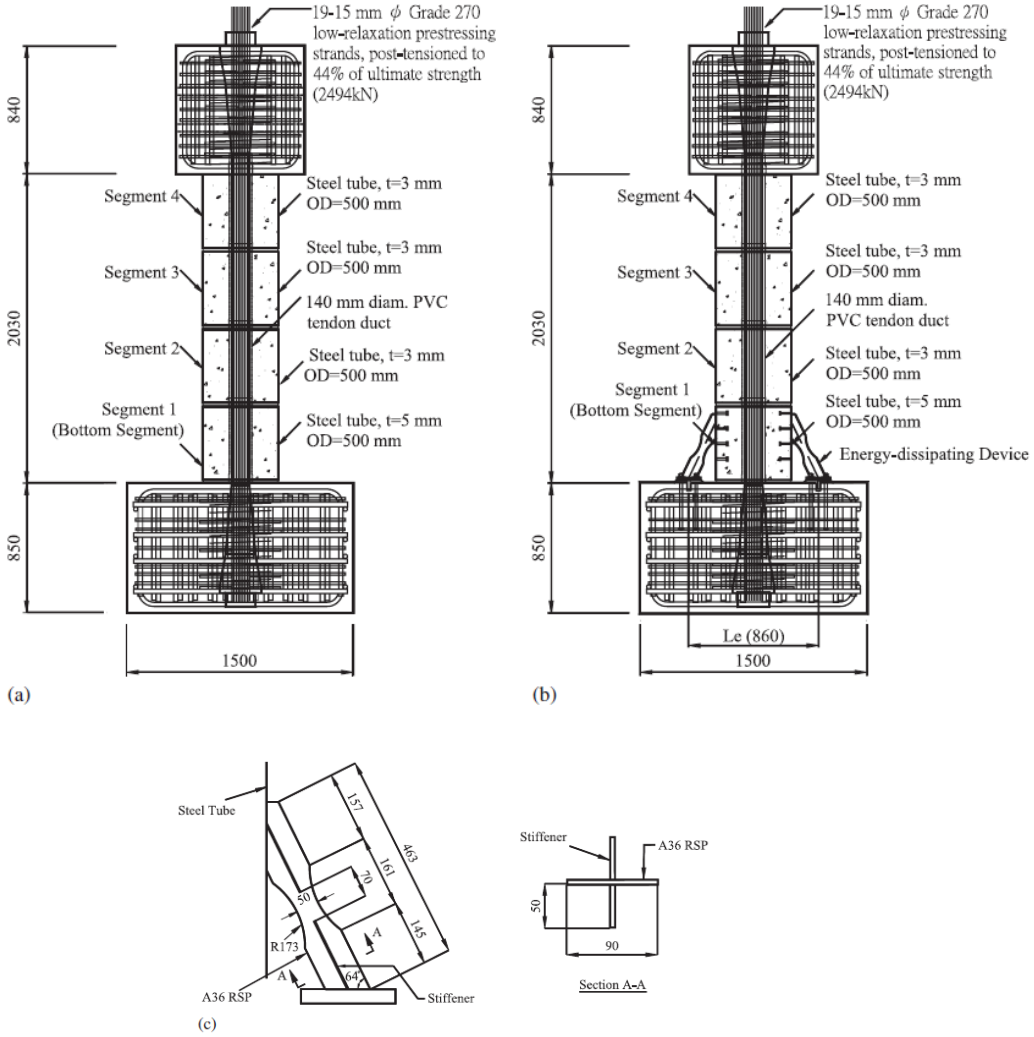

Figure 2.16 Specimen elevation (dimension in mm; 25.4 mm = 1 in.): (a) Specimen-1 with no external energy dissipators, (b) Specimen-1 with external energy dissipators and (c) Close up of energy dissipating device [20].

The external steel tube around the column segments increases the compressive strength and ultimate strain capacity of concrete and thus increases the flexure capacity of the column. The post-tensioning strands are designed to remain elastic and provide restoration force to the deflected column when the applied lateral load is removed. It also holds the segments together and brings the system back to the original position after a seismic event. In

Speicimen-1, a small amount of energy dissipation was resulted by concrete undergoing inelastic strains and the prestressing strands experiencing yielding at large drifts. For specimen-2, shown in Figure 2.16b, the external energy dissipaters were added to increase the energy dissipation capacity of the system and also the moment resistance. The details of the external energy dissipators are shown in Figure 2.16c. The energy dissipating device consisted of 0.2 in. thick A36 Reduced Steel Plate (RSP) and stiffeners at both sides were used to decrease the unbraced length. The bottom end of the dissipater was connected to a stiffener embedded into the foundation while the top end was connected to the bottom segment steel tube.

2.3.2.3 Test Setup

The column was post tensioned to the foundation at the bottom and to the loading stub at the top. The column is laterally displaced along North-South direction using the horizontally positioned actuator, connected to the column stub at the north end and to the strong wall at the south end. The detail test setup is shown in Figure 2.17.

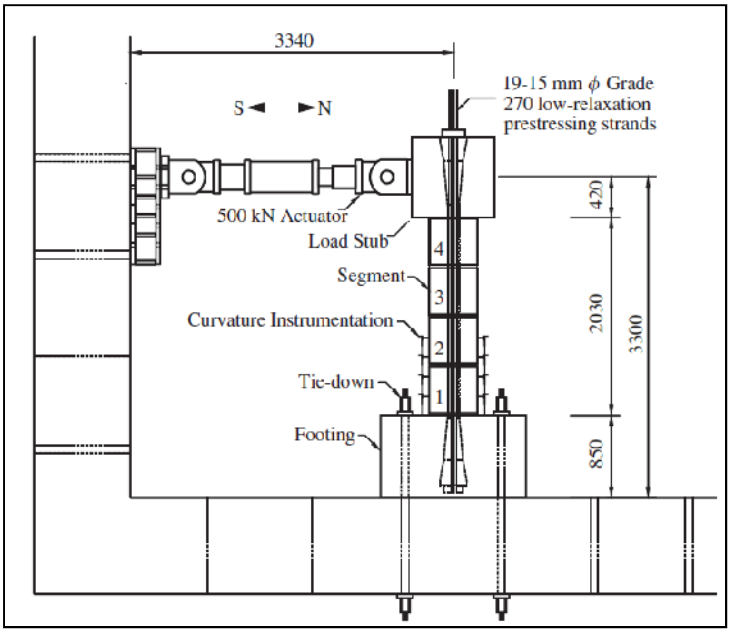

Figure 2.17 Elevation view of test setup with all the equipments labeled [20].

2.3.2.4 Results

The load displacement response for both the tests is shown in Figure 2.13. Both the tests show a maximum displacement of 200 kN at the end of 6% lateral drift. The hysteresis energy was calculated to be 50 % higher for the test two compare to one, which can be clearly observed in Figure 2.18.

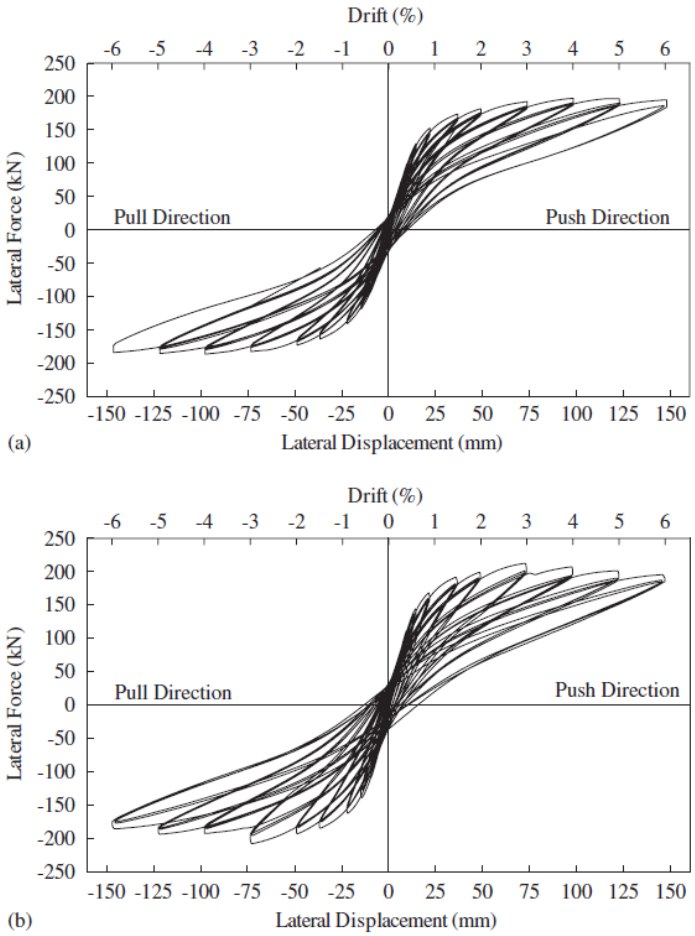

Figure 2.18 Lateral force versus lateral displacement response: (a) Specimen-1 and (b) Speciemen-2.

Until 4 % lateral drifts the lateral load and the area covered by the load displacement envelope is higher for Specimen-2. At first cycle of 4 % lateral drift the steel plates (energy dissipators) failed and from this point onwards the load displacement envelope of Specimen-2 matches closely with Specimen-1 results.

CHAPTER - 3 EXPERIMENTAL INVESTIGATION

3.1 Introduction

Testing of UHPC columns with different connection details is presented in this chapter. Each column was tested under reverse cyclic lateral loading, after it was connected to a steel foundation primarily using a post-tensioning bar. As noted previously there was a soft interface pad placed between the column base and top of the foundation. Altogether three UHPC columns were tested; the first unit was tested only with unbonded post-tensioning connecting the column to the foundation while the next two units were first tested with post-tensioning connection and then with both unbonded post-tensioning and energy dissipating connectors made up of steel angles. Presented first are the experimental setup and instrumentation, which were common for all of the tests. Next, information about the interface pad, loading protocol, test observations and results are presented for each unit.

3.2 Experimental Test Setup

Figure 3.1 shows an elevation view of the test setup, which includes both the post-tensioning and steel angle connectors. The main reason for using an unbonded post-tensioning connections was to eliminate development of large loacalised strains and subsequent fracture of the bar. This allows the column to be displaced to large displacements without yielding the post-tensioning bar, and subsequently experiencing loss in prestress force. Leaving the post-tensioning bar unbonded also prevents any development of large bond stress in the surronding UHPC and the related local damage. Although the columns

were tesetd in parallel to the major axis, there was no lateral support provided to restrain the column movements in the out-of-plane direction, as the movement in this direction was expected to be very small

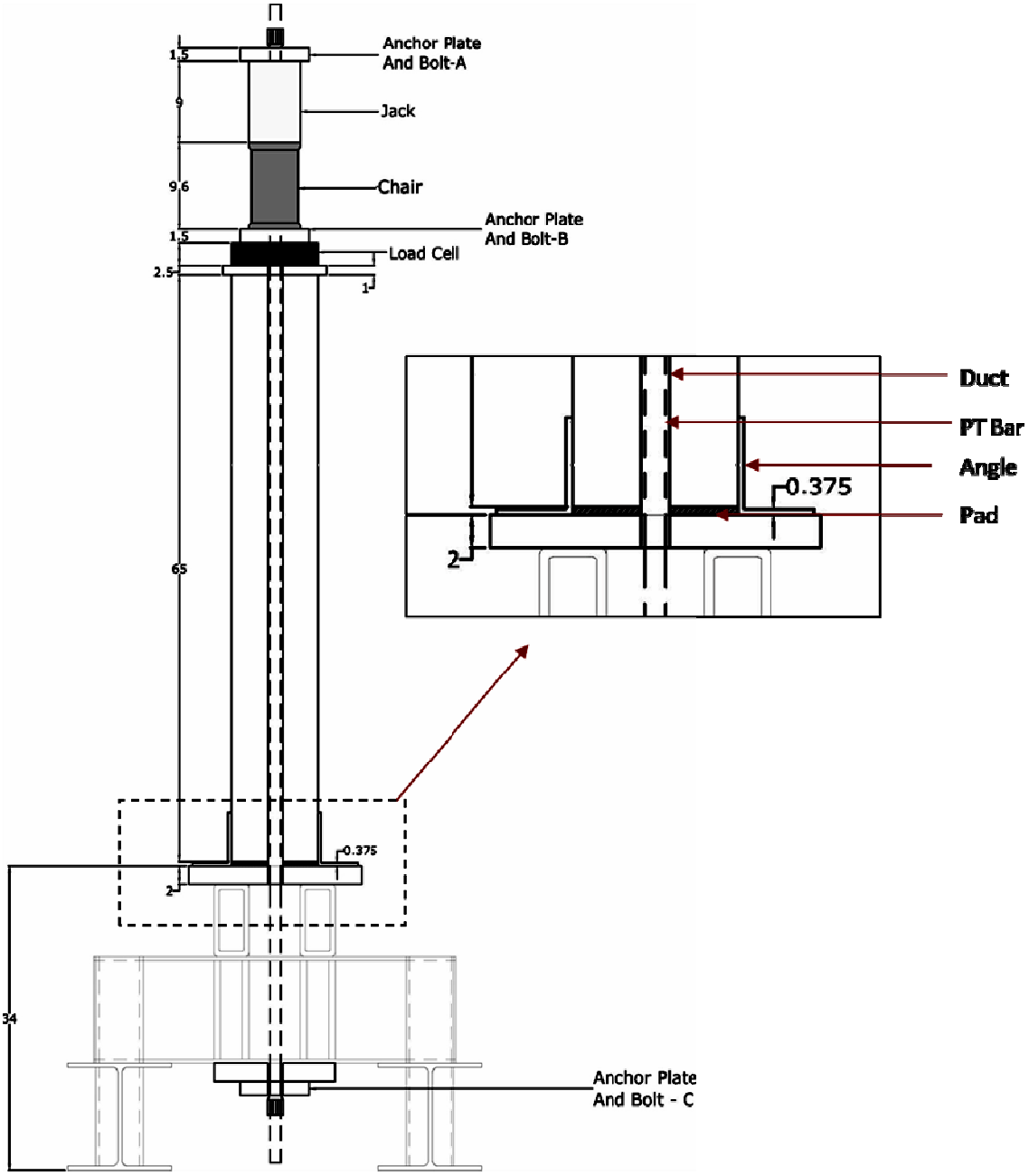

Figure 3.1 Test setup used for the UHPC columns.

Due to the use of unbonded post-tensioning, the UHPC column subjected to lateral loads was expected to rock at the base with a gap opening at one end and compression force transfer occuring through the pad at the other end. This behavior is possible due to concentration of flexural cracks at the base. With the post-tensioning steel designed to remain elastic, it also provides the necessary force to recentre the column when the lateral load is removed. When the steel angles are added as the energy dissipating elements, the recentring of the column can still be expected by apprioprietlysizing the angles. In this case, the UHPC column is expected to exhibhit noticeable energy dissipation by subjecting the steel angle to inelastic deformation.

3.2.2 UHPC Column

The UHPC columns used in all tests were 65 in. tall with a rectangular cross section of 6in. x 10in. as shown in Figure 3.2. The columns were built with a 1.7in.-diameter PVC pipe along its length at the center of the cross section. The post tensioning bar was placed inside the PVC to create the unbounded condition.

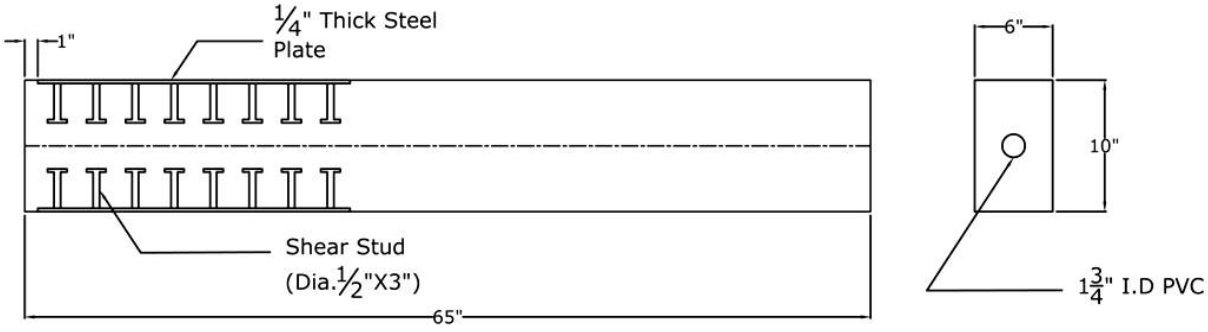

Figure 3.2 Dimensions of the UHPC test columns.

One end of the UHPC column had two steel plates attached to the 6 in. wide sides, which are identified in Figure 3.2. These plates were flushed with the surface and anchored into the column using shear studs. The use of the steel side plates was to enable the column to be connected to the steel foundation using energy dissipating steel connectors. The dimensions and the shear stud details of the steel embedment plate are shown in Figure 3.3. The side plate was 24 in. x 6 in. x ¼ in. (thick) and used 16 shear studs arranged in two rows as shown in Figure 3.3. The length of each shear stud was 3 inches. The first 2 ¾ in length of the stud had ½ in. diameter while the remaining ¼ in. length at the head was 1 inch in diameter.

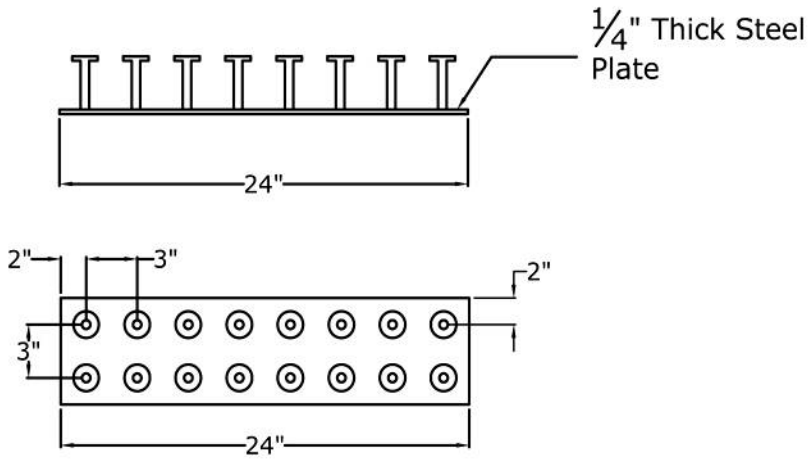

Figure 3.3 Dimension and shear stud details of the steel embedment plates.

3.2.3 Steel Foundation

A steel foundation designed for another research project at Iowa State University was used in all UHPC column tests. This foundation was 48 in. wide x 48 in. long and 36 in. tall and was constructed in three layers using I-beams, plates, stiffeners and tubes of A50 steel.

At the top of the foundation, it included a 2 in. thick 10 in. x 10 in. steel platform at the center, which enabled the connection to be established between the column and the foundation. A 1.5-in. diameter hole was included in the steel platform in order to allow the post-tensioning bar to extend below the base plate and anchor it to the foundation (see Figure 3.1). Fillet welds were used to attach different steel pieces together to form the steel foundation. The foundation also included four circular tubes in the corners, through which it was secured to the strong floor of the laboratory using tie-down bars

3.2.4 Anchorage of Post-tensioning Bar

As shown in Figure 3.1, a jack and an anchor plate/nut set A were used at the top of the jack temporarily to secure the post-tensioning bar in place. The column was then post-tensioned and the prestress bar was secured using anchor plate/nut set B at the top and a plate/nut set C at the bottom of the column.

The post-tensioning bar used in the test was high strength Dywidag bar with yield strength of about 125 ksi. It had an average diameter of 1.25 inches with a nominal area of 1.23 sq. inch. The bar was 11 feet long, passed through the post tensioning duct of the UHPC column, and extended 30 in. above the column for accommodating the post-tensioning setup. It also extended 30 in. below the column as shown in Figure 3.1.

3.2.5 Lateral Load Application

Each column was tested under lateral displacement cycles using a ±20 kip actuator. The actuator had a 10 in. total stroke, allowing the column to be subjected to ± 5 in. lateral displacement. A yoke linkage was used to connect the two twin plate assembly as shown in

Figure 3.6. The yoke linkage assisted in transferring the linear displacement from the actuator to the column as the column deflected. The actuator on the other end was connected to a strong frame through a link I-beam as shown in Figure 3.4.

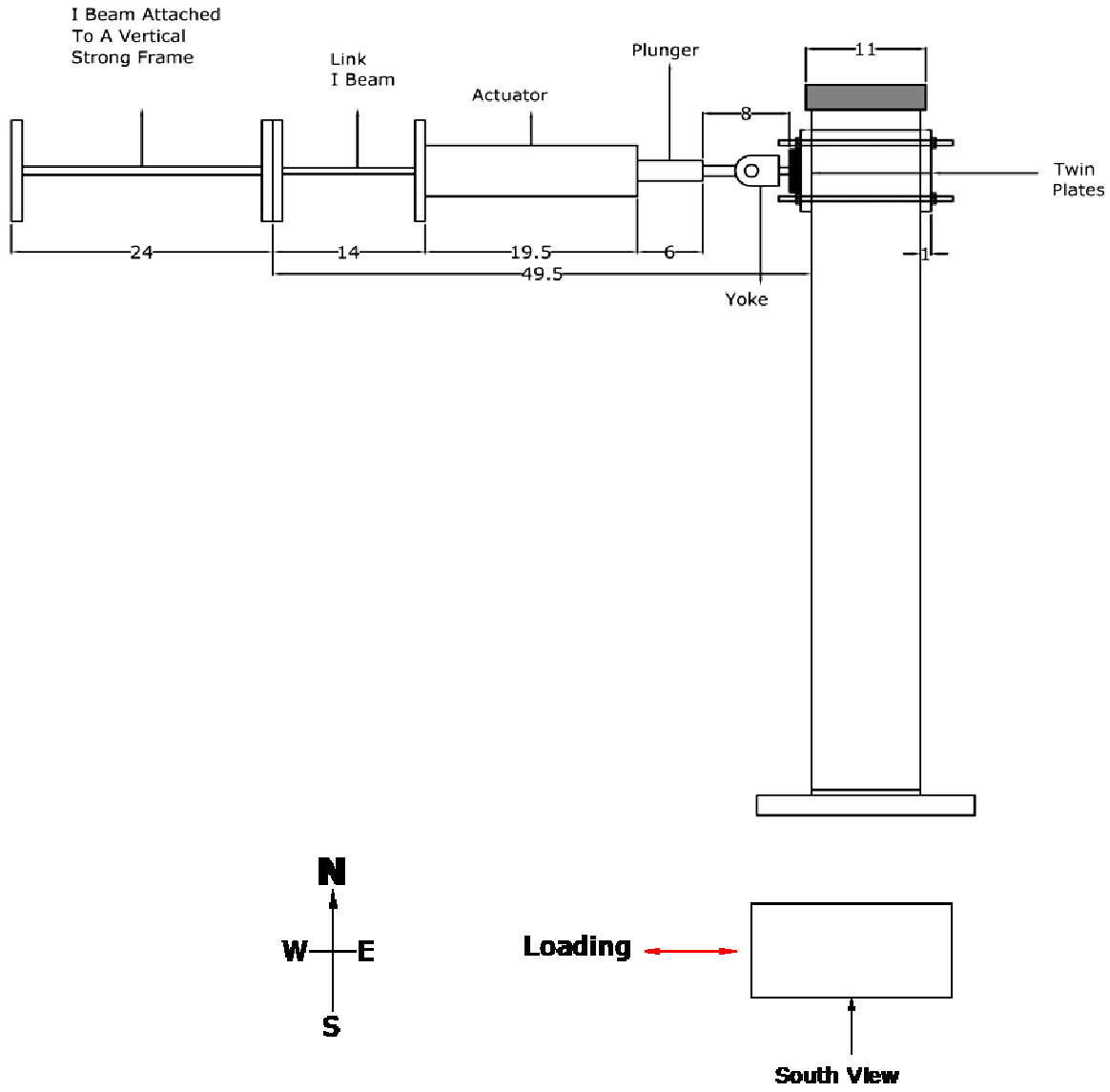

Figure 3.4 Actuator setup and the loading direction.

3.3 Instrumentation

The Instrumentation setup that was used for the UHPC column tests is shown in Figure 3.5 and 3.6. Figure 3.5 shows the setup for the first test and Figure 3.6 shows the setup for the remaining two tests. The Only change between the two instrumentation setup is the strain gauge locations. The different types of instruments used in the tests were: string potentiometers, tilt meters, linear variable displacement transducers (LVDT), strain gauges, and load cells. Locations of the different devices as mounted to the test unit are shown in Figure 3.5 and 3.6 on the four sides of the column. More details of the instruments are presented below.

Load Cells: Two load cells were used in each UHPC column test and their locations can be seen in Figure 3.5. A 200–kip load cell was placed at the top of the column to measure the post-tensioned force in the column. While the second load cell was positioned on the west face of the column. This 20-kip capacity load cell was used to measure the horizontal load applied to the column.

String Potentiometers: Three string potentiometers were used in each test as shown on the north view of Figure 3.5a. One string potentiometer was connected horizontally to the east face at the column top to measure the lateral displacement of the column from its original position. The remaining two devices were connected vertically on the east and west side of the column as shown in Figure 3.5a to measure the column elongation and the uplift at the base.

Strain Gauges: For first test, fifteen strain gauges were mounted in total, all within the bottom 9 in. height of the column. Six strain gauges were attached to the north face of the column to measure the longitudinal strains in two rows as shown in the Figure 3.5a. Four gauges were positioned at 3 in. from the base plate and two were located at a height of 6.5 in. from the base. On the south, east and west faces, there were nine strain gauges attached, which included three gauges along the center line on each face at heights of 2 in., 5 in. and 8in. from the base plate. It was hoped that the four strain gauges at the same height on the north face of the column would help locate the neutral axis depth of the UHPC column section at this height.

For the remaining two tests, fifteen strain gauges were mounted on each specimen, all within the bottom 9 in. height of the column. Six strain gauges were attached to the north face of the column to measure the longitudinal strains in two rows as shown in Figure 3.6a. Four gauges were positioned at 3 in. from the base plate and two were positioned at a height of 6.5 in. from the base. On the south face, 9 strain gauges were attached in three rows at heights of 2 in., 5 in. and 8in. from the bottom column end as shown in Figure 3.6b.

Linear Variable Differential Transducers (LVDTs): There were nine LVDTs used as shown in Figure 3.5d to measure the displacements between two points. Six of these devices were mounted to steel rods embedded into the column on the east and west faces at 6 in., 12 in. and 18 in. from the column base. One LVDT was mounted to each of the rods to measure the vertical extension with respect to the base plate. Two LVDT’s were mounted vertically on the north face of the column at a height of 3 in. from the base plate to record the column

uplift as seen in Figure 3.5d. One LVDT was mounted horizontally at 1 in. from the base plate to measure any slip of the column with respect to the base plate.

Tilt Meters: There were two tilt meters attached to the south face of the column as shown in the south view in Figure 3.5b. One tilt meter was positioned at a height of 2 in. above the base and the other at a height 5 in. below the top of the column. These tilt meters measured the rotation of the columns section at the respective locations.

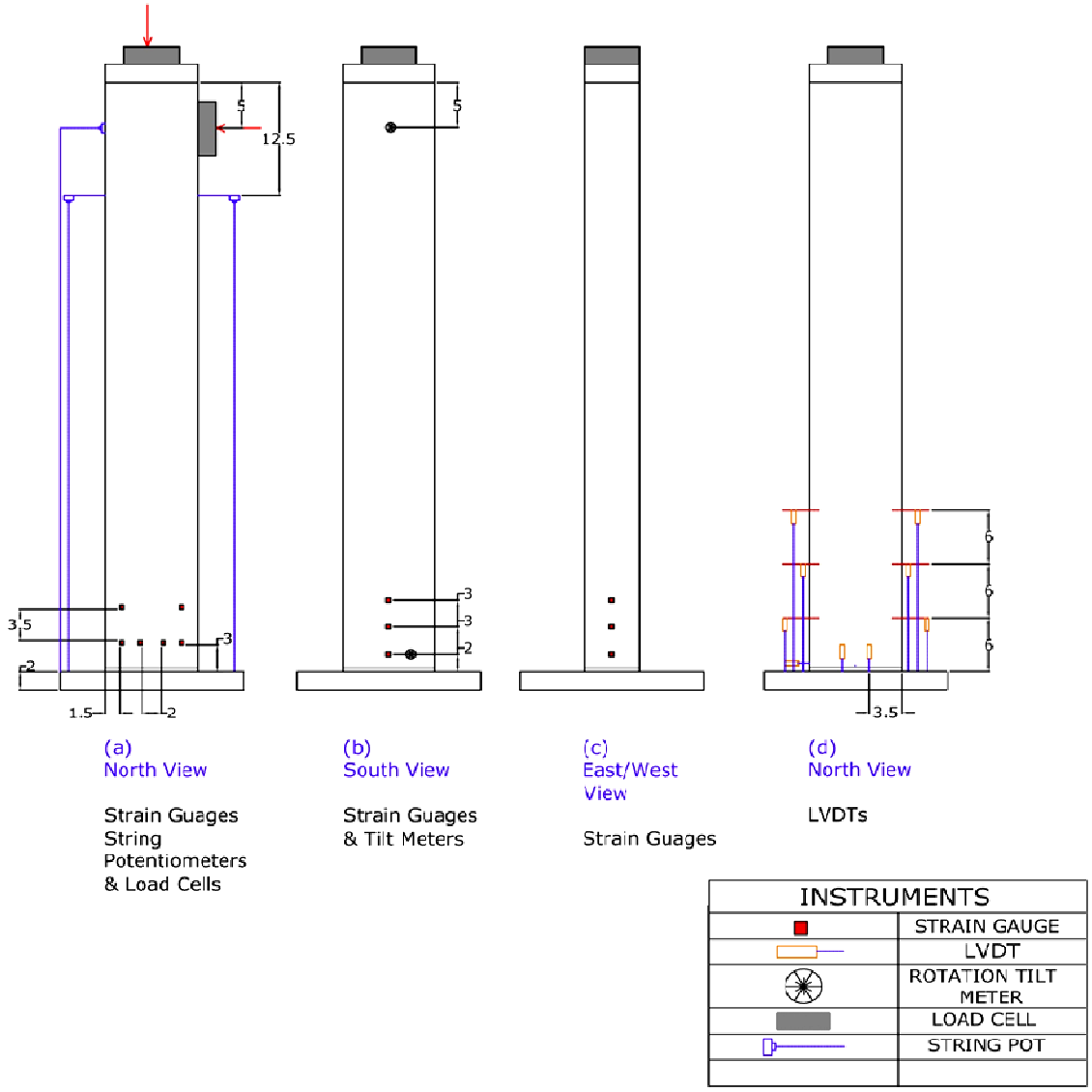

Figure 3.5 Instrumentation used for the first UHPC column test UHPC-C1.

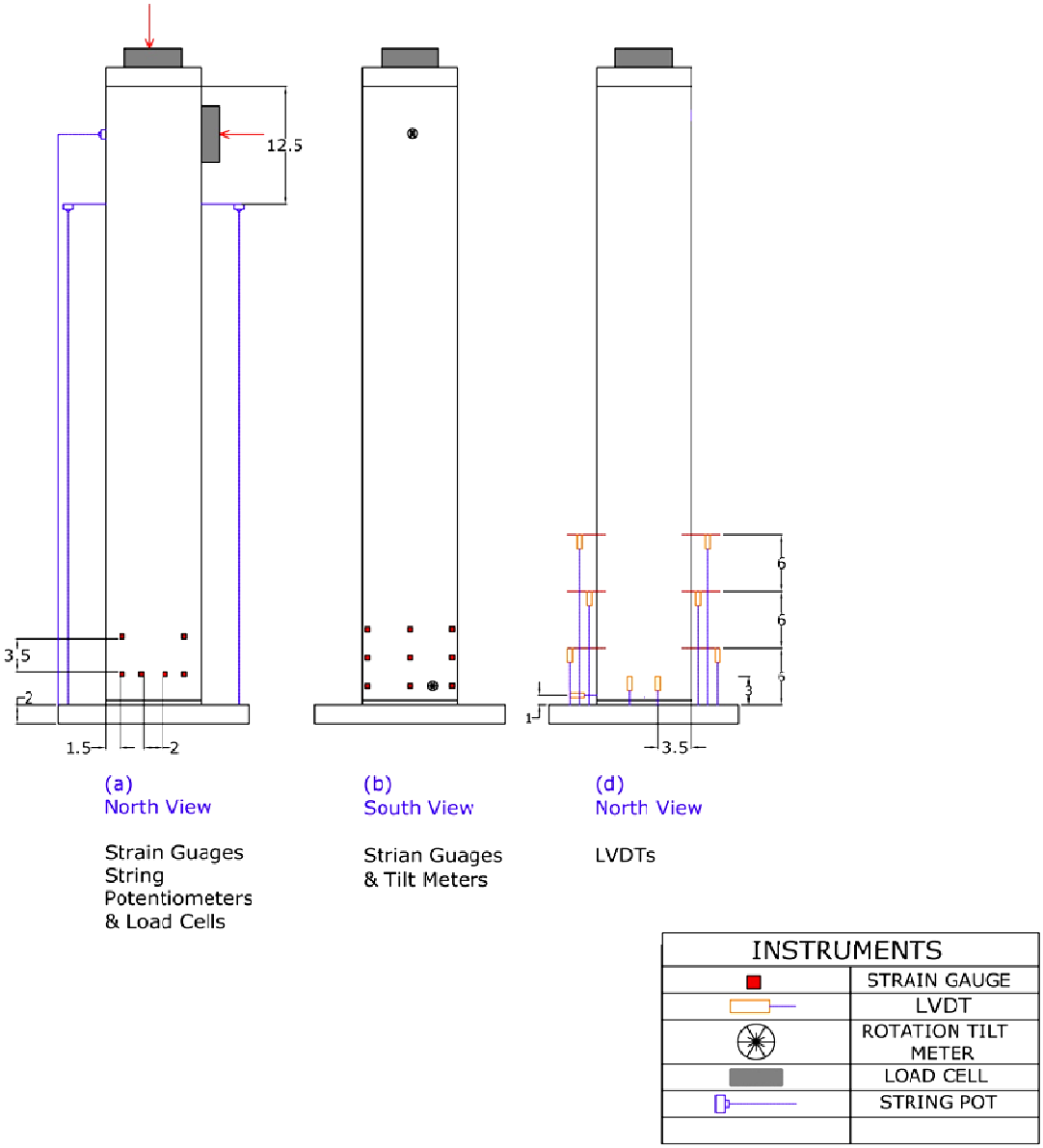

Figure 3.6 Instrumentation used for the second (UHPC-C2) and third (UHPC-C3) UHPC column tests.

Using a data acquisition system, all instruments were recorded during the tests at a 2 seconds interval. The collected data are presented in graphical form in the subsequent sections.

3.4 Lateral Load Tests

Three UHPC column tests were conducted in this studies and a different interface pad was used in each test. The tests were done on three different columns and details of the interface pads are summerized in Table 3.1. These test were identified as UHPC-C1, UHPC-C2 and UHPC-C3. UHPC-C2 and UHPC-C3 were tested with and without a pair of A36 steel angles as energy dissipators. the different identification used for the tests are also included in Table 3.1

Table 3.1 Summary of the UHPC column tests and test designation with respect to energy dissipation.

Test	Pad	Energy Dissipation
C1	Hydrostone	None
C2.a	Steel fiber grout	None
C2.b	Steel fiber grout	Pair of 3/8th inch A36 steel angles
C3.a	Glass fiber epoxy	None
C3.b	Glass fiber epoxy	Pair of 3/8th inch A36 steel angles

3.4.1 UHPC-1

The first column was attached to the foundation using a 0.5 in. thick Hydrostone pad at the foundation interface and 1.25-in. diameter Dywidag post-tensioning bar. The reason for selecting Hydrostone as the interface material was that it is easier to use and is the readily available strongest gypsum cement which can develop considerable early strength. The

selected Hydrostone was expected to develop compressive strength of 6,500 psi in wet condition and 13,500 psi in dry condition within one hour, which is greater than any other gypsum or Portland cement, can develop during the same duration. When it is mixed according to the given water to powder ratio, it provides a dense material with high compressive strength and high resistance to abrasion or wear. Other benefits of using Hydrostone as the interface material include: it sets faster than Portland cement which will speed up construction; it doesn't experience shrinkage strain while have the ability to penetrate and fill any cracks that may exist in the foundation; and it is a flowable material and ensures good contact between the column and the foundation.

Prior to placing the Hydrostone, the column was centered and leveled using a temporary formwork on a 0.5-in. thick, 0.75 in wide Neoprene rubber pad that had a 1.5-in. diameter hole in the middle using a temporary formwork around it. The top and bottom surface of the neoprene pad were sealed using butyl rubber, which in turn ensured a 0.5-inch gap between the column and foundation and prevented any, Hydrostone leaking into the post-tensioning duct. A rectangular wooden form was built around the column to create 8 in. x 12 in. Hydrostone interface pad as shown in Figure 3.7.

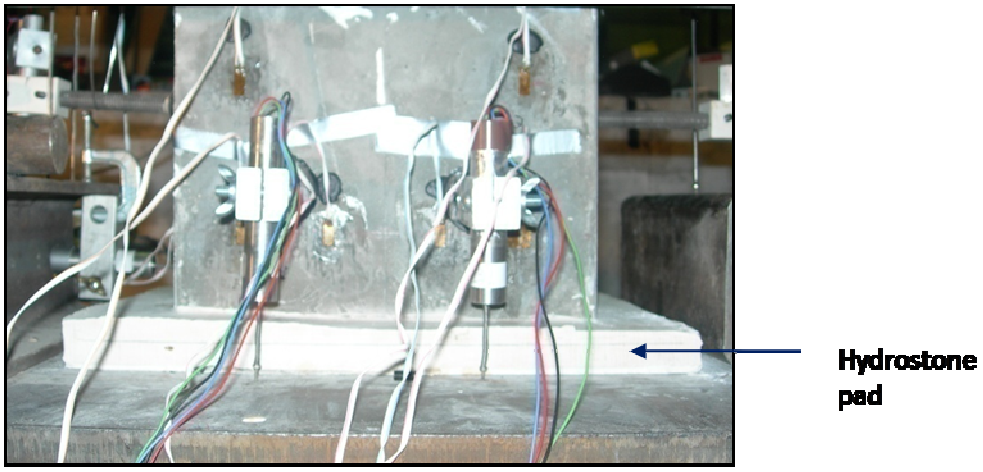

Figure 3.7 Forming a Hydrostone interface pad for UHPC-C1.

3.4.1.2 Loading Protocol

UHPC-C1 was subjected to a cyclic load path with full reversals as shown in Figure 3.8. The test was started under force control in the small displacement range and the following cycles were applied: ± 2 kips, ± 4 kips, ± 6 kips and ± 7.5 kips. For ± 7.5 kips of loading, the column reached maximum lateral load drifts of about ± 1 percent (i.e., lateral displacement of ± 0.6 in.). From this point onwards, a displacement control was used for the test and UHPC-C1 was subjected to ± 0.5% percent drift increments with three cycles at each drift level. When the column reached a lateral drift of ± 5 percent, a 3 percent loss in the initial prestress was noted due to the damage incurred to the Hydrostone pad (see more details in section 3.4.3.). Consequently, after subjecting the column to two cycles at ± 5 percent, the column was brought back to the original position and the post-tensioning bar was re-tensioned to the initial stress of 80.5 ksi. Three more cycles were applied at ± 5 percent, followed by three cycles at ± 6 percent and finally the column was subjected to ± 8 percent drifts. Due to

noticeable drop in the initial pre-stress, the test was terminated after applying two cycles at this drift.

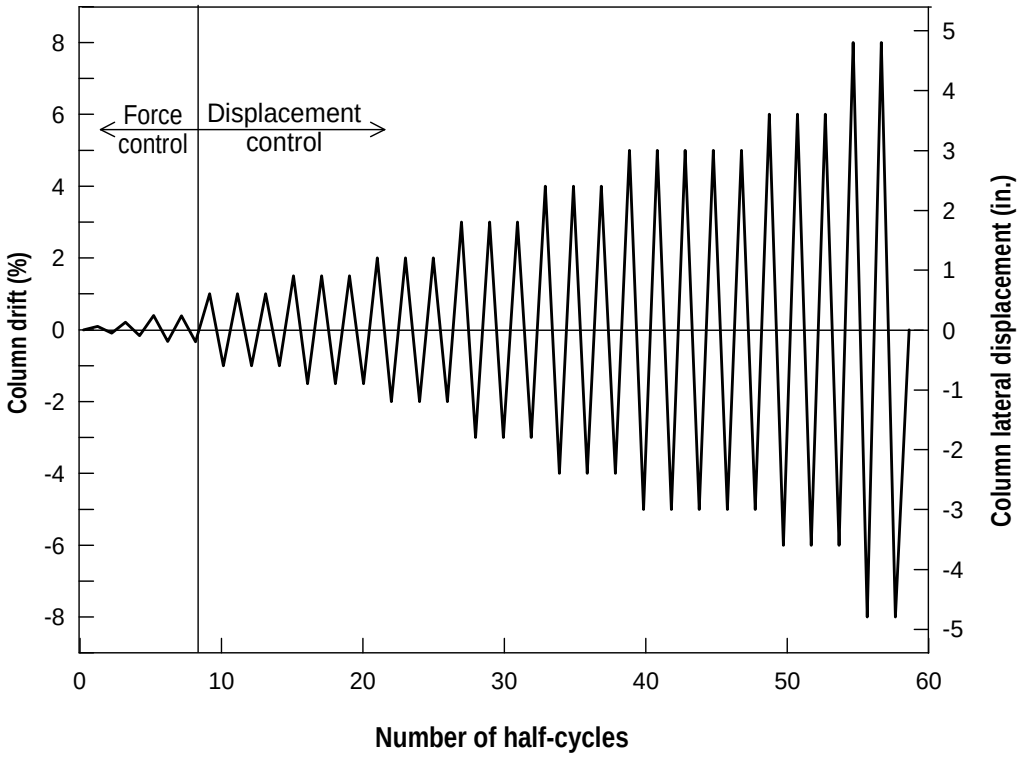

Figure 3.8 Load protocol used for UHPC-C1.

3.4.1.3 Test Observations

With all instruments ready to record data, the column was post-tensioned to 104 kips or a stress of 84.1 ksi. The Dywidag bar was anchored and the jack was released. At this stage, a seating loss of only 0.3 kips was encountered, leaving an initial load of 103.7 kip. The column lateral load test was then followed using the load protocol shown in Figure 3.8. During the force control cycles, the base of the column started to lift off the pad on the

tension side during the ± 6 kip cycle, but there was no damage to the pad or the column observed. During the displacement controlled cycles, the column continued to uplift at the base and during the first cycle at 2 percent lateral drift, the Hydrostone experienced cracking at column faces, indicating incipient crushing of the pad.

During the third cycle at 2 percent lateral drift, the crushing of the pad was clearly visible. More crushing of the pad was observed until the 5 percent lateral drift was reached, but no other major damage was observed to the test unit. At ± 5 percent lateral drift, the test was stopped after two cycles, since the initial post-tension load had dropped by 30 percent. The cyclic load displacement response upto 5 % lateral drift is shown in Figure 3.9a.

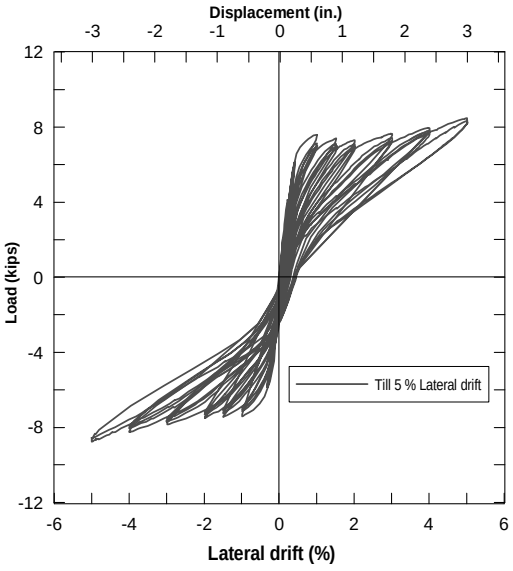

(a) Response till 5 percent lateral drift

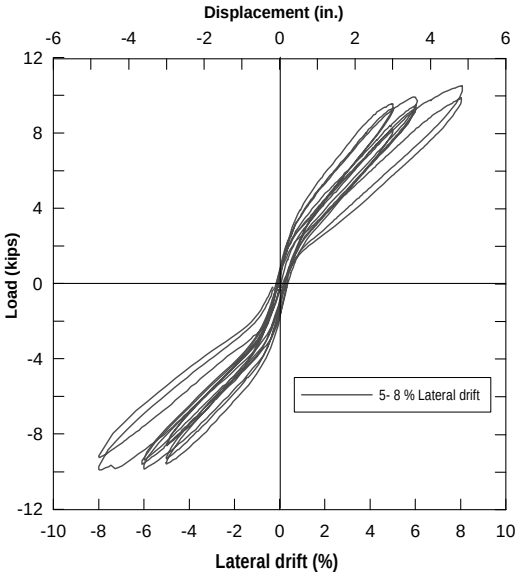

(b) Response from 5 to 8 percent lateral drift

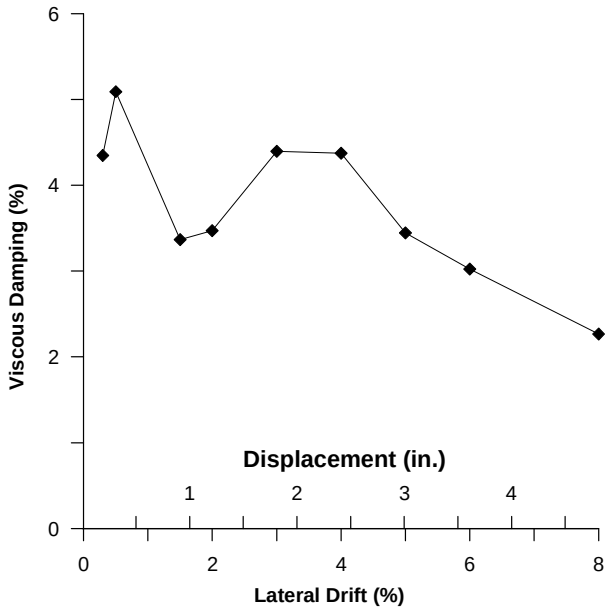

(c) Viscous damping

Figure 3.9 Force versus lateral displacement responses of UHPC-C1 and viscous damping in percentage for first peak lateral displacements.

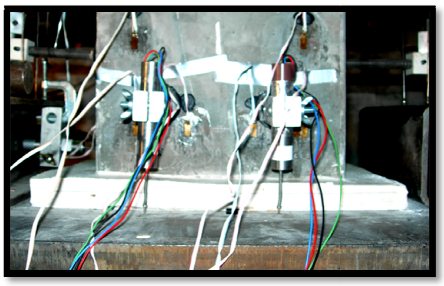

Hydrostone pad at the beginning of the test

Beginning of pad damage after 1 % lateral drift

Before re-tensioning the Dywidag bar at the end of 5 % lateral drift.

Completely crushed hydrostone at the end of 8 % Lateral drift

Figure 3.10 Hydrostone at different stages of the test.

At this stage, the Dywidag bar was re-tensioned to 104 kips. The load dropped to 99 kips due to seating loss after the bar was securely anchored. The column was subjected to two more cycles at 5 percent lateral drift. It was observed during the repeat testing at 5 percent drift, the lateral load increased by 1 kip compared to the first sequence of testing at the same drift, which can be observed in Figures 3.9b and Figure 3.11. Next, the column was subjected to three cycles at 6 percent drift and followed by two cycles at 8 percent lateral drift. During the ±8 percent drift cycles, the initial post-tensioning force started to reduce drastically due to further damage to the pad, and therefore the test was terminated after subjecting the column

to two full cycles at this drift. After the test was completed, the thickness of the pad was measure to be half the initial thickness (i.e., 0.25 in.). Variation of viscous damping with respect to lateral displacement is also shown in Figure 3.9c.

3.4.1.4 Force-Displacement Response

From Figure 3.11, it can be observed that between about 1 percent (0.6 in.) of lateral drift and 5 percent (3 in.) lateral drift, the force displacement curve flattens and the lateral load increases only marginally from 7.27 kip to 8.14 kip, which is due to the loss in initial pre-stressing strain in the Dywidag bar. This loss was due to the crushing damage incurred to the pad. The curve remains flat beyond 5% drift too even after re-tensioning, which is also due to continued loss in the prestressing force in the bar.

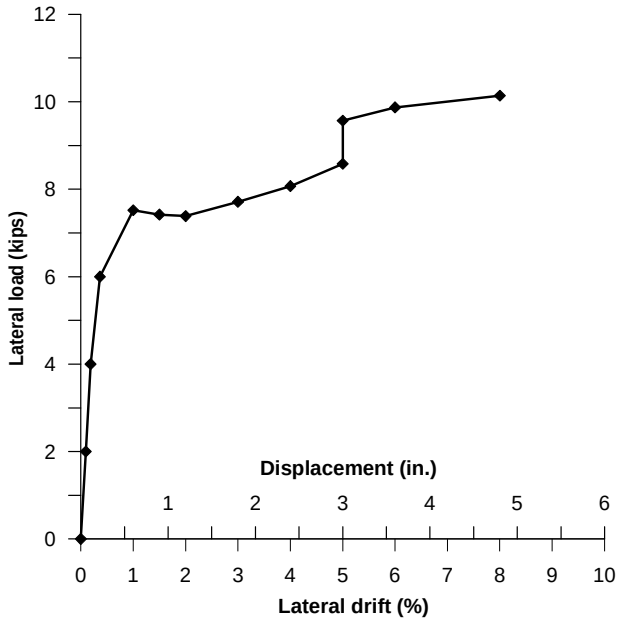

Figure 3.11 Monotonic force versus lateral displacement response using average first peak cycle values of UHPC-C1.

3.4.1.5 Post-tensioning Force

Figure 3.12 shows the variation of post-tensioning force during the test. During zero to 3 in. displacement cycles, the loss of prestressing force was gradual in the beginning, due to minimal crushing of the pad and as the lateral displacement increased the prestress load reduced drastically due considerable amount of crushing to the pad. Even in the 3 in. to 4.8 in. lateral displacements range there was continuous loss of prestressing force with displacement, which can be observed from Figure 3.12b. Even though the pad had crushed significantly and scope for further crushing was minimal, regular loss was observed. This loss in the prestress load might be due to anchorage slip loss as the column was subjected to large displacements.

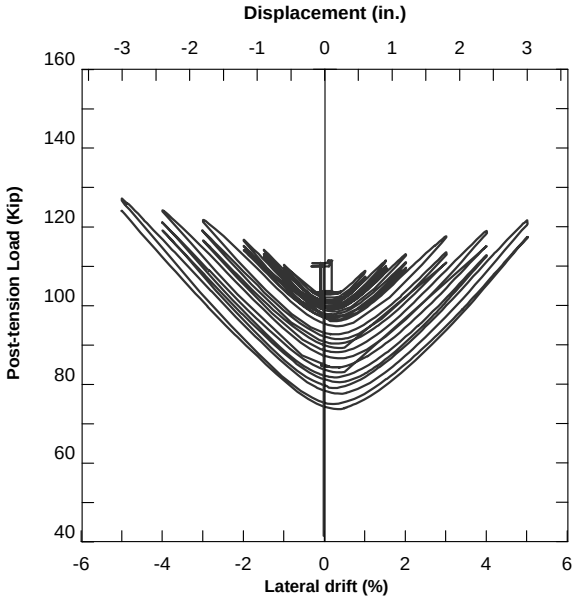

(a) Response till 5 percent lateral drift

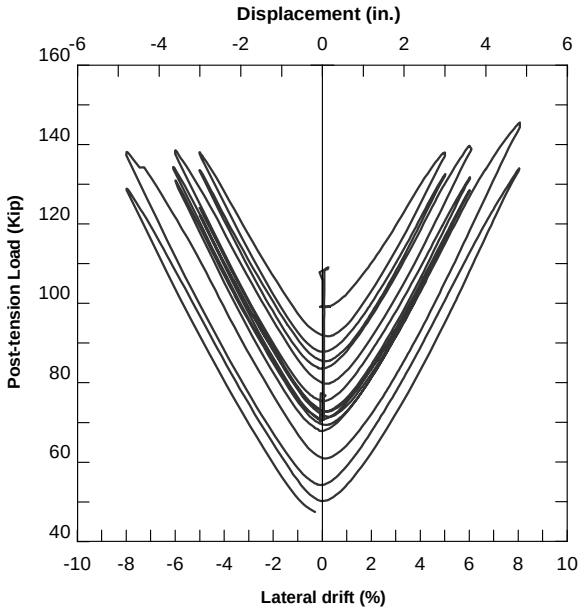

(b) Response from 5 to 8 percent lateral drift.

Figure 3.12 Post-tension load variations with lateral displacement.

3.4.1.6 Tilt Meter Reading

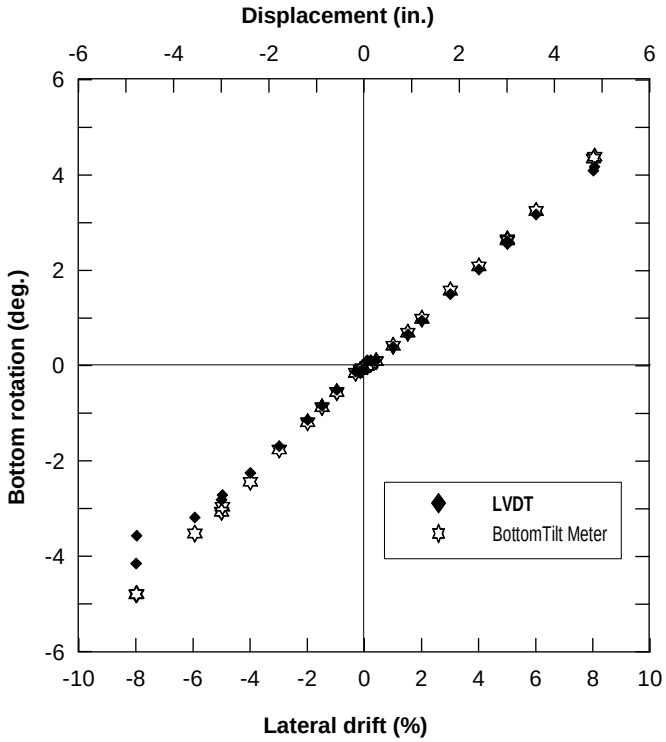

Figure 3.13 Bottom rotations versus lateral displacement calculated from Tilt meter reading and LVDT data.

The bottom rotation of the UHPC column was measured using tilt meter, mounted at 2 in. height from column base and calculated using a set of two LVDTs mounted at 12 in. height from the column base as shown in Figure 3.5. Only the rotation at first peak lateral drift was plotted as shown in Figure 3.13. Data obtained from both the instruments match well showing a linear variation.

3.4.1.7 Neutral Axis Depth

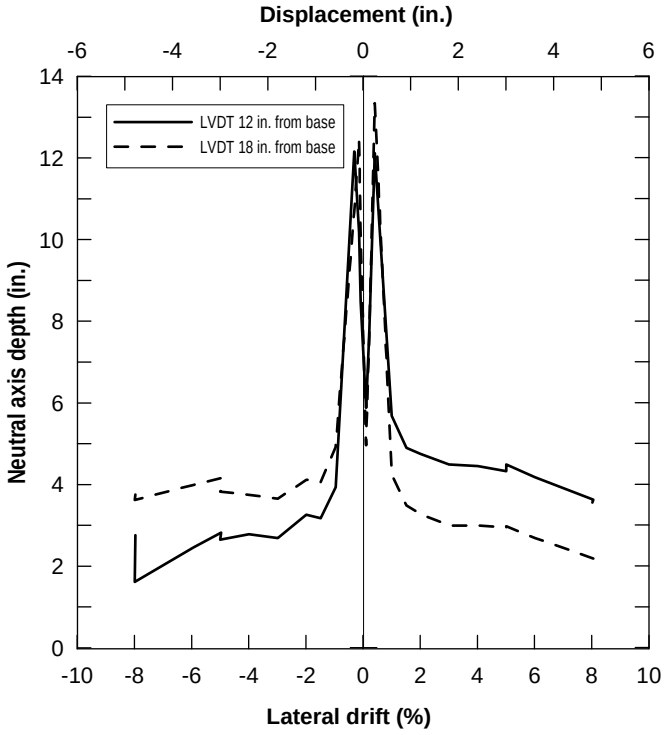

Figure 3.14 Neutral axis depths versus lateral displacement calculated from LVDT data for UHPC-C1.

The neutral axis of the UHPC column was calculated using the data recorded by two sets of LVDTs mounted at 12 in. and 18 in as shown in Figure 3.5. Only the values at first peak drift were plotted as shown in Figure 3.14. The LVDT data measures initially during the force control cycles were inappropriate, which led to drastic variations and reached high values of neutral axis depth greater than the depth of the column which is 10 in. From 1 percent drift onwards the data was appropriate and shows gradual variation. The neutral axis depth reduced gradually with the lateral displacement, due to the drop in post-tensioning load. The neutral axis depth varied within 2 to 4 in. depth

3.4.1.8 Strain Data

Figure 3.15 and 3.16 shows the strain history envelope of two locations on the face of the column, at equal distance from the longitudinal axis of the column and located at extreme edges. Both these locations showed similar strain behavior. First part of the test till the 5 percent lateral drift the column showed zero tensile strains, but later part of the test from 5 to 8 % lateral drift, tensile strains were observed at these positions as the column was subjected to large lateral displacements.

Figure 3.17 and 3.18 shows the strain history envelope of two locations on the face of the column, at equal distance from the longitudinal axis of the column and located close to it. Since the location was close to the center of the column, only compressive strains were observed. For the second part of the test from 5 to 8 % lateral drift the strain envelope shift slightly down with increased compressive strains, due to the post-tension bar restraining done before beginning the second part of the test.

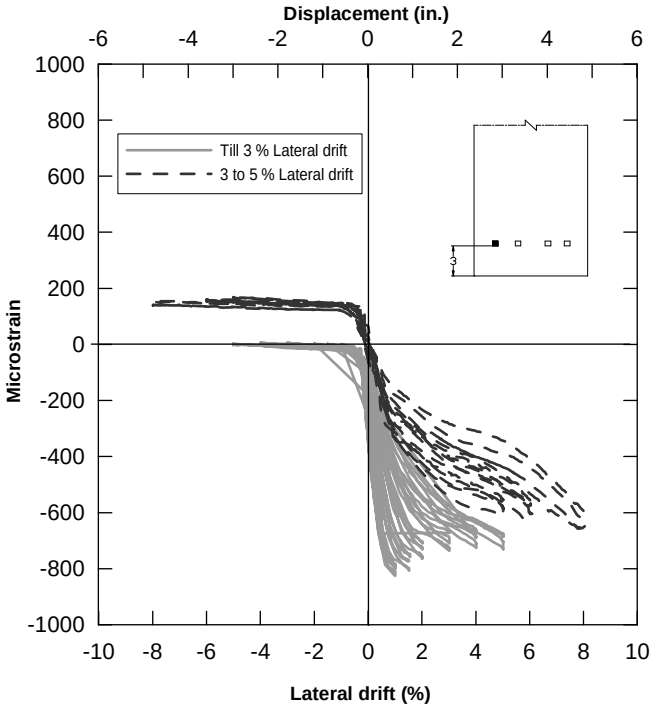

Figure 3.15 Strain histories obtained on the face of the column at 3 in. from the base.

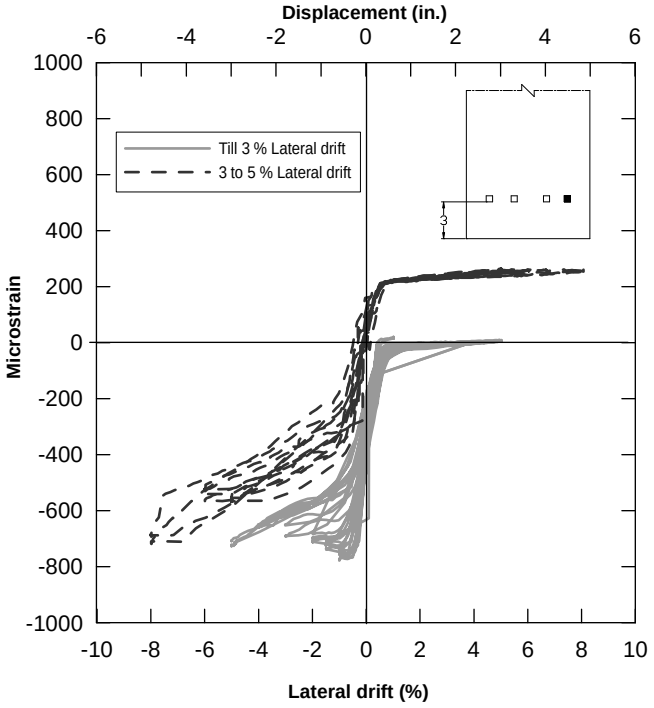

Figure 3.16 Strain histories obtained on the face of the column at 3 in. from the base.

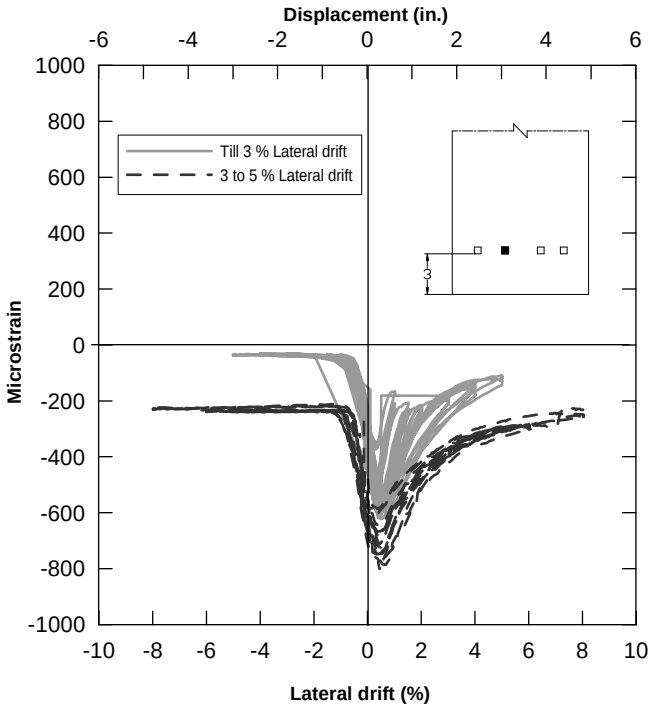

Figure 3.17 Strain gauge history of a strain gauge on the face of the column.

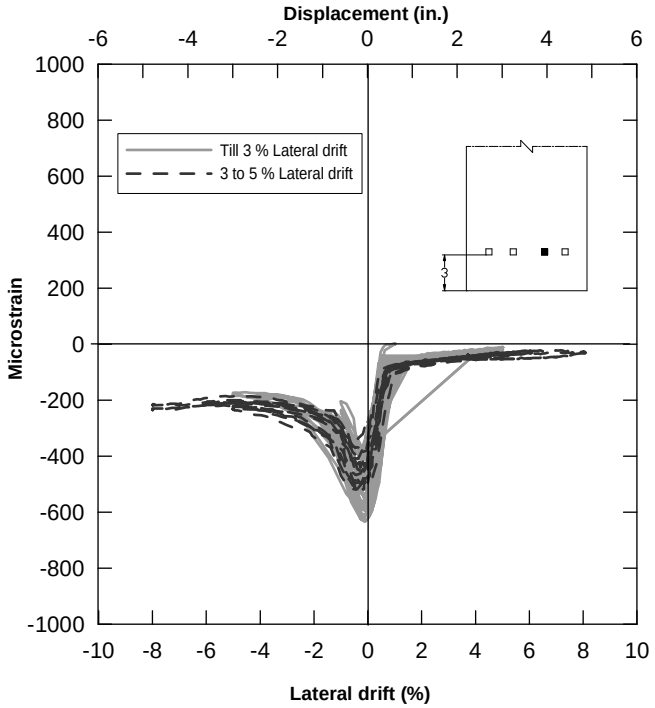

Figure 3.18 Strain gauge history of a strain gauge on the face of the column.

3.4.2 UHPC-C2

After the crushing failure of the Hydrostone pad during the UHPC-1 testing, material with better compressive strength and strain capacity had to be chosen for the UHPC-2 column test. A steel fiber reinforced non-shrink cementetious grout (SFRG) was chosen, this material was usually employed as a base material for heavy load foundations. It showed higher compressive strength compared to Hydrostone and developed a compressive strength of 9 ksi in one day and 13 ksi in a week. The reinforced steel fibers were 0.5 in. long and expected to provide strain capacity to the grout. When the grout is mixed according to the given water to mix ratio, it is supposed to form a dense material with high compressive strength and hard surface, resistant to mechanical burden like beating, grinding and rubbing.

Other benefits of SFRG as the interface material include: It sets faster and develops high early adhesion with high compressive strength; it does not experience shrinkage strain; it is a flowable material and ensures good contact between the column and the foundation; when used in construction parts it improves bending strength as well as shear strength and impact strength to quiet some extent and due to steel fibers reinforcement it shows minimal tensile strength and can employed in construction parts where reinforcement cannot be installed.

Similar to the first test, prior to placing the grout the column was centered and leveled using a temporary formwork on a 0.5-in. thick, 0.75 in. wide Neoprene rubber pad that had a 1.5-in. diameter hole in the middle using a temporary formwork around it. The top and

bottom surface of the neoprene pad were sealed using butyl rubber, which in turn ensured a 0.5-in. gap between the column and foundation and prevented any, grout leaking into the post-tensioning duct. A rectangular wooden form was built around the column to create 8 in. x 12 in. SFRG interface pad as shown in Figure 3.19.

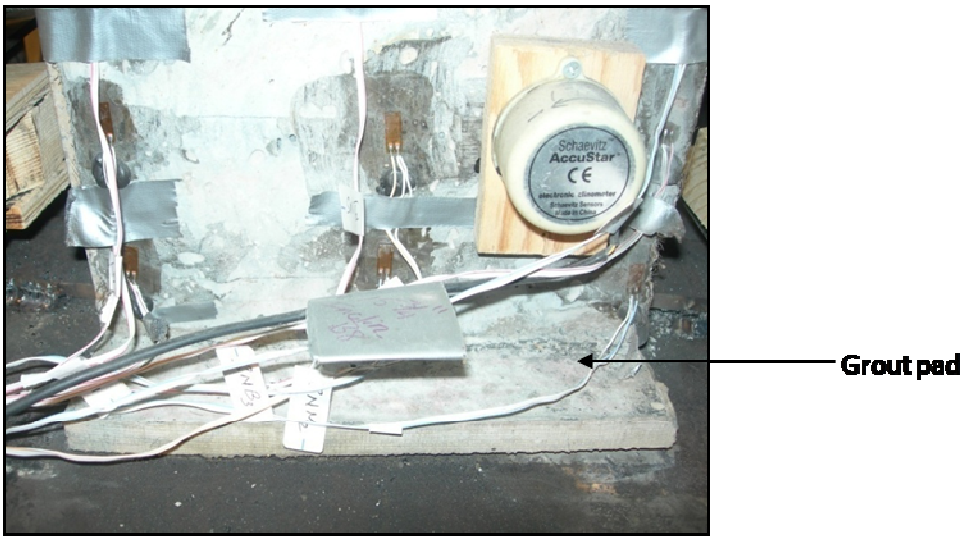

Figure 3.19 Steel Fiber Reinforced Grout (SFRG) pad.

3.4.2.2 Loading Protocol

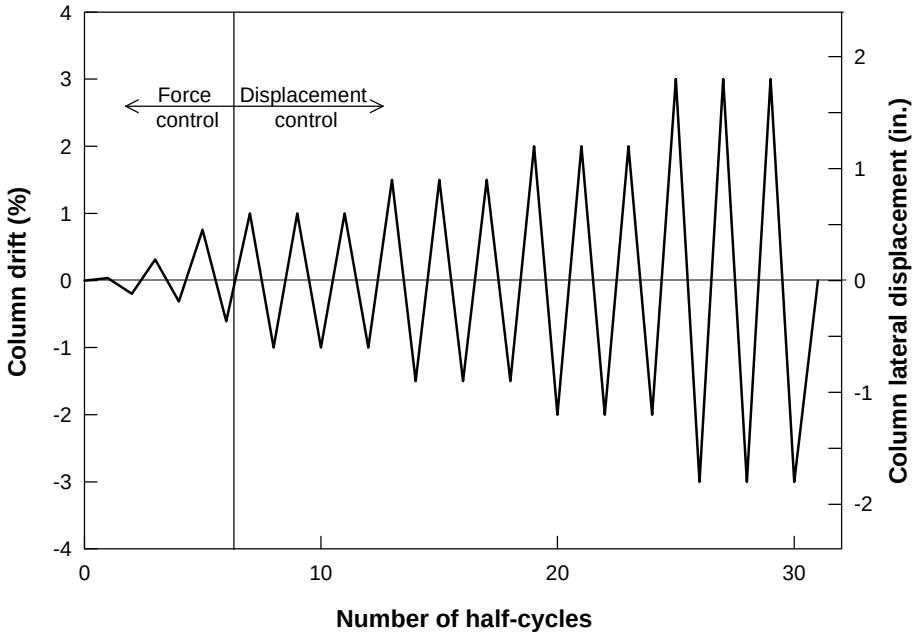

Figure 3.20 Load protocol used for UHPC column without angles (UHPC-C2a).

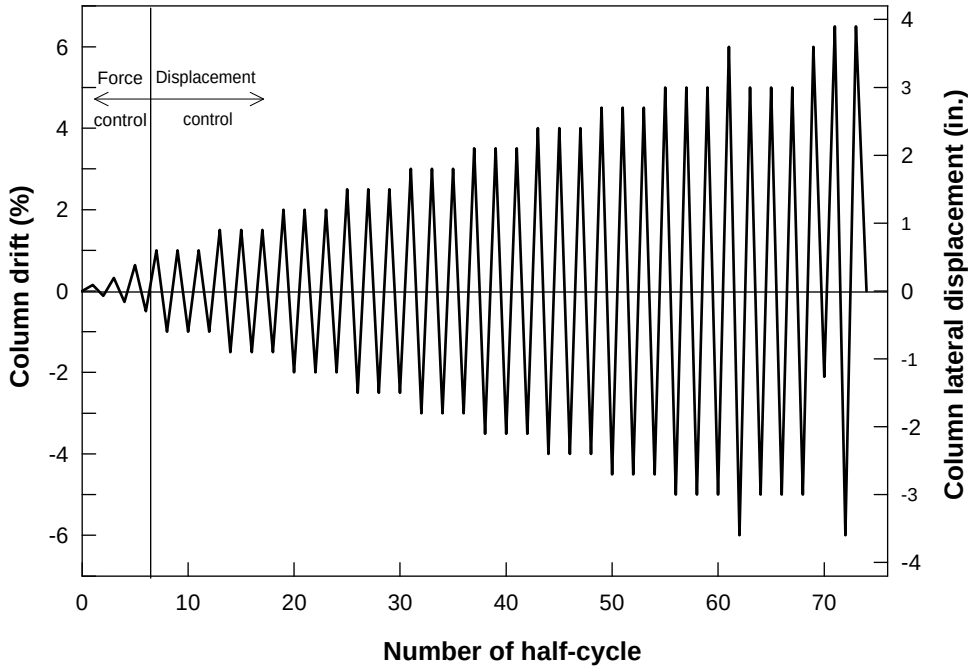

Figure 3.21 Load protocol used for UHPC column with angles (UHPC-C2b).

As shown in Table 3.1 the UHPC test-2 was divided in to two parts based on the presence of dissipation material (steel angles). For the first part of the test UHPC-C2a, (no angle test) the column UHPC-C2 was subjected to a smaller load path as shown in Figure 3.20. Next for the second part of the test UHPC-C2b (with angle test), the column was subjected to a longer load path as shown in Figure 3.21. Both will be explained in detail below.

For test UHPC-C2a, UHPC-C2 was subjected to a cyclic load path with full reversals as shown in Figure 3.20. The test was started under force control in the small displacement range and the following cycles were applied: ± 2 kips, ± 4 kips, ± 6 kips, ± 8 kips and ± 8.5 kips. For ± 8.5 kips of loading, the column reached maximum lateral load drifts of about ± 1 percent (i.e., lateral displacement of ± 0.6 in.). From this point onwards, a displacement control was used for the test and UHPC-C1 was subjected to ± 0.5 percent drift increments with three cycles at each drift level. This test was continued only till 3 percent lateral drift to make sure there was not much damage to the pad, used again for the next part of the test and also enough data is available to verify the column analytical model without the steel angles.

For the UHPC-C2b, UHPC-C1 was subjected to a cyclic load path with full reversals as shown in Figure 3.21. The test was started under force control in the small displacement range and the following cycles were applied: ± 2 kips, ± 4 kips, ± 6 kips and ± 7.5 kips. For ± 7.5 kips of loading, the column reached maximum lateral load drifts of about ± 1 percent (i.e., lateral displacement of ± 0.6 in.). From this point onwards, a displacement control was used for the test and UHPC-C1 was subjected to ± 0.5% percent drift increments with three

cycles at each drift level. When the column reached a lateral drift of ± 6 percent, cracks were observed on the weld connecting the angle and the base plate (see more details in section 3.4.2.3). Consequently, after subjecting the column to one cycle at ± 6 percent, the column was brought back to the original position and the test was stopped. After fixing the weld connections the post-tensioning bar was re-tensioned to the initial stress of 89.4 ksi (110 kips) and the test was started beginning with 5 percent lateral drift. During the first half cycle +5 percent, the angle connected at the east face failed in tension. Three cycles were completed at 5 percent drift, followed by one incomplete half cycle till +2 percent lateral drift, limited due to loud noise heard from the apparatus. Next, the column was pushed to -6.5 percent lateral drift, where the other angle connected on the west face also failed in tension.

3.4.2.3 Test Observation

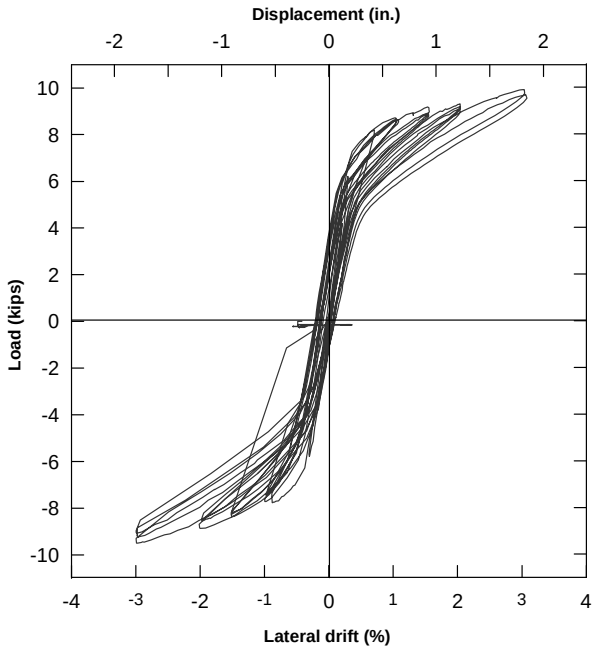

(a) UHPC-C2a reverse cyclic response

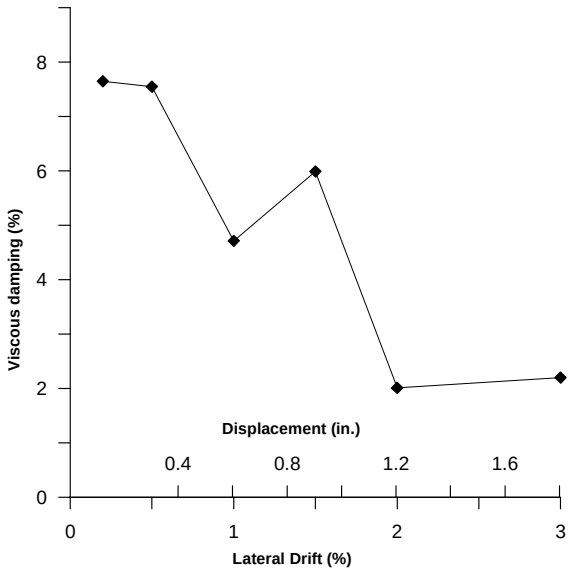

(b) Viscous damping

Figure 3.22 Force versus lateral displacement response of UHPC-C2a (no angles) test and viscous damping in percentage for first peak lateral displacements.

With all the instruments ready to record data, the column was post-tensioned to 112 kips or a stress of 91 ksi. (0.0029 strain). The Dywidag bar was anchored and the jack was released, a seating loss of 0.9 kips was encountered leaving an initial load of 111.1 kips. The column lateral load test was then followed using the load protocol shown in Figure 3.20. During the force control cycle ±8 kips, small cracks were observed on the grout pad, just below the column face indicating crushing of the pad. Later during displacement control cycles, at ± 2 percent deflection the base of the column started to lift off the pad on the tension side. Figure 3.22a shows the load verses displacement curve for UHPC-C2a. No significant changes were observed during this test. The variation of viscous damping with respect to lateral displacement is also shown in Figure 3.22b.

For the second part of the test with the steel angles connected, the column was post-tensioned to 110.3 kips. The Dywidag bar was anchored and the jack was released. A seating loss of 0.3 kips was encountered, leaving an initial load of 110 kips. During the load control cycles no major changes were observed in the test. During displacement control cycles, at 2 percent lateral drift the column base was observed to lift off with the pad on the tension side. During the first cycle of the 2.5 percent lateral drift cracks development was observed on both sides of the grout pad at approximately 3.5 in from the column edges as shown in Figure 3.24. This was due to crushing of the concrete at the edges for width equal to the neutral axis depth. The cracks on the pad continued to widen with increase in displacement. At the end of third cycle 3.5 percent lateral drift hair line cracks were observed developing on the north and south face of the column

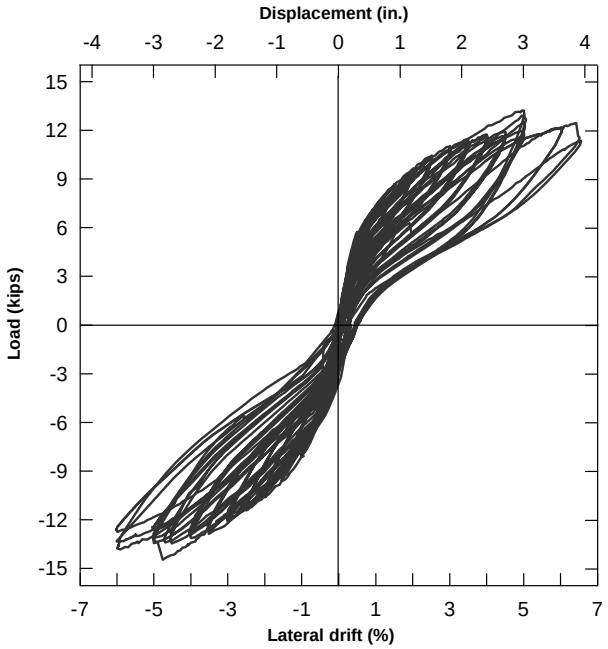

(a) UHPC-C2b reverse cyclic response

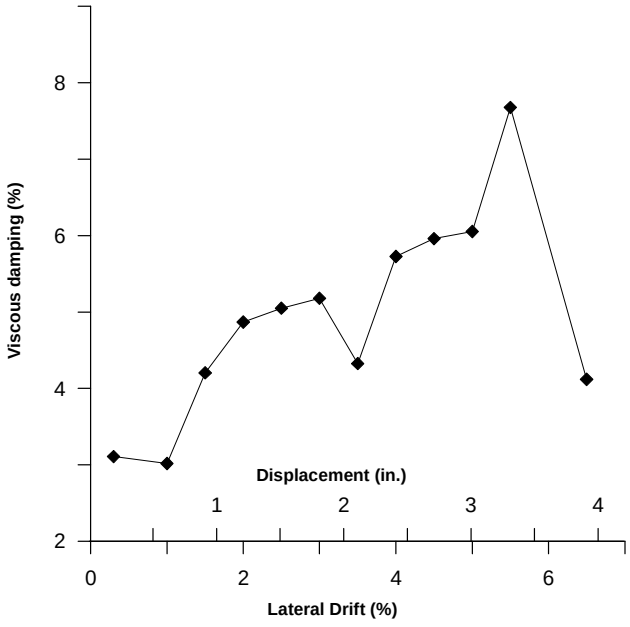

(b) Viscous damping

Figure 3.23 Force versus lateral displacement response of UHPC-C2b test and viscous damping in percentage for first peak lateral displacements.

. On the north face of the column, a crack had developed from the base measuring approximately 3 in. from the edge as shown in Figure 3.24. While on the south face the crack had developed exactly in the middle developed from the column base. Also, at the end of 3.5 percent lateral drift hair line cracks were spotted on the weld connecting the angle to the foundation plate. The weld continued to incur damage from this cycle onwards. The test was continued till second cycle of 5 percent lateral drift and consequently stopped due to the increase in damage to the weld and also due to drop in the initial post-tension load by 16 percent.

The damaged weld was grinded off and the angles were re-welded connecting the column and the base plate. The post-tension bar was re-tensioned to 104 kips and the test was continued. During the immediate first half cycle the angle on the east face fractured at + 5 percent drift. After three cycles at 5 percent drift, the column was pushed to an incomplete + 2 percent half cycle stopped due to a loud noise heard from the setup as shown in Figure 3.23a. During the next half cycle – 6.5 percent drift the other angle also failed. The variation of viscous damping with respect to lateral displacement is also shown in Figure 3.23b.

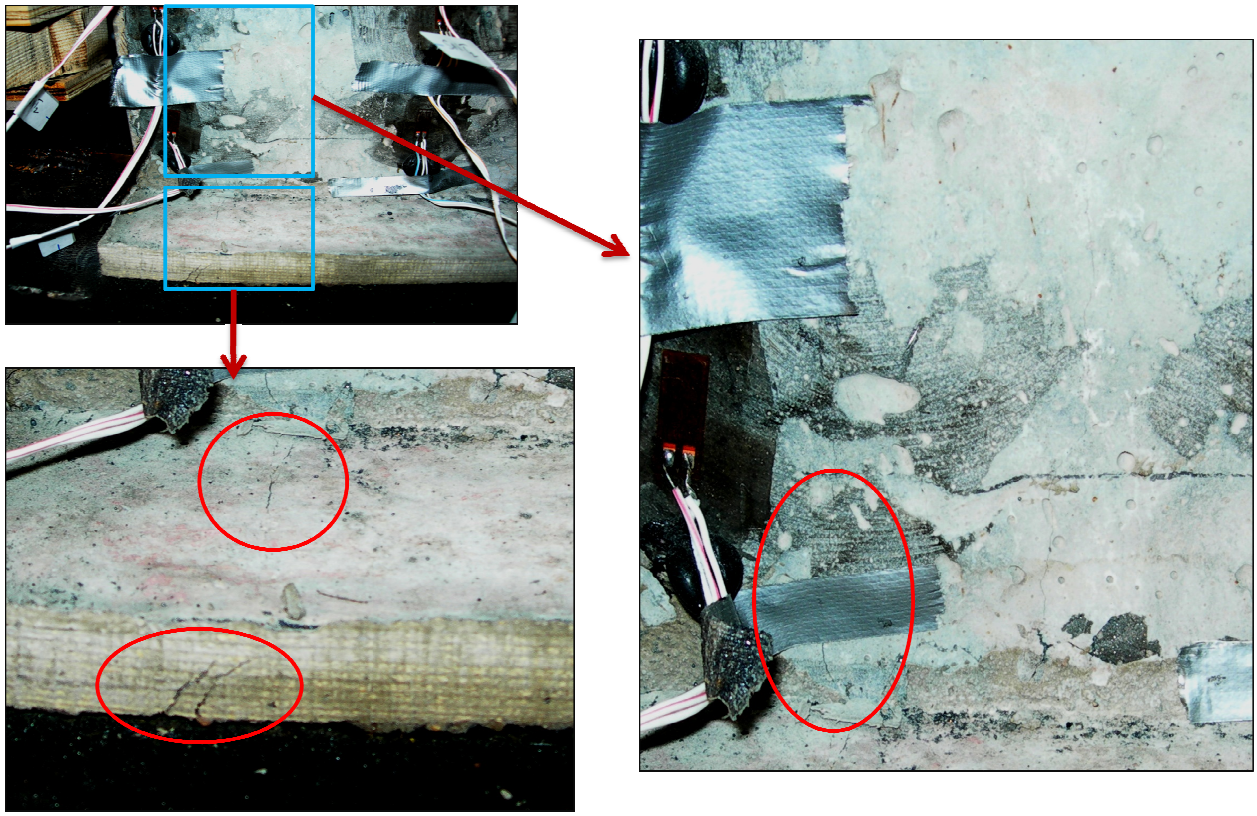

Figure 3.24 Observation during the test of cracks developed on pad and column.

3.4.2.4 Force-Displacement Response

Monotonic force displacement responses for both no-angle and with-angle test are shown in Figure 3.24. During the first test (without angles) the pad was damaged at the edges and its stiffness was reduced. This was evident from the results of the second test. The with-angle test showed less initial stiffness than the no-angle test, which is clearly visible in Figure 3.25.

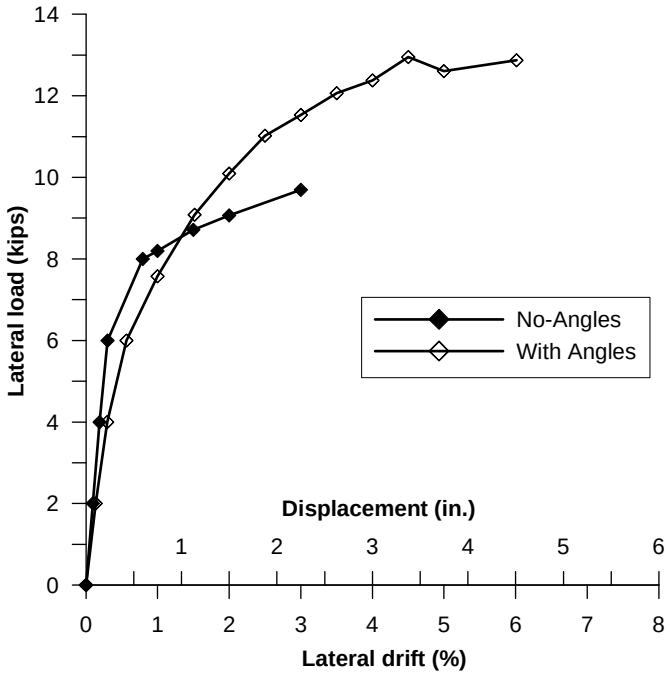

Figure 3.25 Monotonic force versus lateral displacement response of UHPC-C2.

3.4.2.5 Post-tensioning Force

From Figure 3.26 shows the post-tension force variation for the no-angle test UHPC-C2a. There was not much loss in post-tensioning compared to the UHPC-C1 test, at the end of 3 percent displacement only 1.1 kip drop was recorded.

Figure 3.27 shows the post-tension force variation for the with angle test UHPC-C2b. Even during this test the post- tension load drop was only 1.2 kips till 3 percent lateral drift. From 3.5 percent lateral drift onwards the post-tension load started dropping proportionally with increase in displacement. At the end of 6 percent lateral drift when the test was stopped, the initial post-tension load was lost by 22 percent, this may be due to both crushing of the

pad and slip loss. the bar was re-tensioned to 104 kips and the column was subjected to 5 cycles from 5 to 6.5 percent drift , the initial post-tension load was lost by 17 percent , this loss was predominantly due to slip loss as result of large lateral displacements.

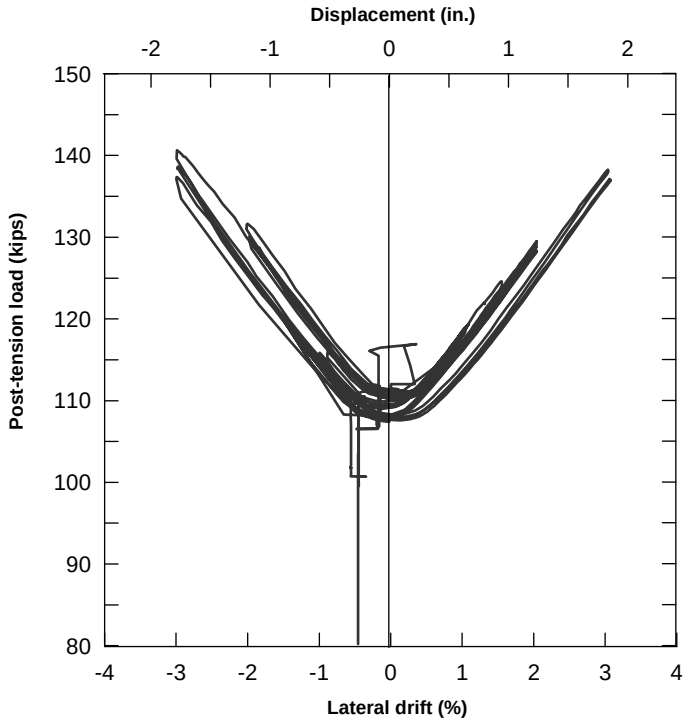

Figure 3.26 Post-tension load variations with lateral displacement of UHPC-C2a (no-angle) test.

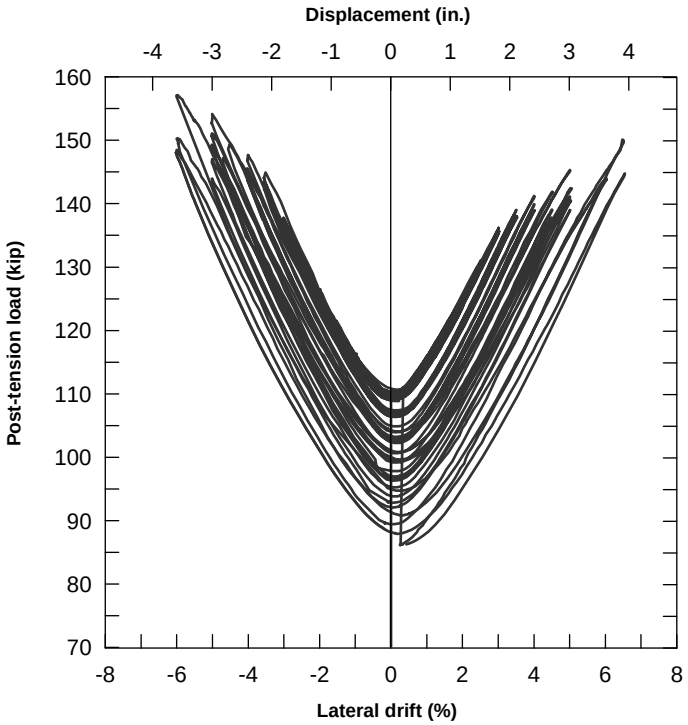

Figure 3.27 Post-tension load variations with lateral displacement of UHPC-C2b test.

3.4.2.6 Tilt Meter Reading

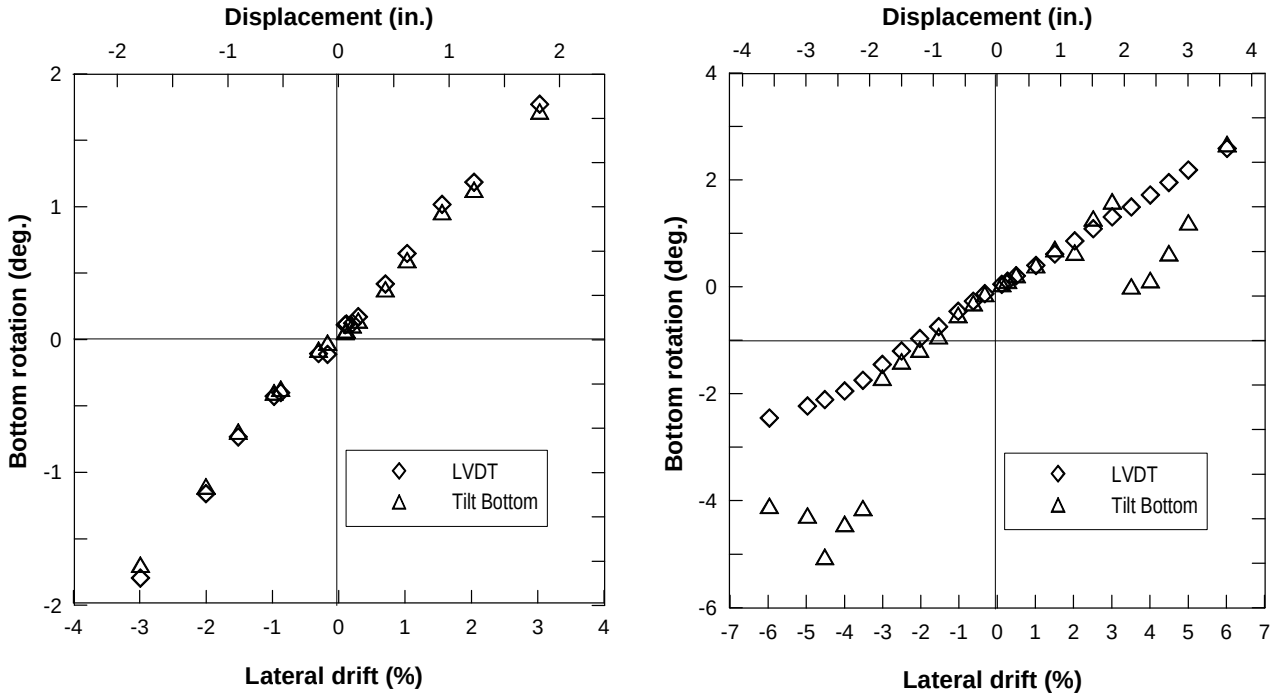

(a) UHPC-C2a rotation till 3 percent drift (b) UHPC-C2b rotation till 6 percent drift

Figure 3.28 UHPC-C2 Bottom rotations versus lateral displacement calculated from Tilt meter reading and LVDT data.

The bottom rotation of the UHPC column was measured using tilt meter, mounted at 2 in. height from column base and calculated using a set of two LVDTs mounted at 12 in. height from the column base as shown in Figure 3.28. Only the rotation at first peak lateral drift was plotted. For the no-angle test data obtained from both the instruments match well showing a linear variation. For the angle test the test data obtained from both the instruments match only till 3 percent lateral drift. This may be due to calibration errors of the measuring instrument.

3.4.2.7 Neutral Axis Depth

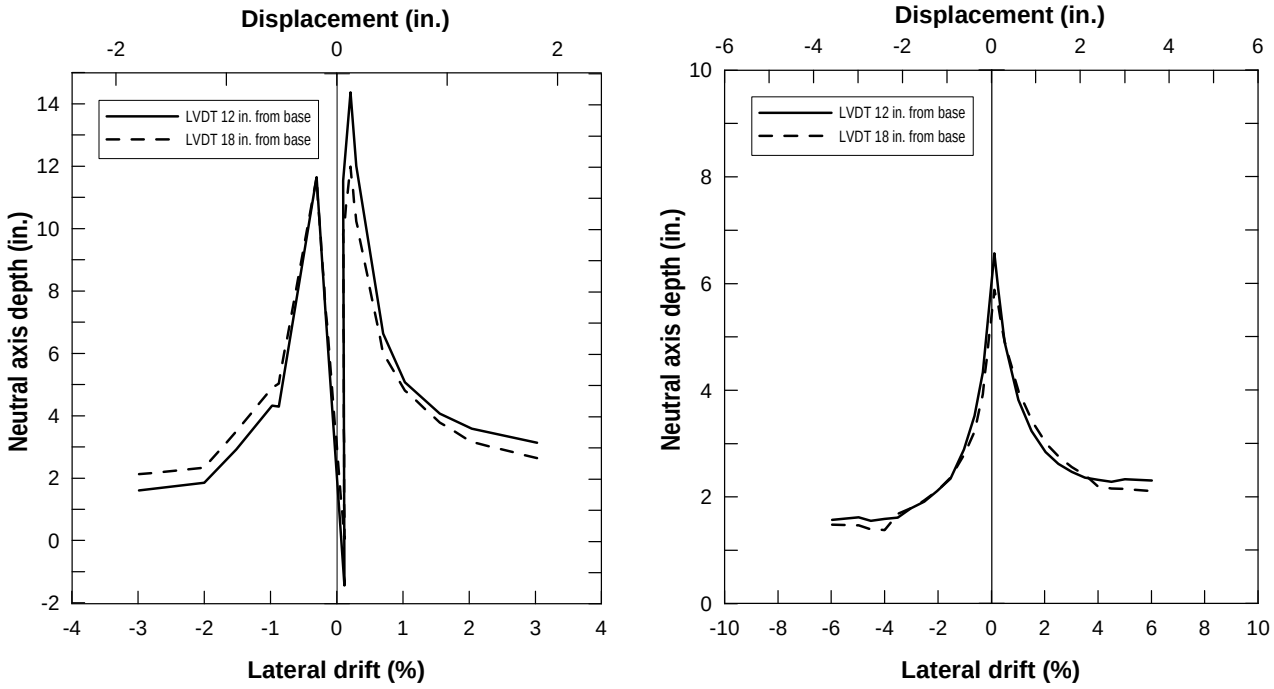

(a) UHPC-C2a N-A depth till 3 percent drift (b) UHPC-C2b N-A depth till 6 percent drift

Figure 3.29 Neutral axis depths versus lateral displacement calculated from LVDT data for UHPC-C2.

The neutral axis of the UHPC column was calculated using the data recorded by two sets of LVDTs mounted at 12 in. and 18 in as shown in Figure 3.5. Only the values at first peak drift were plotted as shown in Figure 3.29. The LVDT data measures initially during the force control cycles were inappropriate, which led to drastic variations and reached high values of neutral axis depth greater than the depth of the column (10 in.) in column 2a. From 1 percent drift onwards the data was appropriate and shows gradual variation. For both the

tests, the neutral axis depth reduced gradually with the lateral displacement and varied in-between 1.5 to 4 in.

3.4.2.8 Strain Data

Figure 3.30 and 3.31 shows the strain history envelope of two locations on the face of the column equal distance from the center of the column and located at extreme edges. Both these locations showed similar strain behavior. For the no-angle test the column shows negligible tensile strains at these locations similar to previous test, till 3% lateral displacement. For with-angle test, tensile strains up to 250 microstrains were recorded in the same locations for similar lateral displacement cyclic path. As the column resisted higher lateral loads due to the inclusion of energy dissipating steel angles in the connection.

Figure 3.32 and Figure 3.33 shows the strain history envelope of two locations on the face of the column equal distance from the center of the column and located close to the longitudinal axis of the column. Since the location was close to the center of the column, only compressive strains were observed with negligible tensile strains for the no-angle test. For with-angle test, tensile strains up to 400 microstrains were recorded in the same locations for similar lateral displacement cyclic path. As the column resisted higher lateral loads due to the inclusion of energy dissipating steel angles in the connection.

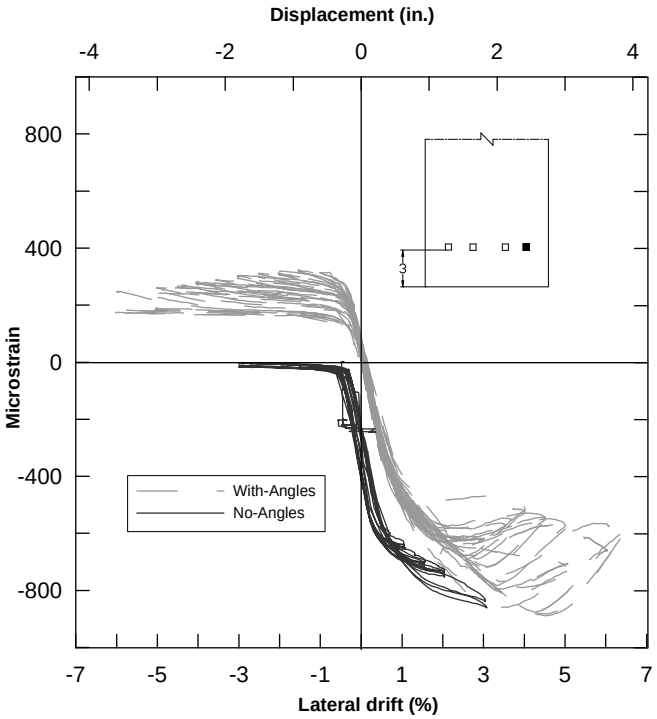

Figure 3.30 Strain histories obtained on the face of the column at 3 in. from the base.

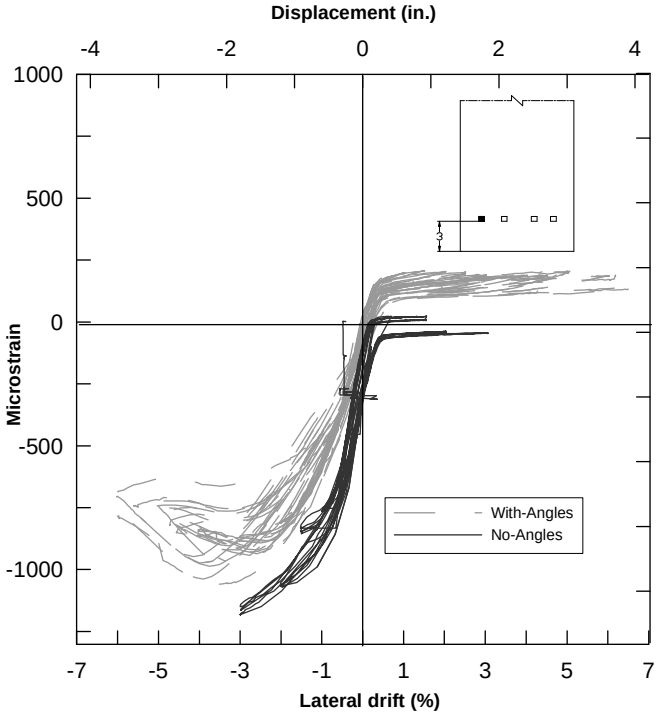

Figure 3.31 Strain histories obtained on the face of the column at 3 in. from the base.

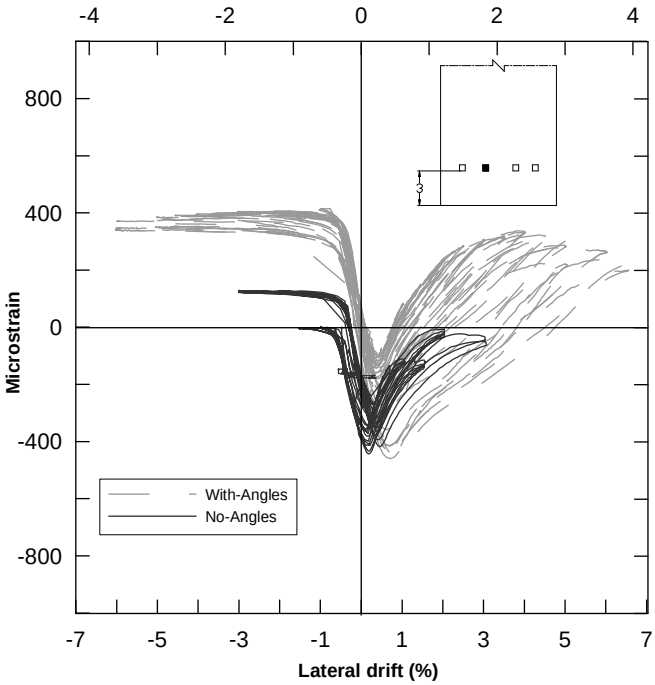

Figure 3.32 Strain histories obtained on the face of the column at 3 in. from the base.

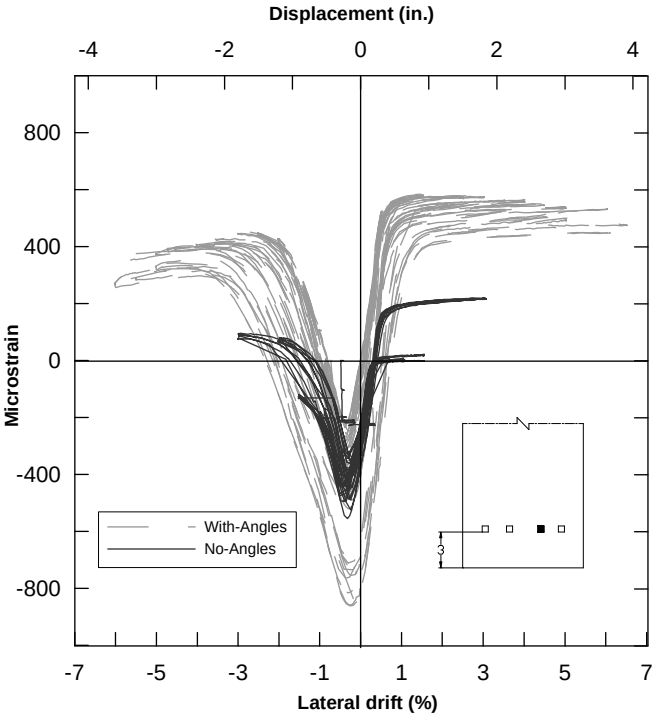

Figure 3.33 Strain histories obtained on the face of the column at 3 in. from the base.

3.4.3 UHPC-C3

Steel fiber reinforced grout performed better then the Hydrostone in compression and strain capacity, but it also failed by crushing when subjected to large displacements. For the third UHPC column test, a material with higher compressive strength and strain capacity had to be chosen. The stress strain property of Glass Fiber Reinforced Epoxy (GFRE) was satisfying the requirement to some extent and hence it was chosen. The preparation of GFRE pad was different compared to Hydrostone and the steel fiber grout, it had to be prepared separately and then placed below the column.

The pad measuring 0.4 in thick and cross section 10 in. x 6 in. was prepared in the laboratory using following materials: Epoxy resin, glass fiber sheets, 14 sq. in. wooden form and a squeegee. First a small amount of epoxy was poured in to the 14 sq. in. wooden form, enough to submerge one glass fiber sheet. Next a glass fiber sheet was placed on the epoxy and smeared using the squeegee till the sheet completely absorbed the epoxy resin, next a new sheet was submerged into the epoxy, with fibers running perpendicular to the previous sheet and it was again smeared using a squeegee. This process was continued until the required thickness was reached, which was around 0.4 in. In the end epoxy was poured on the surface and it was leveled for obtaining a flat surface using the squeegee. Two days later the pad was taken out of the form and the edges were cut off by 2 in. to get rid of the meniscus formation. Next the pad was cut to required size 10 in. x 6 in. and a 1.5 in. hole was drilled to make provision for the post-tensioning bar to pass through, and the pad was placed below the column and anchored to the foundation. No leveling of the column was required in this case because of the smooth leveled flat surface of the pad.

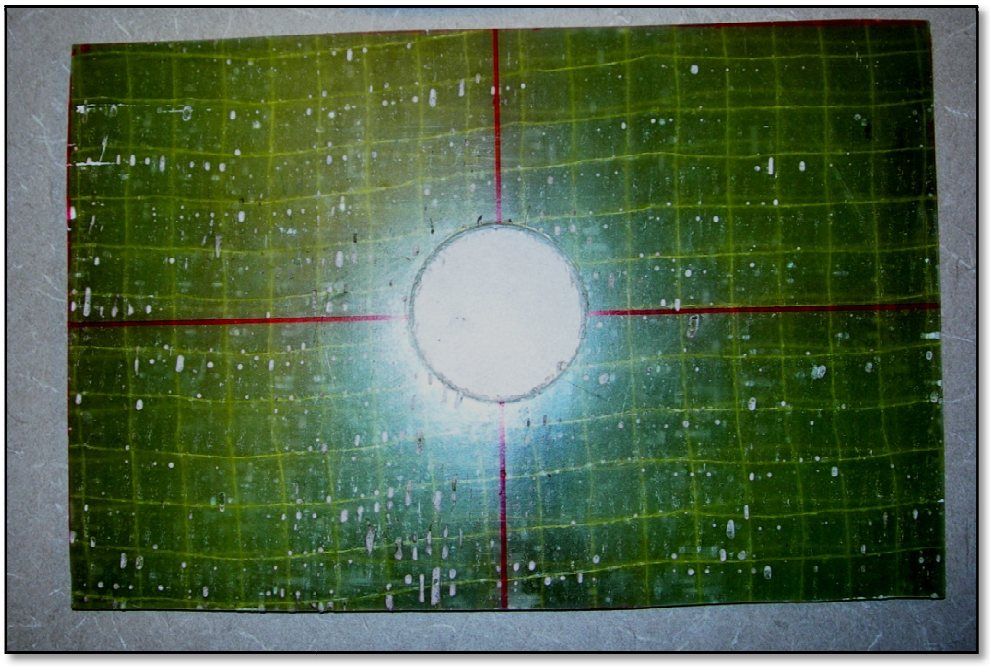

Figure 3.34 Glass Fiber Reinforced Epoxy pad used for Test UHPC-C3 measuring 10 in. x 6 in. and thickness 0.4 in.

3.4.3.2 Loading Protocol

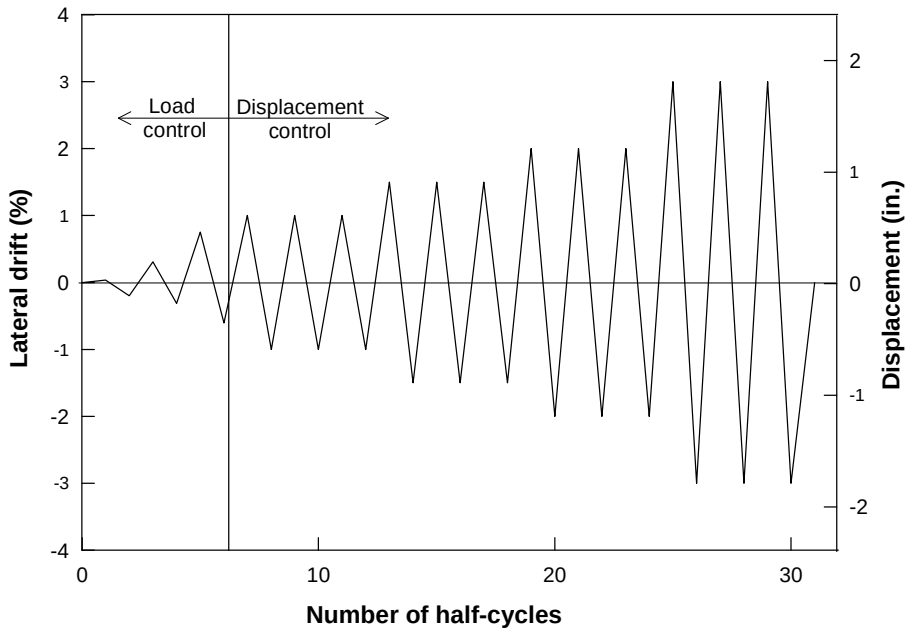

Figure 3.35 Load protocol used for UHPC column without angles (UHPC-C3a).

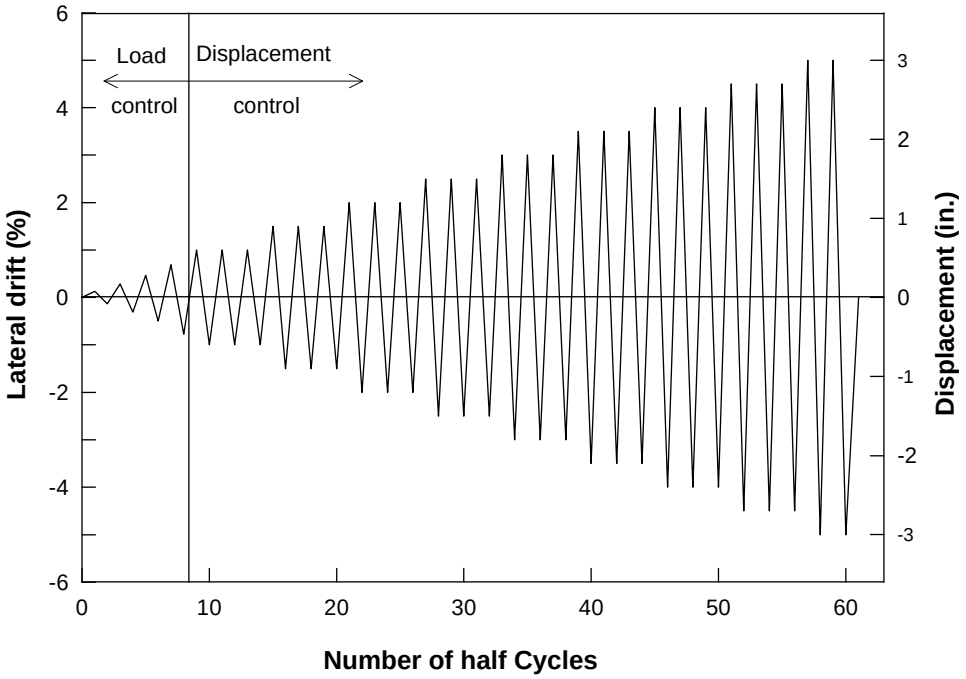

Figure 3.36 Load protocol used for UHPC column without angles (UHPC-C3b).

As shown in Table 3.1 the UHPC test-3 was divided in to two parts based on the presence of the dissipation material (steel angles). For the first part of the test UHPC-C2a, (no-angle test) the column UHPC-C3 was subjected to a smaller load path as shown in Figure 3.35. Next for the second part of the test UHPC-C2b (with angle test), the column was subjected to a longer load path as shown in Figure 3.36. Both will be explained in detail below.

For test UHPC-C3a, UHPC-C3 was subjected to a cyclic load path with full reversals as shown in Figure 3.35. The test was started under force control in the small displacement range and the following cycles were applied: ± 2 kips, ± 4 kips, ± 6 kips, and ± 7 kips. For ± 7 kips of loading, the column reached maximum lateral load drifts of about ± 1 percent (i.e., lateral displacement of ± 0.6 in.). From this point onwards, a displacement control was used for the test and UHPC-C1 was subjected to ± 0.5 percent drift increments with three cycles at each drift level. This test was continued only till 3 percent lateral drift to make sure there was not much damage to the pad, used again for the later part of the test and also enough data is available to verify the column analytical model for without angles.

For the UHPC-C3b, UHPC-C3 was subjected to a cyclic load path with full reversals as shown in Figure 3.36. The test was started under force control in the small displacement range and the following cycles were applied: ± 2 kips, ± 4 kips, ± 6 kips, ± 8 kips and ± 9.5 kips. For ± 9.5 kips of loading, the column reached maximum lateral load drifts of about ± 1 percent (i.e., lateral displacement of ± 0.6 in.). From this point onwards, a displacement control was used for the test and UHPC-C3 was subjected to ± 0.5% percent drift increments

with three cycles at each drift level. This was continued till 4.5 percent lateral drift and stopped after only two full cycles at 5 percent drift. The reason for ending the test was due to weld failure of the angle foundation connection and loss in the initial post-tension load by 23 percent.

3.4.3.3 Test Observation

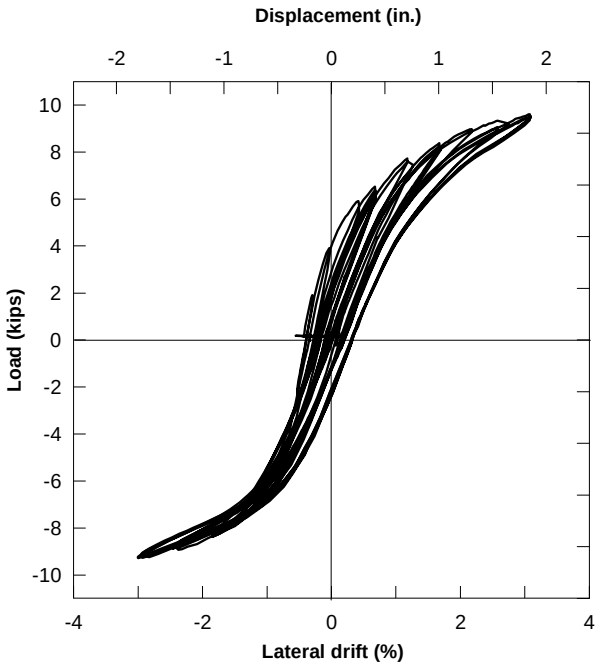

(a) UHPC-C3b reverse cyclic response

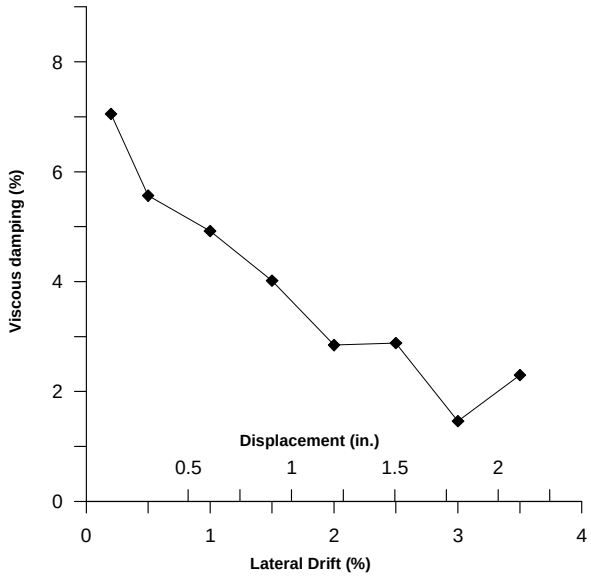

(b) Viscous damping

Figure 3.37 Force versus lateral displacement response of UHPC-C3a (no-angle) test and viscous damping in percentage for first peak lateral displacements.

With all the instruments ready to record data, the column was post-tensioned to 115 kips or a stress of 93.5 ksi. The Dywidag bar was anchored and the jack was released. At this stage, a seating loss of only 3 kips was encountered leaving an initial pre-stress of 112.1 kips. The column lateral load test was then followed showing the load protocol shown in the Figure 3.37.There was string extension problem encountered with the column lateral displacement measuring string potentiometer, which was fixed after completing 1.5 percent lateral drift cycles. This was the reason for the wider distribution of the force-displacement envelope at zero displacement as shown in Figure 3.37a. Except this there was no noticeable changes observed during this part of the test. The variation of viscous damping with increase in lateral displacement is also shown in Figure 3.37b.

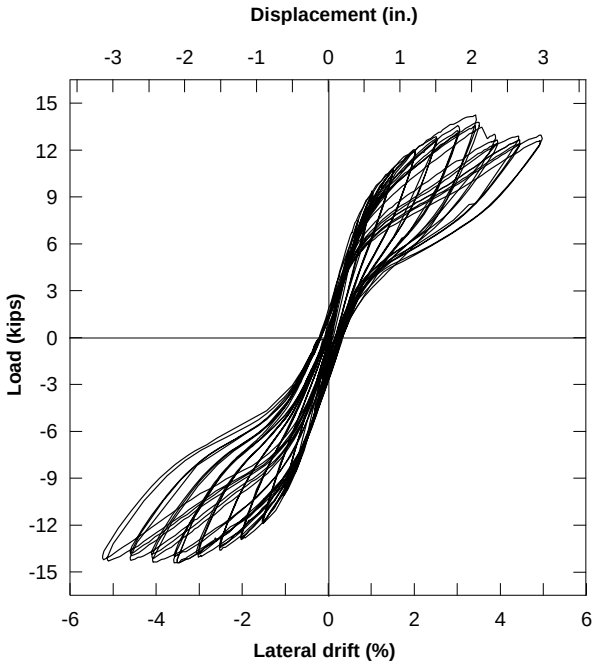

(a) UHPC-C3b reverse cyclic response

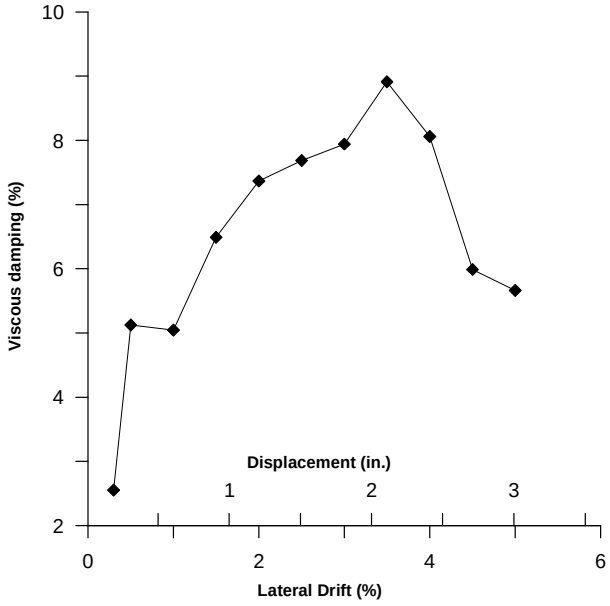

(b) Viscous damping

Figure 3.38 Force versus lateral displacement response of UHPC-C3b test and viscous damping in percentage for first peak lateral displacements.

For the second part of the test with angles the column was post-tensioned to 110.3 kips. The Dywidag bar was anchored and the jack was released. A seating loss of 0.3 kips was encountered, leaving an initial load of 110 kips. During the load control cycles no major changes were observed in the test. During displacement control cycles, a steady increase in the load was seen with displacement until last cycle of 3 percent lateral drift, at the end of first cycle of 3.5 percent lateral drift the load-displacement curve started to flatten as shown in Figure 3.38, due to the fracture development in the weld joint connecting the angle and foundation plate. The test was halted temporarily, the fractured weld was grinded off and the angle was re-welded to the foundation plate. The test was continued again from 3.5 percent drift and remaining two cycles were completed. Next during first half cycle of 4 percent lateral drift the angle on the east face failed in tension. This led to sudden drop in the load displacement curve in the first quadrant as shown in Figure 3.38a. The test was continued till the second cycle of 5 percent lateral drift and then had to be stopped due to failure of the weld connecting the angle and the foundation at the west face of the column. The variation of viscous damping with increase in lateral displacement is also shown in Figure 3.38b.

3.4.3.4 Post-tensioning Force

Figure 3.39 shows the variation of post-tension load with lateral displacement for UHPC-C3a. There was not much post-tension load loss compared to the previous two tests. Only 6 percent loss was recorded in the initial post-tension load at the end of the test.Figure 3.40 shows the variation of post-tension load with lateral displacement for UHPC-C3b. Similar to the previous UHPC column test with angle (UHPC-C2b) the loss in the initial post-tension load was very low (2.5 percent) till the 3 percent lateral drift, from 3.5 percent onwards the post-tension load loss was steady and proportional to the increase in the lateral displacement. The loss in the post-tensioning load may be due to both compression of the pad and anchorage slip loss of the Dywidag bar.

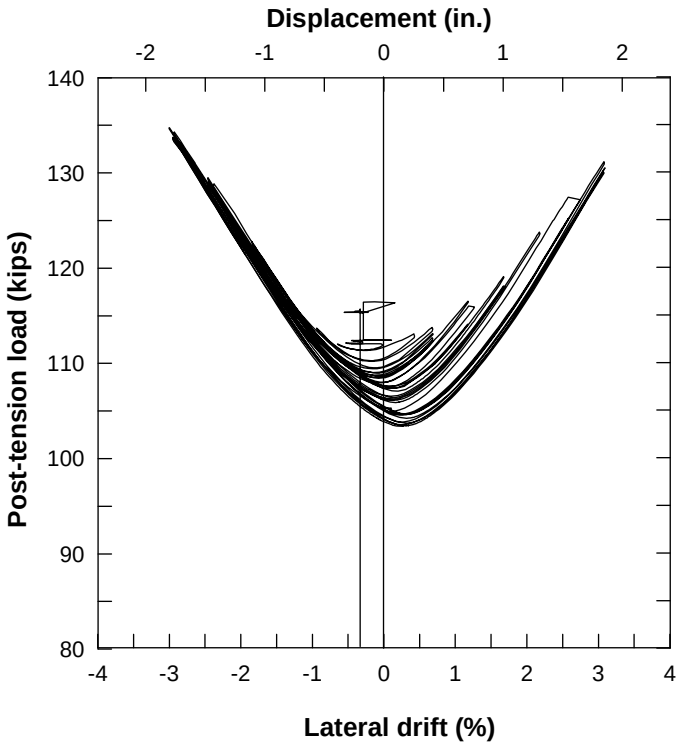

Figure 3.39 Post-tension load variations with lateral displacement of UHPC-C3a.

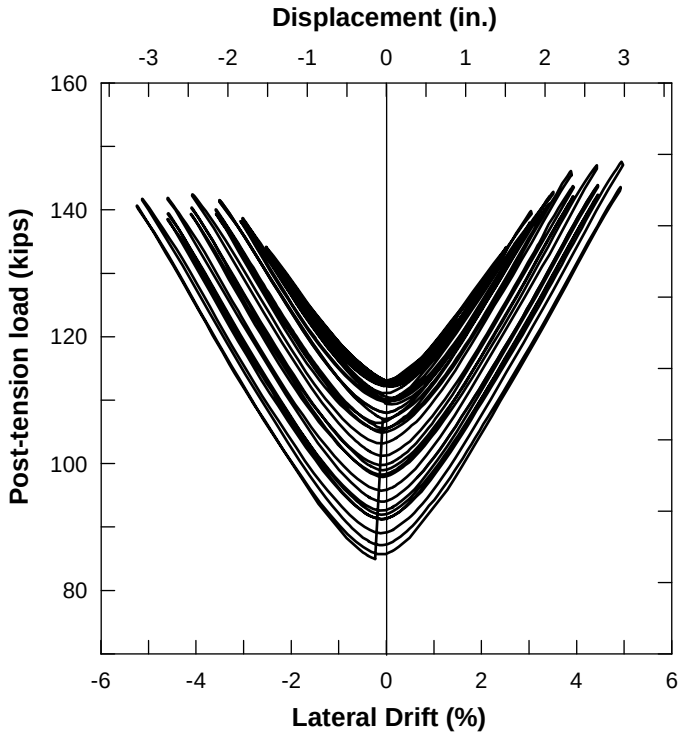

Figure 3.40 Post-tension load variations with lateral displacement of UHPC-C3b test.

3.4.2.5 Force-Displacement Response

Monotonic force displacement responses for both no-angle and with-angle test are shown in Figure 3.41. The Glass fiber reinforced pad showed no difference in the initial stiffness when re-tested with steel angles. This indicates the resilient strain capacity of the material.

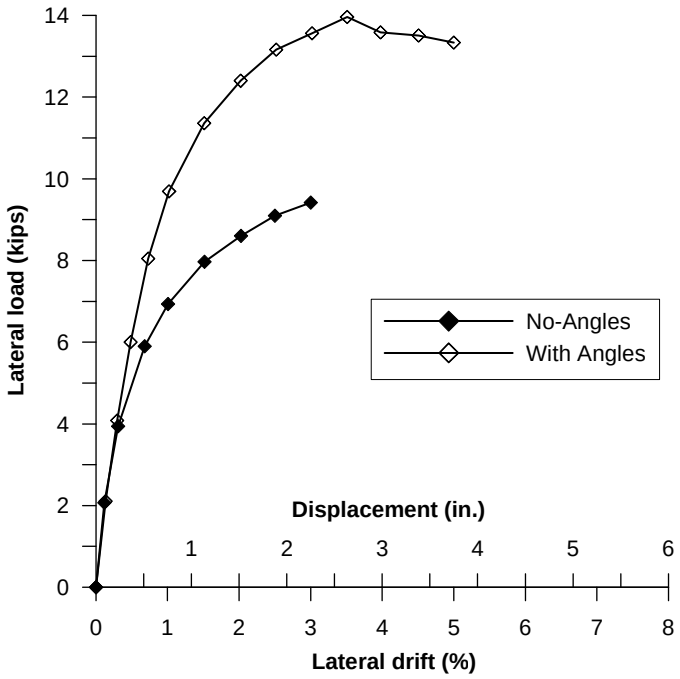

Figure 3.41 Monotonic force versus lateral displacement response of UHPC-C3.

3.4.3.6 Tilt Meter Reading

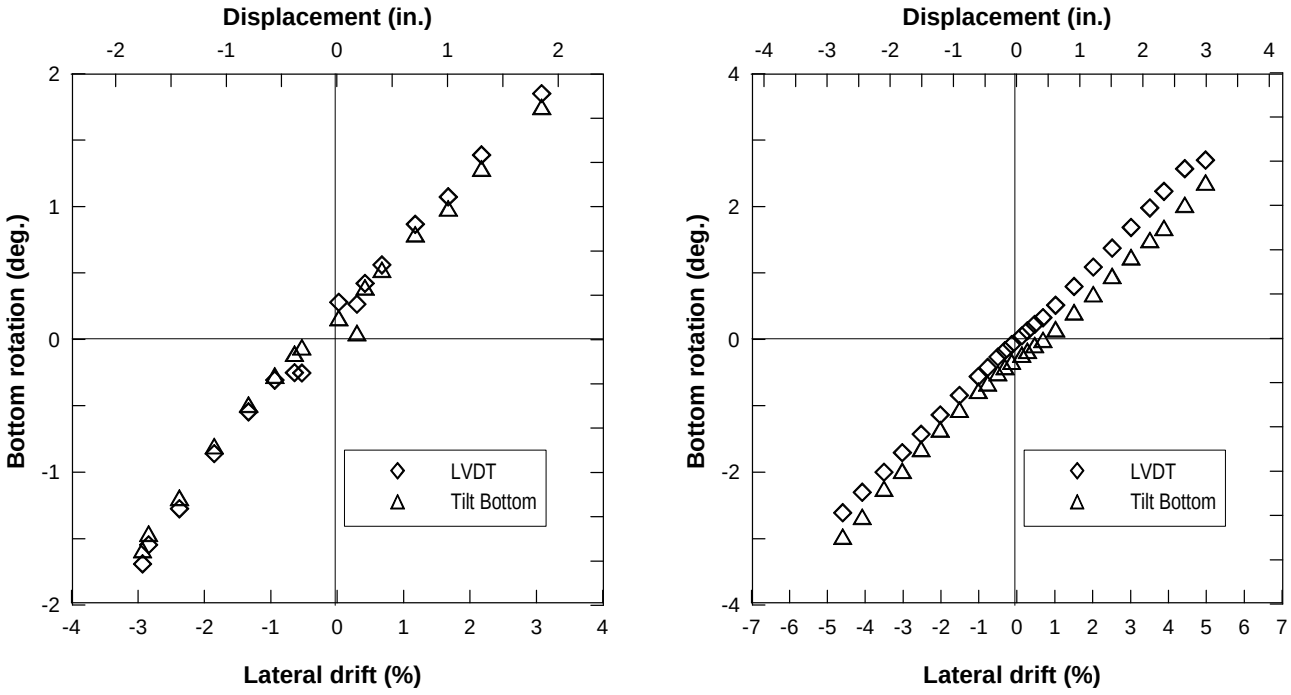

(a) UHPC-C2a rotation till 3 percent drift (b) UHPC-C2b rotation till 6 percent drift

Figure 3.42 UHPC-C2 Bottom rotations versus lateral displacement calculated from Tilt meter reading and LVDT data.

The bottom rotation of the UHPC column was measured using tilt meter, mounted at 2 in. height from column base and calculated using a set of two LVDTs mounted at 12 in. height from the column base as shown in Figure 3.25. Only the rotation at first peak lateral drift was plotted. For both the tests with and without angle, the data obtained from both the instruments match well showing a linear variation.

3.4.3.7 Neutral Axis Depth

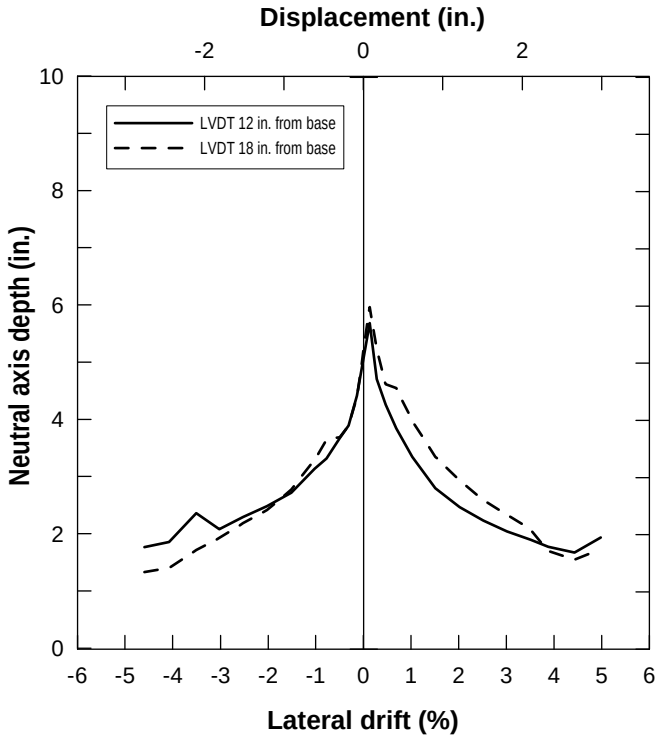

Figure 3.43 Neutral axis depths versus lateral displacement calculated from LVDT data for UHPC-C2.

The neutral axis of the UHPC-C3 column was calculated using the data recorded by two sets of LVDTs mounted at 12 in. and 18 in as shown in Figure 3.25. For the no-angle test the LVDT data was inappropriate hence it is not shown. Only the values at first peak drift were plotted as shown in Figure 3.38. From 1 percent drift onwards the neutral axis data was appropriate and shows gradual variation with increase in lateral drift. At the end of the test the neutral axis reaches 2 in. The decrease in neutral axis depth to such low value with increase in displacement was due to regular loss in the post-tensioning force.

3.4.3.8 Strain Data

Figure 3.44 shows the strain history envelope for one of the locations on the face of the column, close to the longitudinal axis of the column. The strain history envelope at the same position for previous other tests were entirely different, they showed tensile strains during both the positive and negative cycle displacements this may be due to the change in pad stiffness property. Glass fiber epoxy is less stiff compared to both the previous materials. The strain envelope shows negligible tensile strains, but the compressive strains are very high especially for the second part of the test. The loss in post-tensioning load was less in these two tests which is one of the reasons for high compression strains.

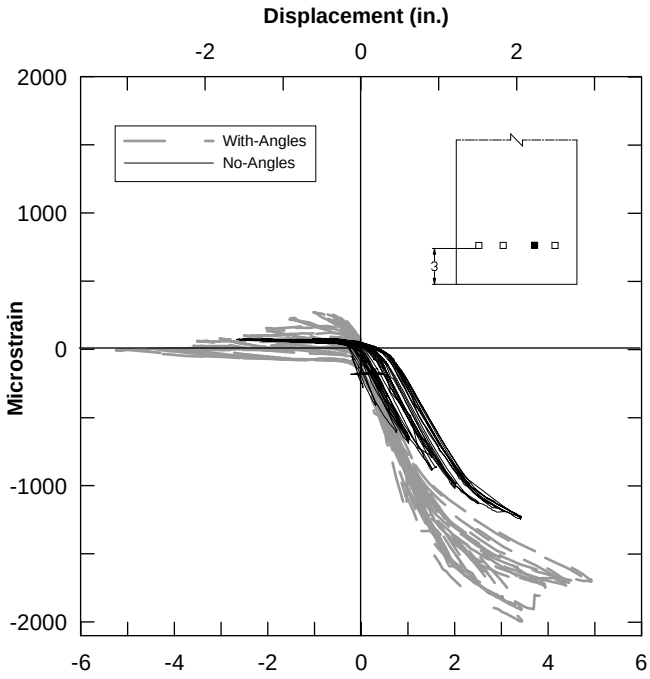

Figure 3.44 Strain histories obtained on the face of the column at 3 in. from the base.

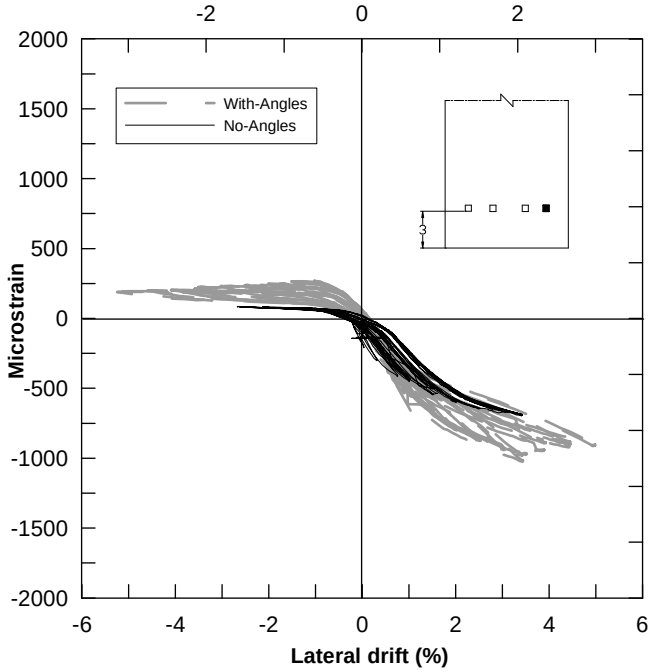

Figure 3.45 Strain histories obtained on the face of the column at 3 in. from the base.

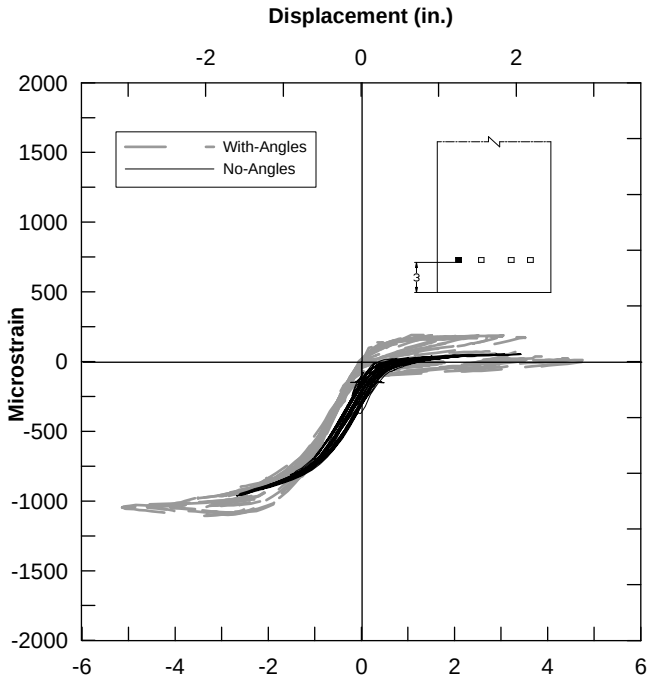

Figure 3.46 Strain histories obtained on the face of the column at 3 in. from the base.

Figure 3.45 and 3.46 shows the strain history envelope of two locations on the face of the column, at equal distance from the longitudinal axis of the column and located at extreme edges. Both these locations showed similar strain behavior. For the no-angle test till the 3 percent lateral drift the column showed very low positive tensile strains, but for the with-angle test tensile strains show noticeable increase to 250 microstrains due to large column lateral drifts and more resistance at the base due to the steel angles. Compression strains is reduced by half when compare to the previous strain history envelopes (Figure 3.44) due to the position being closer to the edges.

CHAPTER - 4 ANALYTICAL MODELING

4.1 Introduction

A Finite element models was developed in ANSYS for analyzing the behavior of the UHPC column and characterize the behavior under monotonic loading. The model was first used to predict the behavior of the columns prior to the test and later modified to improve their response based on the experimental observation. In this chapter an introduction to different elements used in the model is first summarized, followed by the UHPC column model is presented. Then, the pre-test analysis results of the FEM models are discussed. Finally, the post-test analysis results are presented for each test together with comparison of critical experimental and analytical results.

ANSYS [21] is general purpose finite element software that is suitable for analyzing linear and non-linear structures under static, dynamic, creep and thermal loading. The ANSYS program library has a number of elements that can be used to model structures with complex geometry as well as linear and nonlinear material behavior in both 2-D and 3-D forms. It has a Graphical User Interface for creating structural models, selecting material models, defining the appropriate properties, applying boundary conditions, run the model and performing analysis using the pre-processing option and viewing the recorded analysis results in a required format using the post-processor.

4.2 Chosen Elements

A two-dimensional (2-D) model was preferred for the UHPC test columns because there was not much variation expected in strains along the Z-axis and all the required properties in the XY plane could be adequately captured using this model**.** The finite element model of the UHPC columns was developed using 2-D solid elements and the thickness option available for this element was used for specifying the measurement in the third dimension. Similarly, angles and plates used for the column were modeled using 2D solid elements, with the thickness of the element defining the width along the Z-axis. For modeling the post-tensioning bar, one dimensional link element was used; the other two dimensions were included by accurately defining the cross sectional area for the Link element. The entire model was developed using the direct generation of nodes and elements method available in ANSYS so that the analysis could be executed efficiently. The different elements used in the UHPC column model are listed in Table 4.1 and more descriptions for each element are provided below.

Table 4.1 A Summary of different elements used for developing the model for the UHPC columns.

Element Type	Structural Members
2-D solid 4 node element with a defined thickness	Column, steel plates, and steel angles
1-D link element with a defined cross-section area	Post-tensioning bar
1-D combination element	Contact region between pad and foundation plate

4.2.1 Plane-42

Plane-42 [22] element was used to model column, pad, steel plates and steel angles. This element is defined by four nodes, with each node having two degrees of freedom (i.e., translation in X and Y directions). The Plane-42 element was used as a plane element with its thickness assigned in the Z-axis. This element has plasticity, creep, swelling, stress stiffening, large deflection, and large strain capabilities. The element input data includes location of the four nodes, thickness and orthotropic material properties. Loads can be applied directly on the nodes and/or as surface loads by defining an appropriate pressure.

4.2.2 Link-1

Link-1 [22] element has a wide variety of use and can be modeled as a truss, a spring or a link element depending upon the requirement. This is a uniaxial tension/compression element defined by two nodes, each having two degree of freedom (i.e., translation in X and Y directions), but no bending is permitted. Link-1 is incorporated by providing the locations of the two nodes, cross-sectional area, an initial strain and the relevant material properties. The initial strain in the element was given by Δ/L, where Δ is the change in length, and L is the original length of the element. This element was used to model the post-tensioned bar with the appropriate initial prestress.

4.2.3 Combine-39

Combine-39 [22] is a unidirectional element with generalized force-displacement capability, which can be used in any analysis. The element can be modeled as a longitudinal element or torsion element in 1-D, 2-D or 3-D. The element was used in this structure as a

longitudinal element, but no bending or torsion was considered. This element is defined by two nodes, each having three degrees of freedom (i.e., translation in X, Y and Z direction). A generalized force versus deflection curve is assigned to the element by defining data points (D1, F1), (D2, F2)…(Dn, Fn), where F represents the force and D represents the displacement in the longitudinal direction. For the element in the longitudinal direction, the uniaxial tension/compression behavior was defined using a force displacement curve, It is necessary that the force-displacement curve should be defined from third quadrant (i.e., compression) to the first quadrant (i.e., tension). If the element has no compressive resistance, the force-deflection curve does not need to be extended to the third quadrant.

4.3 Modeling

Modeling of different materials used in the experimental test apparatus is presented in this section.

4.3.1 Column

As-built dimensions of the UHPC column (10 in. height x 65 in. width) were used to define the geometry of the column in the analytical model, using 2-D Plane-42 elements. As-built column thickness of 6 in. was used to define the thickness of Plane-42 elements. A mesh size of 0.5 in. x 0.5 in. was used for the column, except at the side edges where a mesh size of 0.25 in. x 0.5 in. was used. The mesh dimension was controlled by the need to accommodate the steel studs and the steel side plates. Apart from these constraints, a small mesh size was preferred so that the nonlinear effects of the critical regions such as angle to

column joint region, pad contact regions and shear studs to column contact regions could be captured accurately.

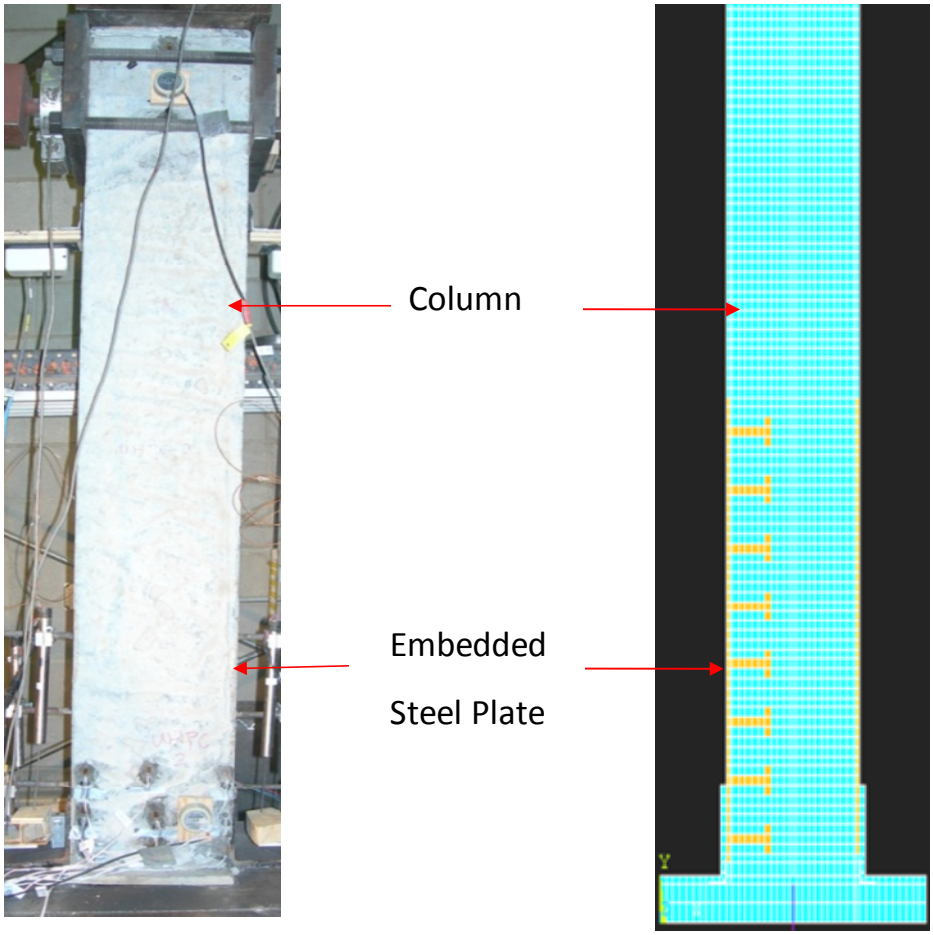

Figure 4.1 Comparing a test column with the ANSYS model.

The embedded side plates on either side of the column were also modeled with as built dimensions of 0.25 in. x 20 in. x 6 inches. For the shear studs an equivalent area to volume method was used, as there were two studs in each row on the steel plate. A single equivalent

stud element was modeled at each row having the volume and shear area of two studs as shown in Figure 4.1.

The column was modeled using two different elements one with UHPC compression characteristics curve shown in Figure 4.7 and other with UHPC tension characteristic curve shown in Figure 4.8. From the experimental results presented in Chapter-3 and analytical trials, the neutral axis of the column was calculated to lie within 4 in. from the rocking edge of the column. Hence, the compression elements were used to model only for the 4 in. width of the column on the compression side along the entire column height. The remaining 6 in. width was modeled using tension elements as shown in Figure 4.2. The approach was necessary because two different stress-strain responses could not be modeled for a single element in ANSYS.

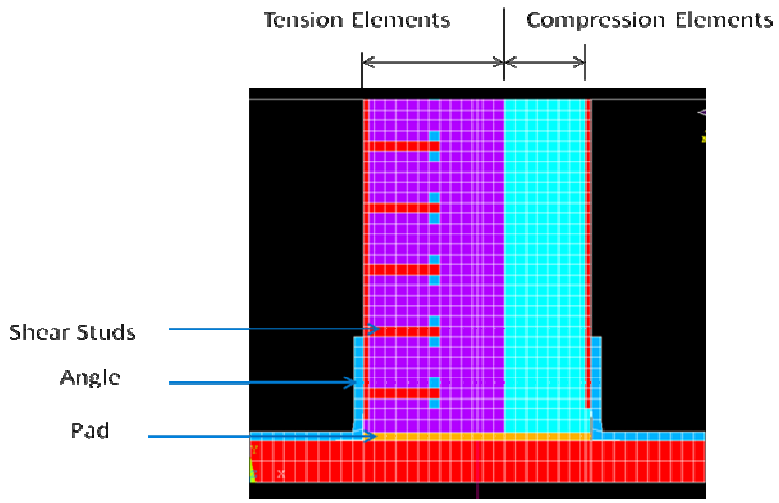

Figure 4.2 Finite element model of column showing locations of UHPC compression and tension elements.

4.3.2 Post-Tensioning Bar

The post-tension bar was modeled using one-dimensional link elements. The nominal cross-sectional area of the chosen 1.25 in. diameter Dywidag bar is 1.23 in^2. This area and as-built unbonded length of (9 ft) of the prestressing bar were used to define the area and length of the link element. An appropriate initial strain was assigned to the link element to simulate the effects of initial prestress. To ensure the curvature of the post-tensioning bar is the same as that of the column edge during lateral load, nodes of the link elements at every 3 in. were constricted in X-direction to the adjacent nodes of the column elements. At the top end the link element node was connected to the steel plate measuring 5 in. from column top surface. At The bottom end, the link element node was constrained (fixed) 24 in. below the column base, following the test setup details.

4.3.3 Plates

In the experimental setup, a 2.5 in. thick load cell and 1 in. thick base plate were placed on the top of column. Above that a 1.5 in. thick anchor plate and bell nut were used to anchor the post-tensioning bar as shown in Figure 4.3. The load cell and steel plates were modeled as a single 5 in.-thick plate as shown in Figure 4.3. The plate was modeled using Plane-42 element with the A-36 steel properties. The mesh size used for the steel was identical to that used for the column (typical element size: 0.5 in. x 0.5 in.) to facilitate continuity and easy connection between elements. The column was resting on a foundation base plate measuring 20 in. x 20 in. x 2 in. This plate was modeled with the same dimension using Plane-42

element and having A-36 steel properties. A mesh size of 0.5 in. x 1 in. was used for maintaining continuity and easy connection to the column elements.

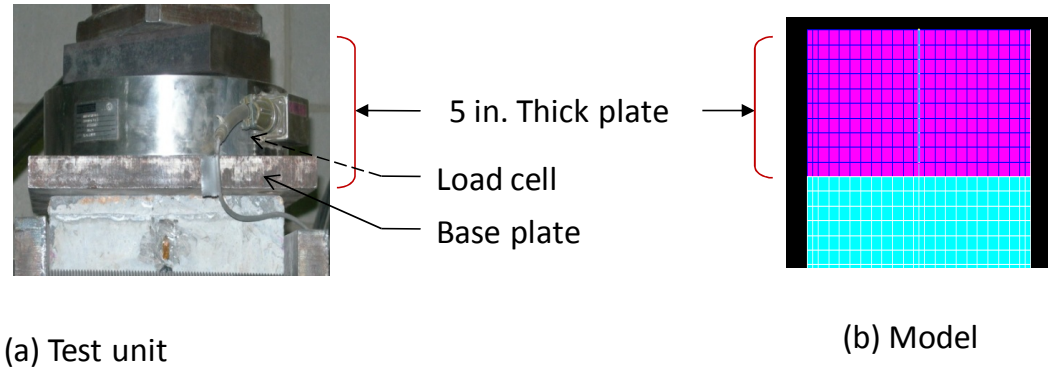

Figure 4.3 Modeling of plates and load cell placed above the column.

4.3.4 Angles

The steel angle chosen for the experimental investigation had a thickness of 0.375 inch, the length of the leg connecting the angle to the column was 5 in. and the length of leg connecting to the base plate was 4.625 inches. The steel angle was modeled using Plane-42 elements with A36 steel properties. A mesh size of 0.325 in. x 0.5 in. was used so that the angle could be easily connected to the column side plates as shown in Figure 4.4 the out-of-plane dimension of the angle was defined using the thickness option. The length of welds connecting the angle to base plate and the column side plates, were modeled by constraining the appropriate nodes. In the experimental investigation the weld length connecting angles to column side plate was 9 in. and the weld length connecting angle to base plate was 8.25 in. and the same was followed in the model.

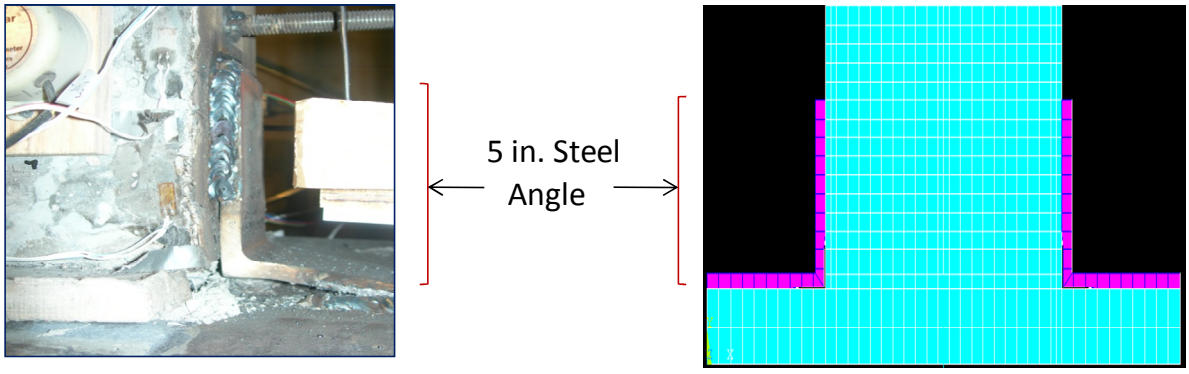

(a) Test unit (b) Model

Figure 4.4 Energy dissipating externally connected angles used in the test and analysis model.

4.3.5 Interface Material

The interface material placed between the column and the foundation to ensure continuity was modeled using Plane-42 elements. The cross-sectional dimension of the interface pad was identical to that of the column with a thickness of 0.5 in. or 0.4 in. depending on the test. As with the column, a mesh size of 0.5 in. x 0.5 in. was used to model the interface so that the top nodes of the pad would be connected to the column at the top and base plate at the bottom through the combination element as shown in Figure 4.5.

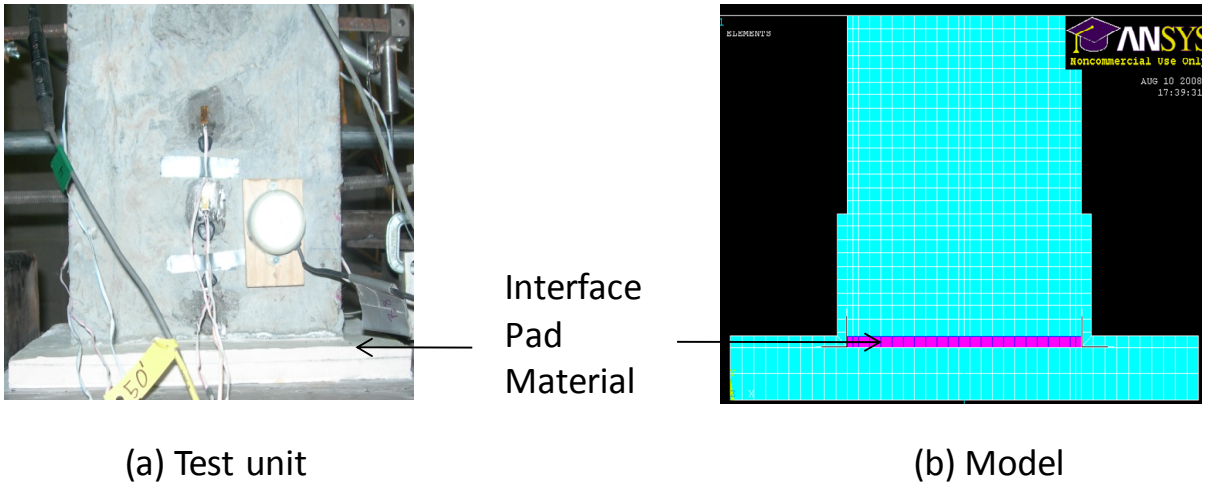

Figure 4.5 Pad used in the test and modeled pad.

4.3.6 Combination Element

The Combin-39 element was used as a zero-length unidirectional element in the UHPC column model with a non-linear force-deflection behavior. This element was used in two places in the model: first as an interface element to connect the pad to the foundation base plate and second as a gap element to connect the angle and the base plate on the compressive face of the column. Between the column and the base plate combin-39 element was modeled as a one-dimensional zero length spring element. As discussed in section 4.2.3 before the element behaves according to input values of force-displacement curve, with the compression response as defined in the third quadrant and tension response as defined in the first quadrant. In the third quadrant (or compression) very large force values were assigned for negligible displacement values of the element for complete transfer of compressive load through the interface material to the steel plate whereas in the first (or tension) quadrant negligible force

resistance was assigned for very large displacement to ensure zero tension resistance in the unidirectional element. The sliding possibility of the column with respect to foundation was prevented by restraining the zero length elements in the x direction.

For the angle connected at the compression side of the column, there was a small gap between the angle and the base plate formed after welding of the angles as shown in the Figure 4.6. The angle was found to establish contact with the base plate by closing the 0.05 in. gap only after the column reached a lateral displacement of about 1 in. at the top as shown in Figure 4.7. A Combin-39 element was used to connect the angle and base plate. The force-displacement values were defined in the post-test model such that the angles come in contact with the base plate at column lateral displacement of 1 in., at which point compressive force is permitted transfer on to the base plate.

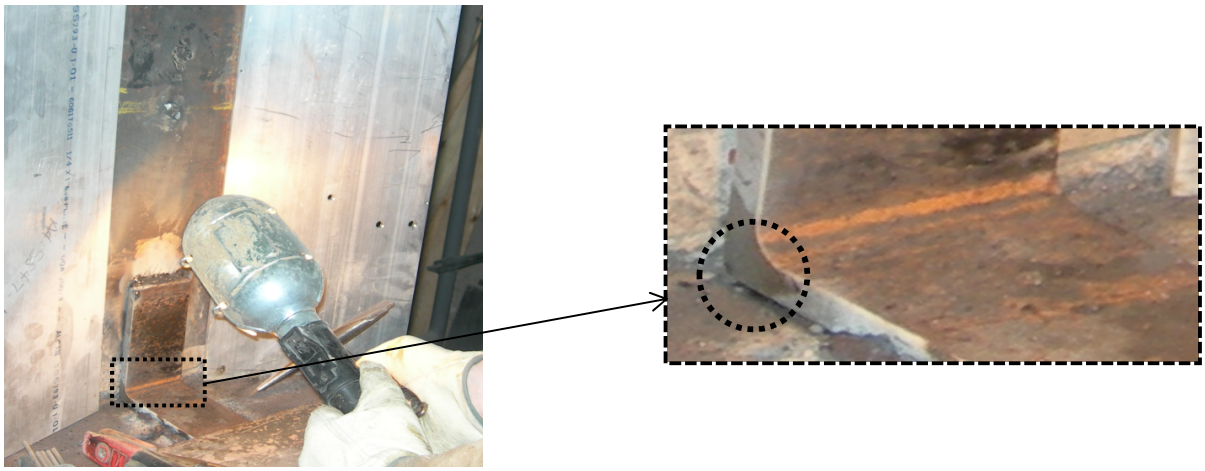

Figure 4.6 Gap formed in the bottom corner of angle after welding is completed.

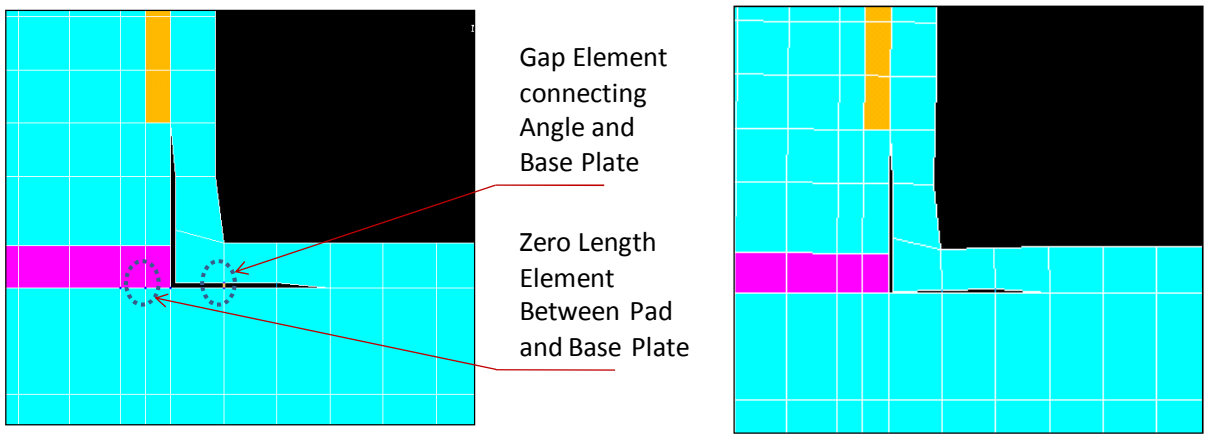

(a) Gap at zero column lateral displacement

(a) Gap at 1 in. column lateral displacement

Figure 4.7 Location and behavior of the Combin-39 element in the analysis model.

4.3.7 Coupling

The coupling [22] command may be used to define, modify, delete, list, or generate coupling between different degrees of freedom (DOFs) for the element in the structural model. One or all DOFs of a set of nodes may be coupled. Each set contains a master node and one or more slave nodes. One or more degrees of freedom of the master node can be coupled with that of slave nodes. Once coupled, the displacement of the coupled degrees of freedoms of slave nodes will be the same as that of the degree of freedom of the master node. The link element was coupled to the column longitudinal edge at every 3 in. length to follow its bending profile during the lateral displacement of the column.

4.4 MATERIAL PROPERTIES

Presented in this section are the stress-strain responses of materials used for the element in the finite element model. All materials responses were modeled using piece–wise linear curves as this approach was considered to be simple and sufficiently accurate.

4.4.1 UHPC Compression

Typical Compressive stress-strain curve of a UHPC cylinder is shown in the Figure 4.8a. This stress-strain curve is based on tests conducted by Acker and Behloul (2004) on UHPC cylinders. The post-peak stress is clearly visible in the figure as discussed in section 2.2.4 (under strain limits).For comparison of the compressive strength the stress-strain behavior of normal concrete is also shown. The actual stress-strain curve was idealized to a multi-linear stress-strain curve as shown in Figure 4.8b for analysis simplicity and to be sufficiently accurate.

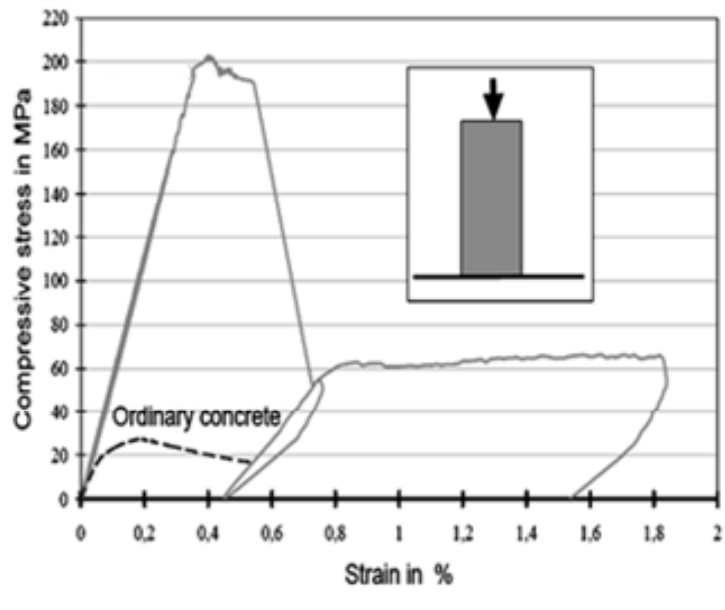

(a) Compressive stress-strain curve chosen for UHPC column [23]

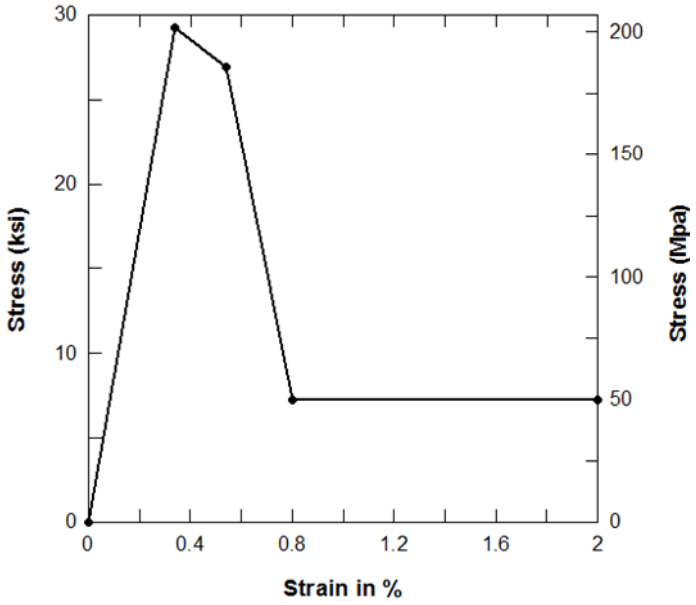

(b) Idealized UHPC stress-strain curve as used in the model

Figure 4.8 Actual and idealized UHPC compression stress-strain curves.

4.4.2 UHPC Tension

Typical tensile stress-strain behavior of UHPC is shown in Figure 4.9a. This multi-linear stress-strain behavior was based on tests conducted by Bristow and Sritharan (to be published) using dog-bone shaped UHPC specimens. The tensile stress-strain behavior of UHPC can also be represented in the form of equations. Equations 1 to 4 was developed by Bristow and Sritharan with recommended variables values.

$$f_t = E_c \times \boldsymbol{\varepsilon} \quad for\ \boldsymbol{\varepsilon} \leq {f'_{te}}/{E_c} \tag{1}$$

$$f_t = f'_{te} + \frac{\left(f'_{t,MAX} - f'_{te}\right)(\varepsilon - f'_{te}/E_c)}{0.00125} \quad for \frac{f'_{te}}{E_c} < \varepsilon \leq 0.0014 \tag{2}$$

$$f_t = f'_{t,MAX} \quad for\ 0.0014 < \varepsilon \leq 0.0024$$

$$f_t = f'_{t,MAX} - 0.672 \cdot \ln(\varepsilon) - 4.062 \quad for\ \varepsilon > 0.0024\ until\ f_t\ reaches\ 0\ ksi \tag{3}$$

$$where:\ f_t = tensile\ stress$$

$$E_c = elastic\ modulus\ of\ UHPC\ in\ compression\ and\ tension\ (8000ksi)$$

$$\varepsilon = tensile\ strain\ (ksi)$$

$$f'_{te} = elastic\ tensile\ strength\ (1.3\ ksi)$$

$$f'_{t,MAX} = maximum\ tensile\ strength\ (1.7\ ksi)$$

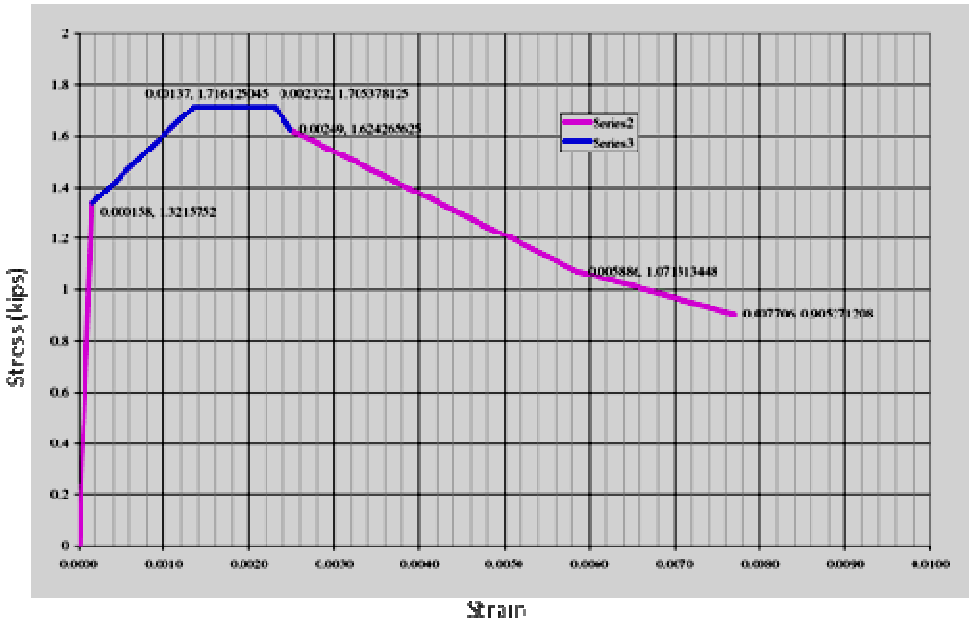

(a) Tensile stress-strain curve chosen for UHPC [24].

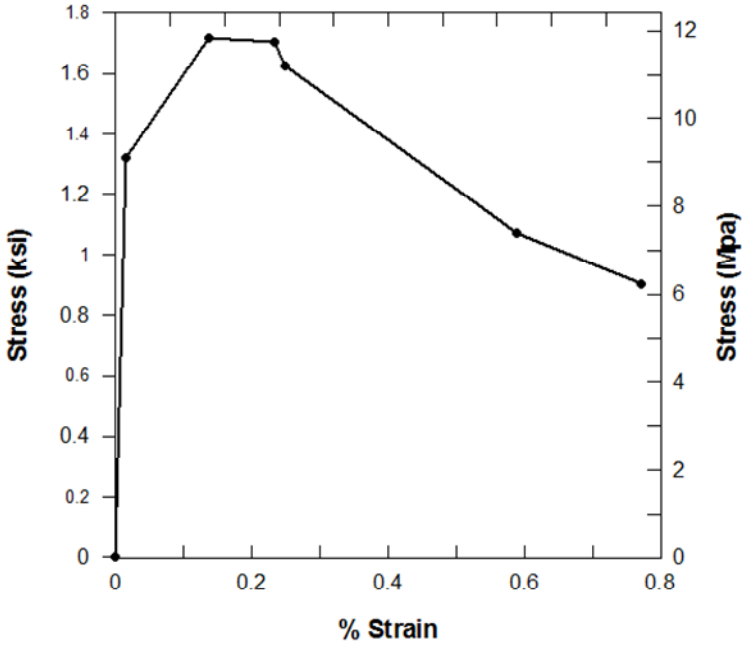

(b) Idealized stress-strain curve as represented in the model.

Figure 4.9 Actual and idealized UHPC tensile stress-strain curve.

4.4.3 A36 Steel

Typical stress-stain curve of A36 carbon steel is shown in Figure 4.10 a. All the steel plates and external connection angles used in the experimental test were made of A36 carbon steel. The actual stress-strain curve was idealized to a multi-linear stress-strain curve as shown in Figure 4.10b for analysis simplicity and to be sufficiently accurate.

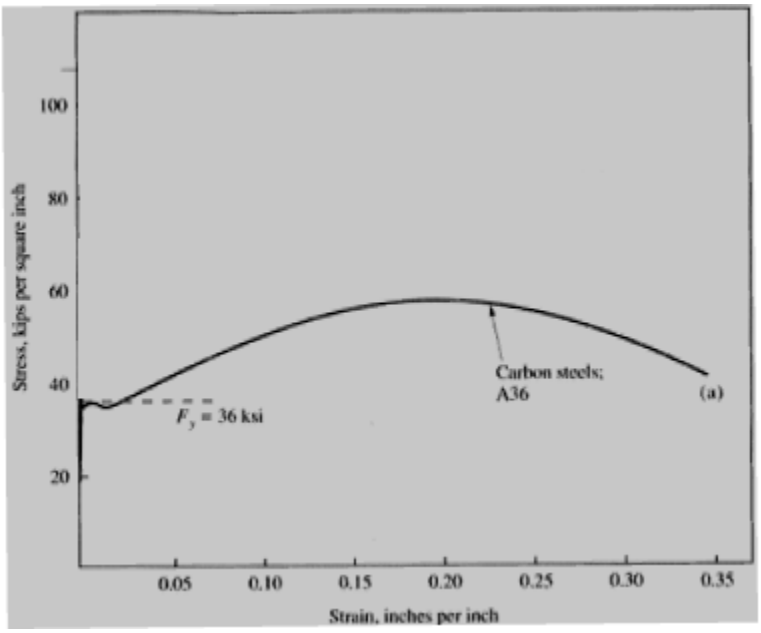

(a) Chosen A-36 Steel stress-strain curve [25]

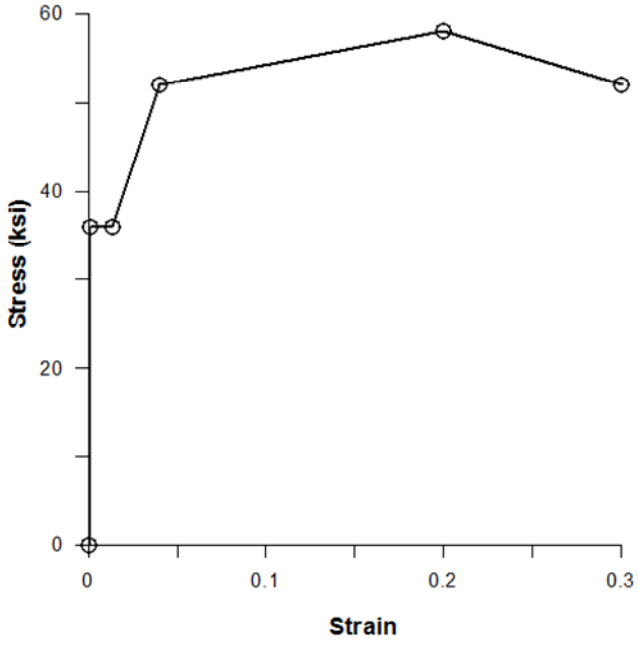

(b) Idealized stress-strain curve as represented in the model

Figure 4.10 Actual and Idealized A36 steel stress-strain curves.

4.4.4 Post-Tensioning Bar

Typical stress-strain curve of 160 grade alloy bar is shown in Figure in 4.11a. 160 Grade Dywidag bar was used for post-tensioning the UHPC column in all the experiments. The bar size and grade were chosen based on its yield strength so that the bar remained in its elastic range for a column lateral displacement of 5-6%. The actual stress-strain curve was idealized to a multi-linear stress-strain curve as shown in Figure 4.11b for analysis simplicity and to be sufficiently accurate.

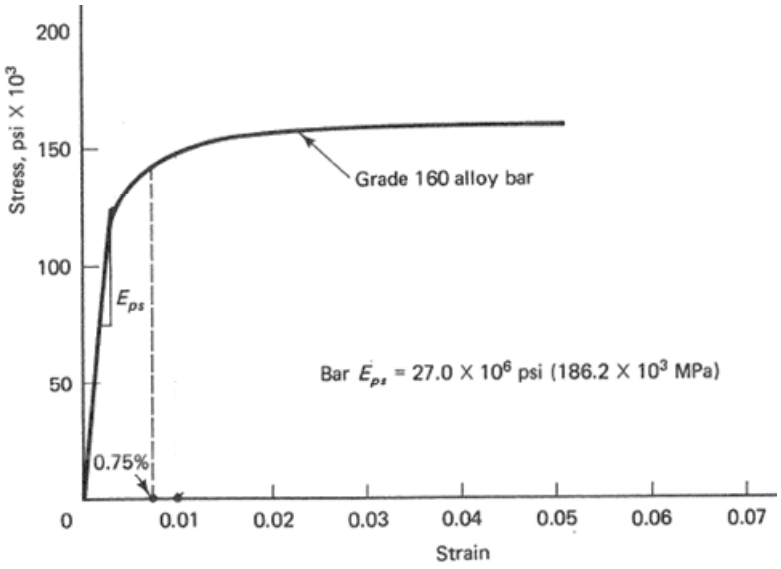

(a) Chosen Prestress Bar stress-strain curve [26]

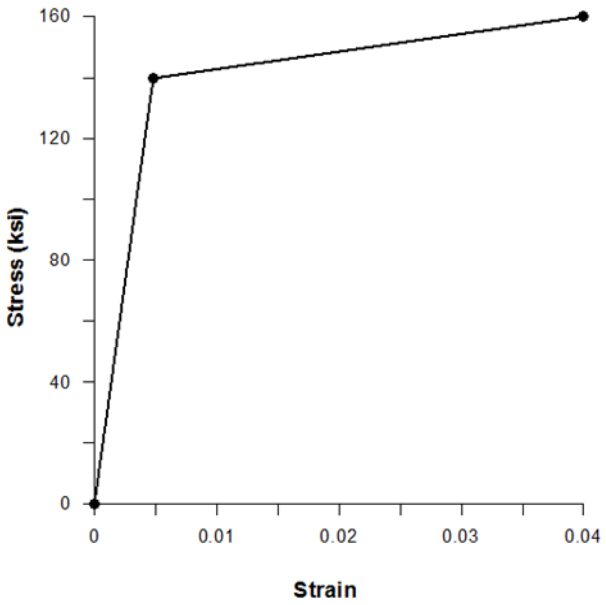

(b) Idealized stress-strain curve as represented in the model

Figure 4.11 Actual and Idealized Stress-strain curves of Post-tensioning Dywidag bar.

4.5 Pre-Test Analysis

Prior to the column tests in the laboratory, the finite element model was used to predict the monotonic lateral load behavior of the UHPC columns. All material properties for the analysis were available except for the interface pad materials. A simple stress versus strain behavior was assumed for the pad behavior as shown in Figure 4.11 which was based on the required properties of the pad like high strain capability and resilience property. Accordingly, as shown in Figure 4.12 the interface pad behavior was assumed to be elastic – perfectly plastic material with elastic limit at a stress of 10 ksi with a corresponding strain of 0.002. Within the elastic strain of the pad (stain < 0.002), when unloaded the pad returns to its original un-deformed shape, but beyond this point (stain > 0.002) the material will behave as a perfectly plastic material and there will be permanent residual strain developed in the pad.

The material models defined in the previous section and the assumed pad behavior, displacement control analysis were conducted. Three different cases were considered: With no- angles, with angles having 2.67 in. out of plane width and with angles having 4 in. out plane angle width. Predicted behavior for all three cases is shown in Figure 4.12.

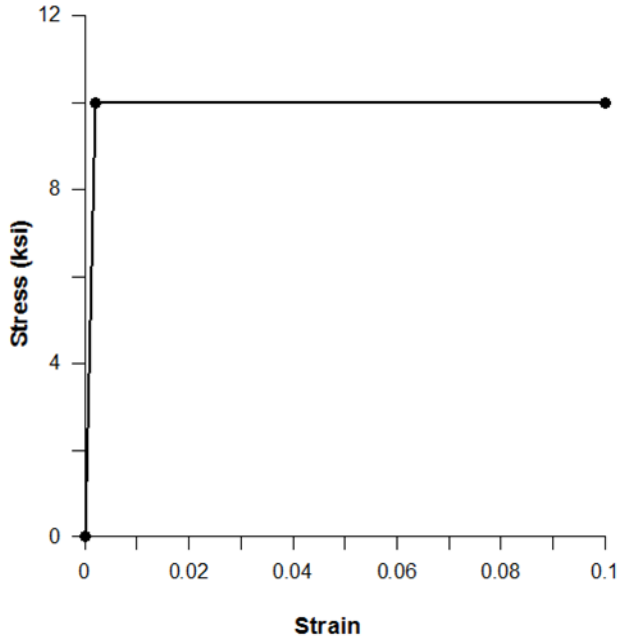

Figure 4.12 Assumed stress/strain behavior of the interface pad for the pre-test analysis of UHPC column.

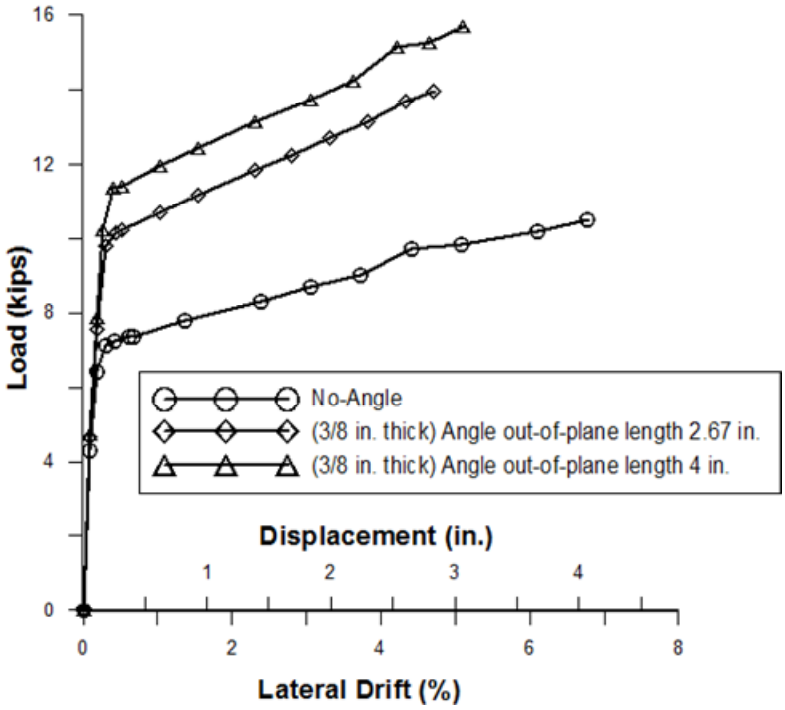

Figure 4.13 Load-displacement behavior predictions for all three test cases.

4.6 Post-Test Analysis and Results

As part of the UHPC column tests, the stress-strain behavior of the interface pad material was also examined using a load controlled compression test in a universal testing machine. The stress-strain behavior of the pad was recorded, which was then used in post-test analysis of the columns. No further modifications to the analysis model were made. The results of the post-test analysis of all three columns are presented below together with the companion of experimental results where appropriate.

4.6.1 UHPC-C1

4.6.1.1 Hydrostone Interface Pad

For the first test UHPC-C1, a 0.6 in. thick hydrostone interface pad was used. Figure 4.14 shows the stress–strain behavior of the hydrostone established from the universal compression test. As shown in the figure, a bilinear idealized curve was used in the analysis to maintain simplicity.

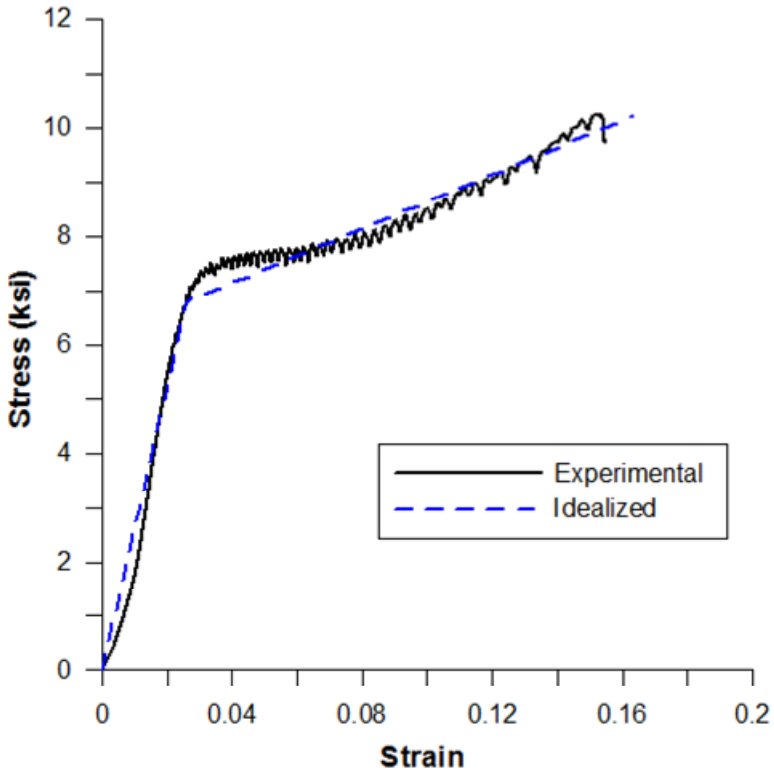

Figure 4.14 Stress-strain behavior of Hydrostone pad established from a 6 in. thick sample size of 2 in. x 2 in.

4.6.1.2 Force-displacement Response

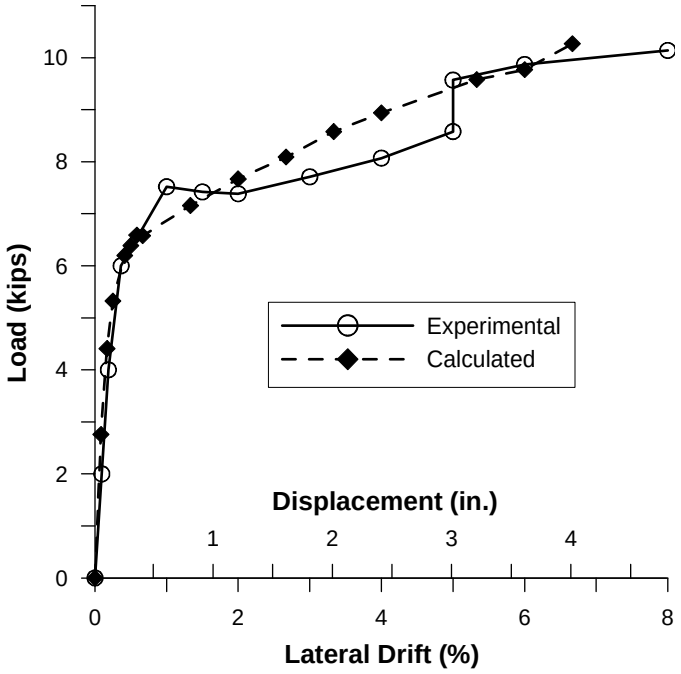

Figure 4.15 Comparison of the experimentally measured force-displacement response of UHPC-C1 with the calculated response.

The calculated monotonic lateral force versus displacement curve is compared with the experimental response envelop that was established from the average first peak responses in the push and pull directions in Figure 4.15. The response calculated from the ANSYS finite element model matches the experimental response well up to the lateral force of 6.5 kips. Beyond this point, the two responses deviated with the experimental curve showing no noticeable increase in strength up to 3 in. of lateral displacement. This discrepancy is primarily due to crushing of the pad (see Figure 3.10 for pictures) that was observed during the test, causing reduction in the prestressing force and no significant increase in the lateral force resistance. This was not modeled in the analysis. At this displacement, the prestressing in C1 was adjusted to a value of 135 kips and thus it produced resistance similar to that

calculated from the analysis. Based on these observations, it is clear that the finite element model adequately modeled the test unit C1.

4.6.1.3 Post-tensioning Force

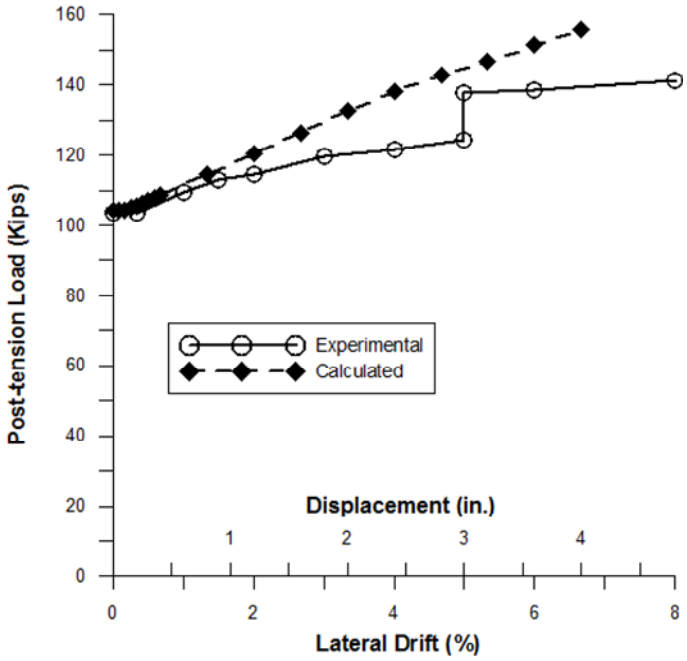

Figure 4.16 Comparison of the experimentally measured post-tensioning force-displacement response of UHPC C-1 with the calculated response.

The calculated monotonic post-tensioning force versus displacement curve is compared with the experimental response envelop, which was established from the average first peak responses in the push and pull directions in Figure 4.16. The response calculated from the ANSYS finite element model matches with the experimental response well up to a lateral displacement of 0.8 in. Beyond this point, the two responses deviated with the experimental curve showing very gradual increase in force up to 3 in. of lateral displacement. This discrepancy was primarily due to observed crushing of the pad as discussed in the previous

section (see Figure 3.10 for pictures), causing reduction in the prestressing force. At this displacement, the prestressing was adjusted to a value of 135 kips but the experimental response remained flat for further lateral displacement. However, the calculated response showed steady and gradual increase in force with increase in lateral displacement.

4.6.1.4 Strain Comparison

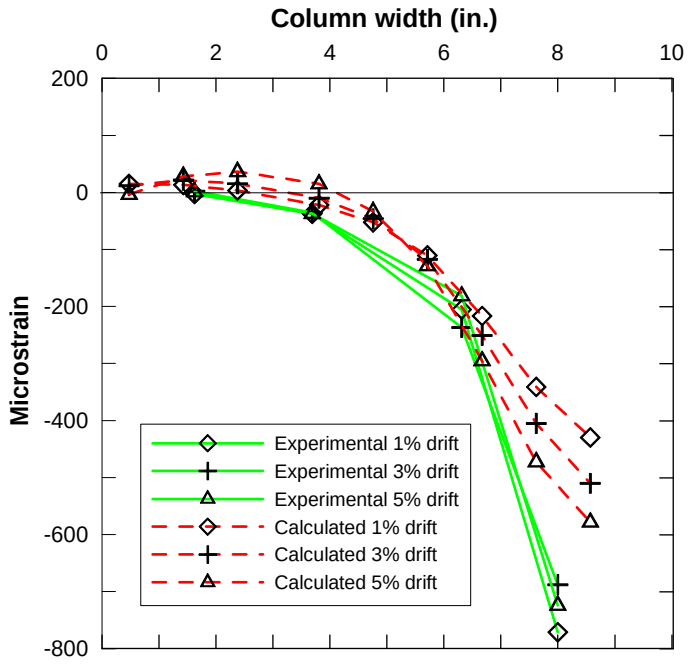

Figure 4.17 Comparing the experimentally measured and analytically calculated UHPC-C1 longitudinal strain variation at 3 in. height from the base of the column.

The calculated longitudinal strain along the 10 in. face of column was compared with experimentally measured strains as shown in Figure 4.17. The calculated strains cross the zero strain axis (i.e., change from tension to compression) between 3 and 4 in. and the experimental values cross the zero strain between 1.5 and 2.5 in. Strains up to 6 in. column width the set of curves follow similar profile and for the remaining width, which is close to

the compression end of the column the curves deviate away. This indicates that the column model was under less compression compared to the actually tested column. This difference may be due to the reason that strain gauges measured the surface strains of the column and the analytically calculated values give the average compression values for the 6 in. width of the column along the Z- axis.

4.6.2 UHPC-C2

4.6.1.1 Steel Fiber Reinforced Grout Interface Pad

For the second UHPC column (C2), a 0.6 inch thick Steel Fiber Reinforced grout interface pad was used. Figure 4.18 shows the stress–strain behavior of the pad established from the universal compression test. As shown in the figure a multi-linear idealized curve was used in the analysis to maintain simplicity.

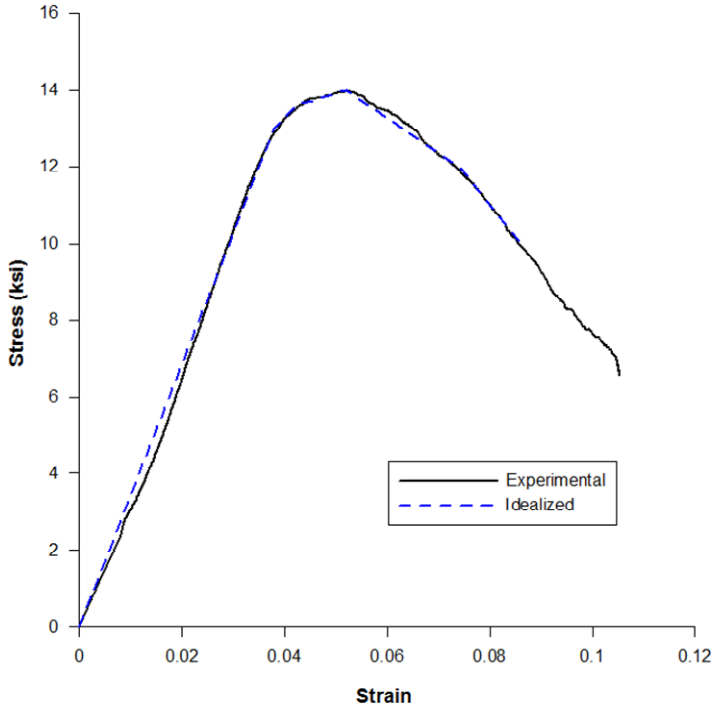

Figure 4.18 Stress-strain behavior of steel fiber grout pad established from a 0.6 inch thick sample of size 2 in. x 2 in.

4.6.1.2 Force-displacement Response

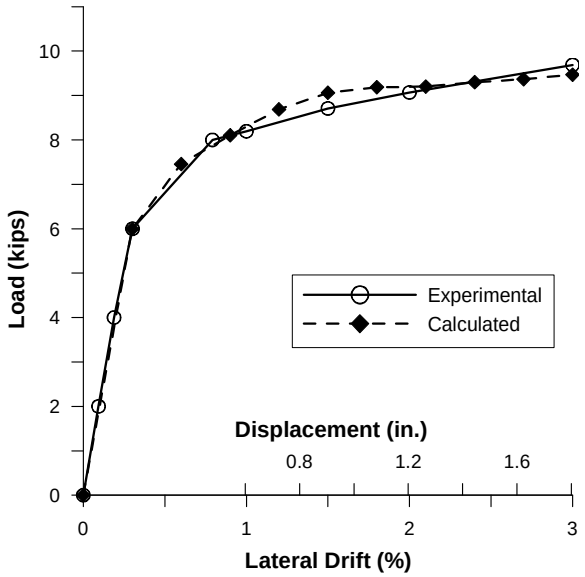

(a) UHPC-C2a test force displacement response comparison.

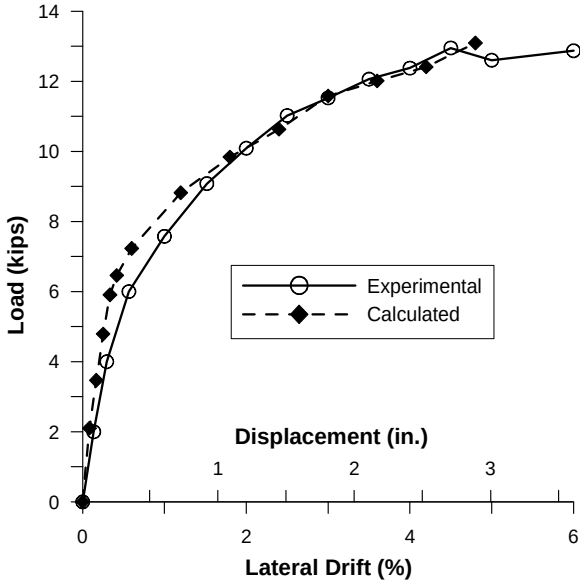

(b) UHPC-C2b test force displacement response comparison.

Figure 4.19 Comparison of the experimentally measured force-displacement response of UHPC-C2 with the calculated response.

The calculated monotonic lateral force versus displacement curve is compared with the experimental response envelop which was established from the average first peak responses

in the push and pull directions in Figure 4.19. For the no-angle test the response calculated from the ANSYS finite element model matches the experimental response well up to 1 percent lateral drift and beyond this point small deviation can seen from the calculated value with in ± 0.5 kips. For the angle test the response calculated from the ANSYS finite element model do not match the experimental response well up to 1 percent lateral drift, the calculated value exceed to 1 kip till 0.5 percent lateral drift and then reduces to zero deviation at 1 percent lateral drift. Beyond this point onwards both the responses match well. The calculated response exceeds the experimental response till 1 percent lateral drift, this may be due to the loss in the stiffness of the interface pad during the no-angle test this condition can be observed in Figure 3.24 of chapter 3.

4.6.1.3 Post-tensioning Force

The calculated monotonic post-tensioning force versus displacement curve is compared with the experimental response envelop which was established from the average first peak responses in the push and pull directions in Figure 4.20. For the no-angle test the calculated response is constantly higher than the experimental response. The difference at 0.5 percent lateral drift is 3 kips and at 3 percent lateral drift it is 8 kips. This may be due to the constant losses in the prestressing force in the experimental test. For the angle test the calculated response was close to the experimental response up to 2 percent drift and from this point onwards the calculated response reduced constantly. This means for lesser lateral displacement the analysis calculated post-tensioning force response matched with the

experimental but for higher lateral displacement the calculated values underestimated the experimentally measured post-tensioning force.

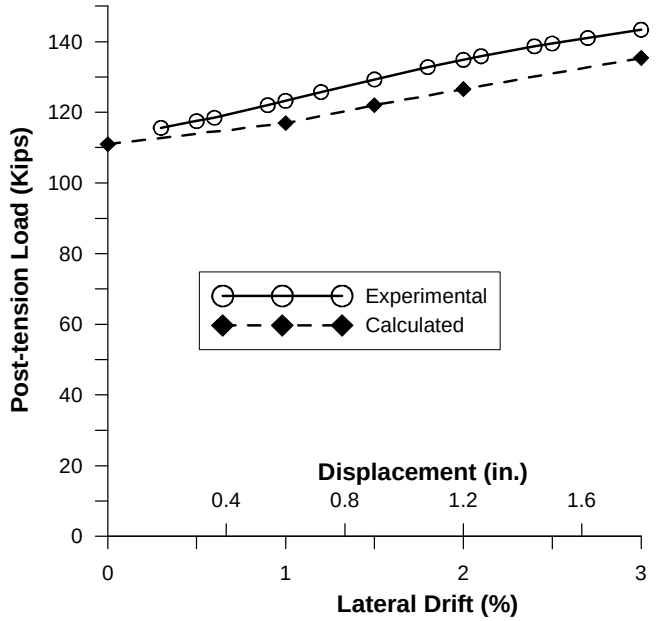

(a) UHPC-C2a Post-tensioning force-displacement comparison.

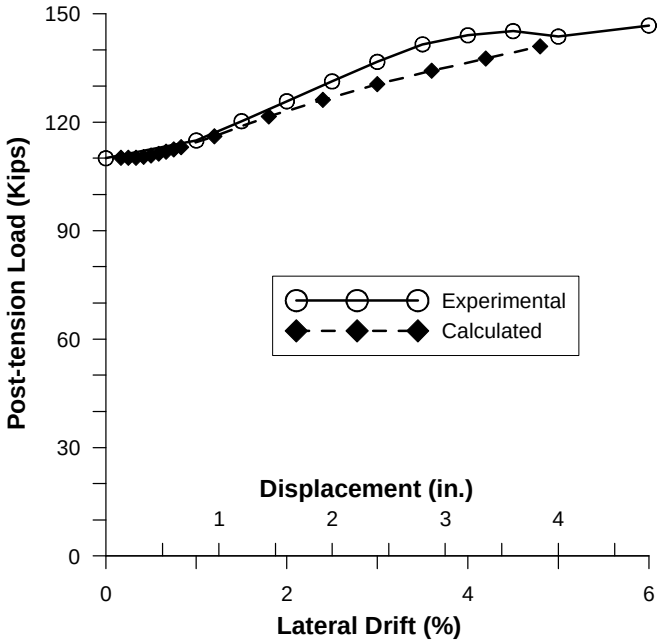

(b) UHPC-C2b Post-tensioning force -displacement comparison.

Figure 4.20 Comparison of the experimentally measured post-tensioning force-displacement response of UHPC C-2 with the calculated response.

4.6.2.4 Strain Comparison.

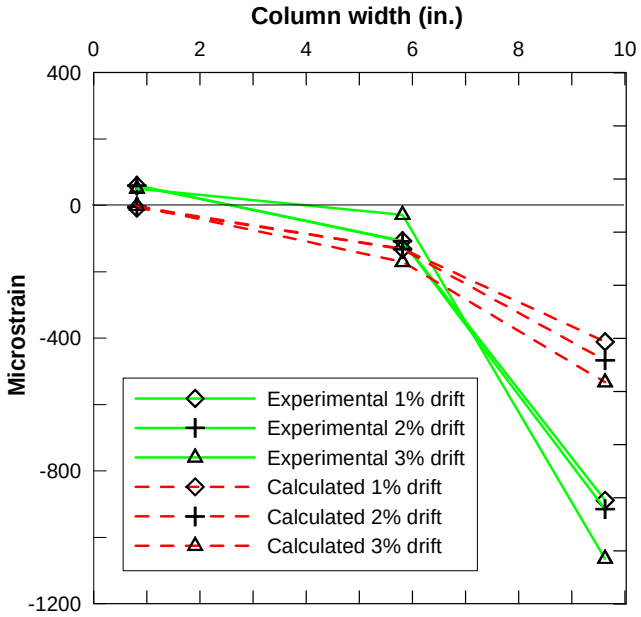

(a) UHPC-C2a Strain comparison at column base.

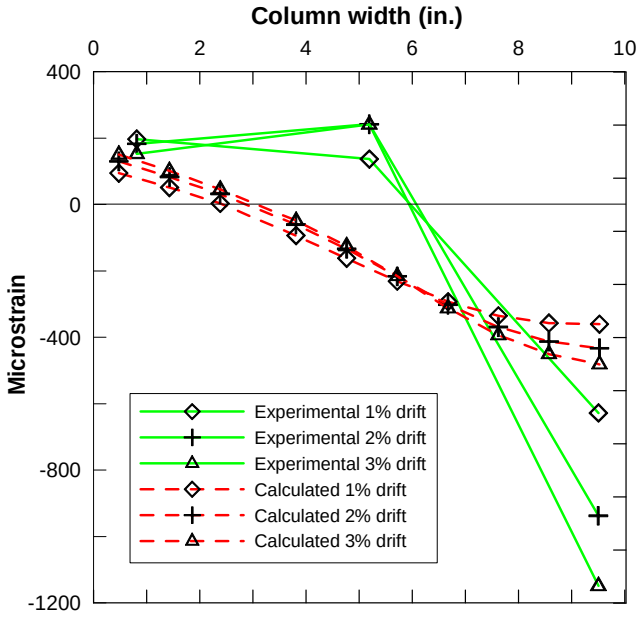

(b) UHPC-C2b Strain comparison at column base.

Figure 4.21 Comparing experimentally measured and analytically calculated UHPC-C2 longitudinal strain variation at 3 in. height from the base of the column.

The calculated longitudinal strain along the 10 in. face of column was compared with experimentally calculated strains as shown in Figure 4.21. For the No-angle test the calculated strains cross the zero strain (change from tension to compression) between 2 and 4 in. and the experimental values cross the zero strain between 0 and 0.5 in. For strains up to 6 in. width, both the set of curves follow similar profile and for the remaining width, which is closer to the compression edge they deviate away. This indicates that the column model was under less compression compared to the actually tested column difference may be due to the reason that strain gauges measure the surface strains of the column and the analytically calculated values give the average compression values for the 6 in. width of the column along the Z- axis. For the angle test the calculated data do not match with the experimental data, difference is very large at the 5 in. and 10 in. column width this erroneous data may be due to the failure of the stain gauges.

4.6.3 UHPC-C3

4.6.3.1 Steel Fiber Reinforced Grout Interface pad

For the third UHPC column (C3) a 0.4 inch Glass Fiber Reinforced Epoxy interface pad was used. Figure 4.22 shows the compressive stress–strain behavior of the pad.

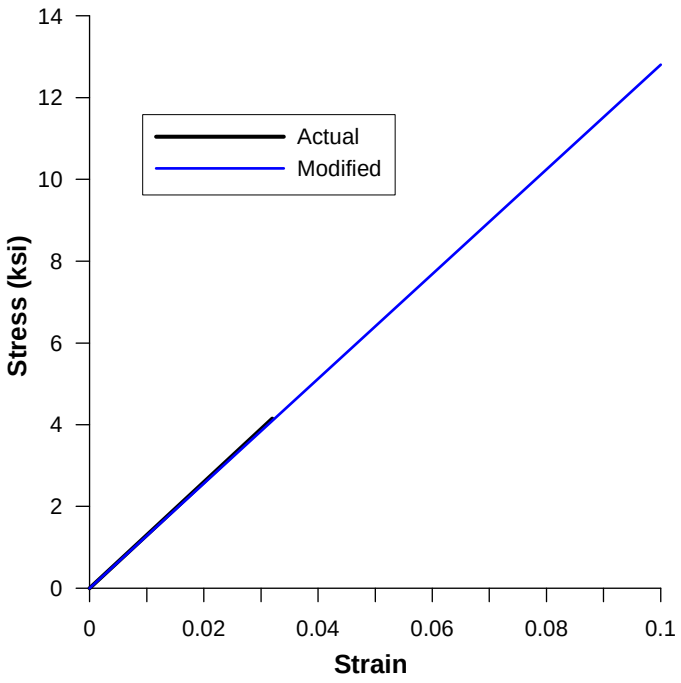

Figure 4.22 Stress-strain behavior of Glass Fiber Reinforced Epoxy pad [27].

4.6.3.2 Force-displacement Response.

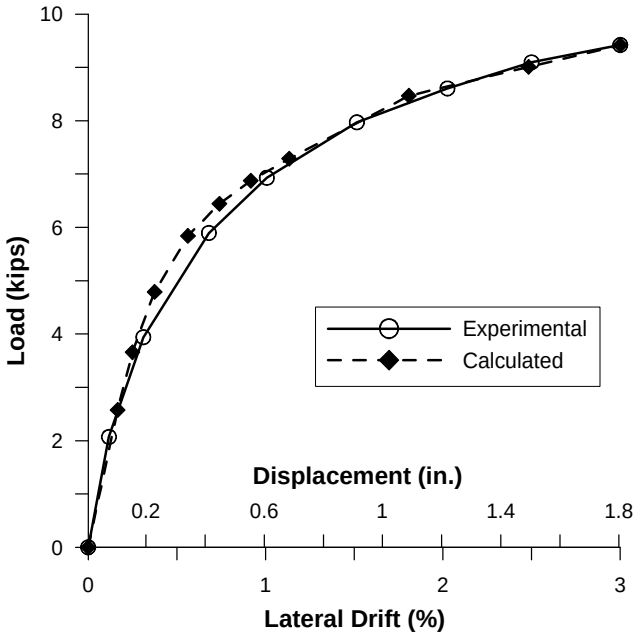

(a) UHPC-C3a Force displacement response comparison.

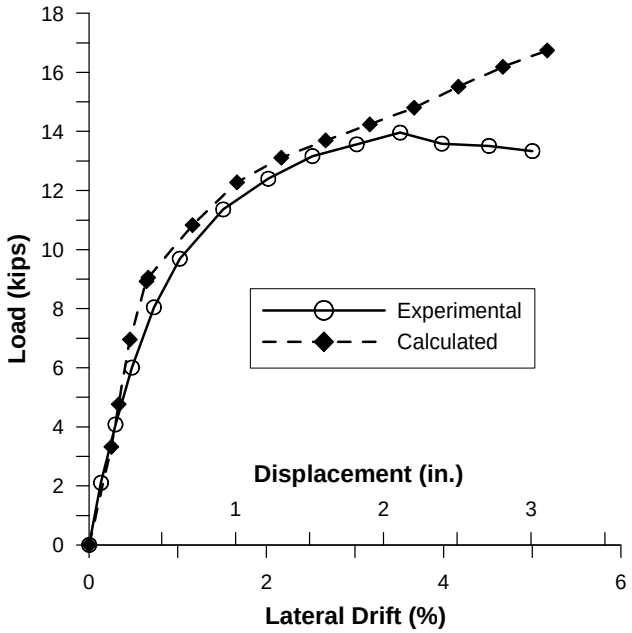

(b) UHPC-C 3b Force displacement response comparison.

Figure 4.23 Comparison of the experimentally measured force-displacement response of UHPC-C2 with the calculated response.

The calculated monotonic lateral force versus displacement curve is compared with the experimental response envelop which was established from the average first peak responses in the push and pull directions in Figure 4.23. For the no-angle test the calculated response matches very well with the experimental response.

For the angle test the calculated response matches very well with the experimental response up to 4 percent lateral drift and beyond this point onwards the experimental response starts deviating away from the calculated response, this was due to the failure of the angles during the experimental testing.

4.6.3.3 Post-tensioning Force

The calculated monotonic post-tensioning force versus displacement curve is compared with the experimental response envelop which was established from the average first peak responses in the push and pull directions as shown in Figure 4.24. For the no-angle test the calculated response increased at a constant slope, whereas the experimentally measured response, the post-tensioning force increased with decreasing slope and deviated away from calculated curve with increase in lateral displacement due to constant loss in prestressing force.

For the angle test the calculated response matches well with the experimental response from 1 to 3 percent lateral drift and beyond this point onwards the experimental response deviated away from calculated response constantly till 4 percent lateral drift, due to sudden loss in the prestressing force.

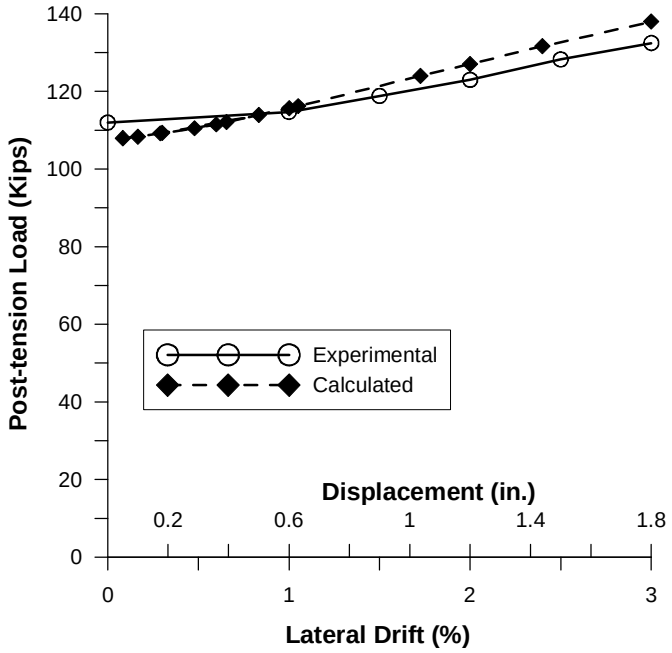

(a) UHPC-C2a Post-tensioning force-displacement comparison.

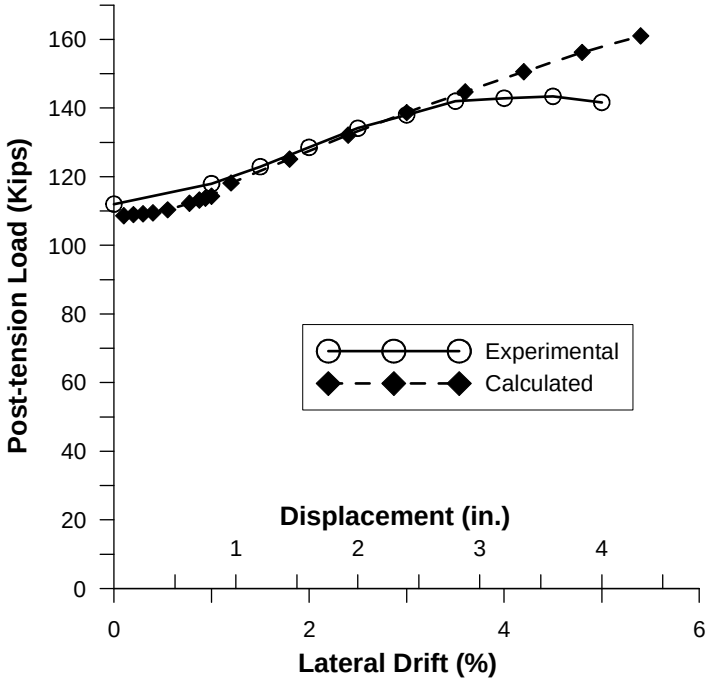

(b) UHPC-C2b Post-tensioning force-displacement comparison.

Figure 4.24 Comparison of experimentally measured post-tensioning force-displacement response of UHPC C-2 with the calculated response.

4.6.2.4 Strain Comparison.

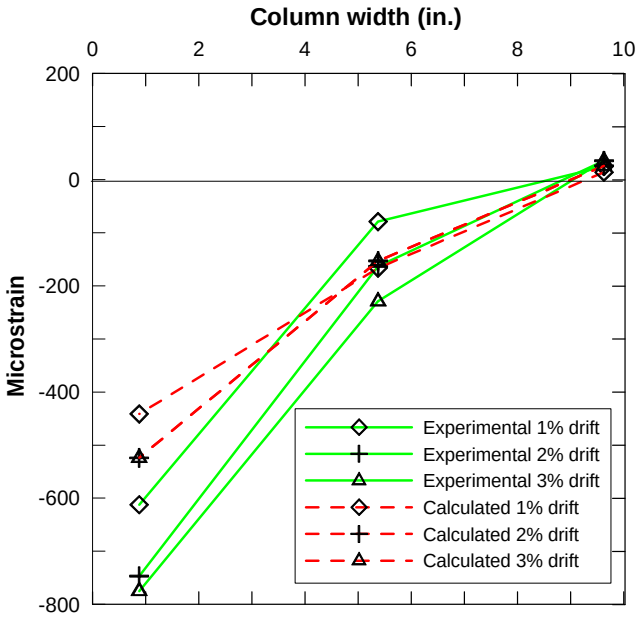

(a) UHPC-C3a strain comparison at column base.

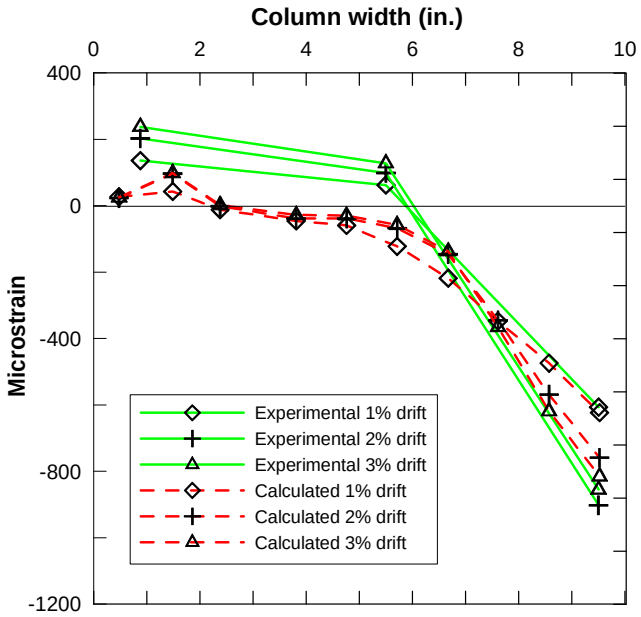

(b) UHPC-C2b Strain comparison at column base.

Figure 4.25 Comparing the experimentally measured and analytically calculated UHPC-C3a longitudinal strain variation at 3 in. height from the base of the column.

The calculated longitudinal strain along the 10 in. face of column was compared with experimentally measured strains as shown in Figure 4.25. For the No-angle test the calculated and experimental strains cross the zero strain (change from tension to compression) at 9 in. Two percent lateral drift response matches well till 5 in. width, from this point onwards the strain responses deviate away. This indicates that the column model was under less compression compared to the actually tested column. Difference may be due to the reason that strain gauges measure the surface strains of the column and the analytically calculated values give the average compression values for the 6 in. width of the column along the Z- axis. For the angle test the calculated and experimental strains match well at the 10 in. width which is close to the compression edge and the strain difference lie within the 200 microstrains at the mid and zero width locations.

4.7 Hollow Section Analysis

The UHPC columns showed very high strength capacity during the lab tests, even after subjecting the columns to several cycles of lateral displacements reaching up to 6% lateral displacement, only minor hair line cracks and repairable column edge spall were observed. This observation led to further extending the analysis to predict the behavior of hollow UHPC section under lateral displacement. The Finite element models used for calculating the experimental test results were used to investigate the hollow section performances and the results are discussed below.

4.7.2 Hollow Section Column

The hollow column section chosen for the analysis work is as shown in Figure 4.26. The column has a rectangular hollow section in the center extending along the full length of the column, cross-section measuring 3.5 inches in-between the steel studs along the 10 inches height and 3 inches along the 6 in. width, leaving a minimum concrete width of 1.5 in. as shown in the cross-section of Figure 4.26.

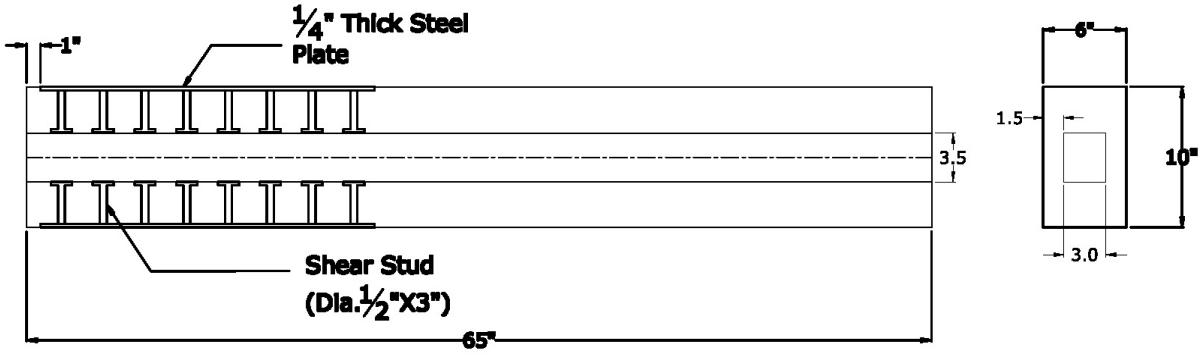

Figure 4.26 Imaginary hollow section used for analysis.

4.7.3 Calculated Hollow UHPC Section Analysis Results

Analysis was performed for all the five tests using the hollow sections and their force displacement responses were compared with the already calculated solid section results. All the five test results are shown in Figures 4.27 – 4.31. Although there was reduction of the cross-section area by 15 percentage there was no significant change observed in the lateral load-displacement responses. Hence the section can be further reduced and checked until an optimum section size is reached without reduction in the lateral load

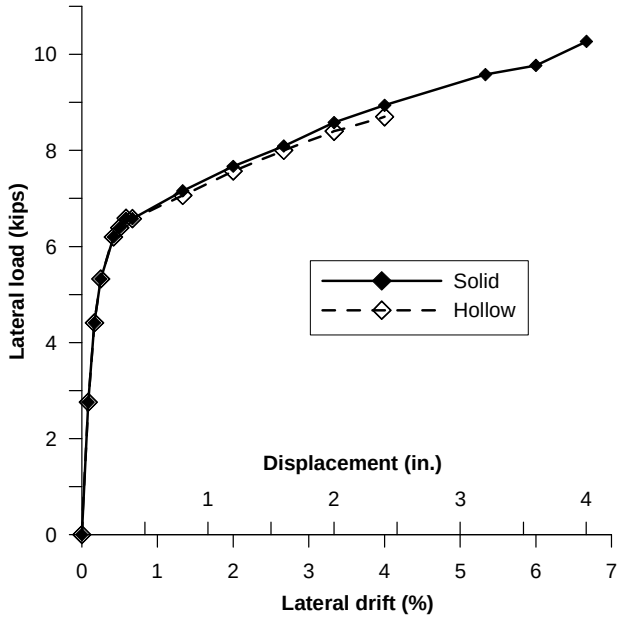

Figure 4.27 Calculated force displacement responses for UHPC-C1.

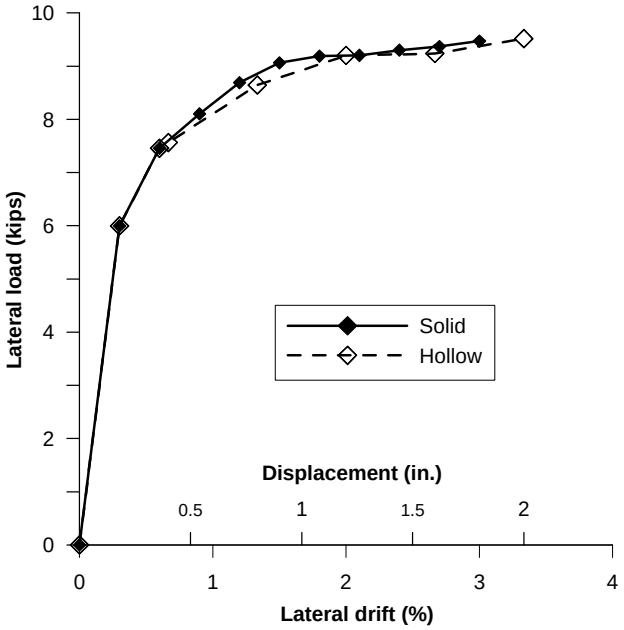

Figure 4.28 Calculated force displacement responses for UHPC-C2a.

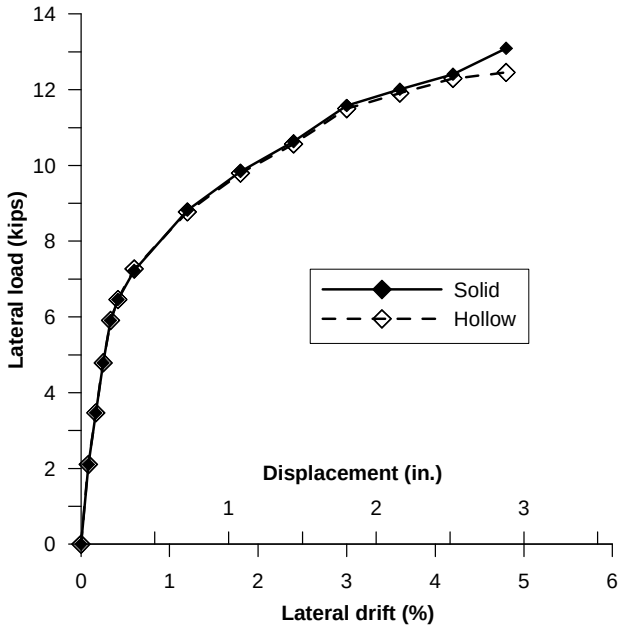

Figure 4.29 Calculated force displacement responses for UHPC-C2b.

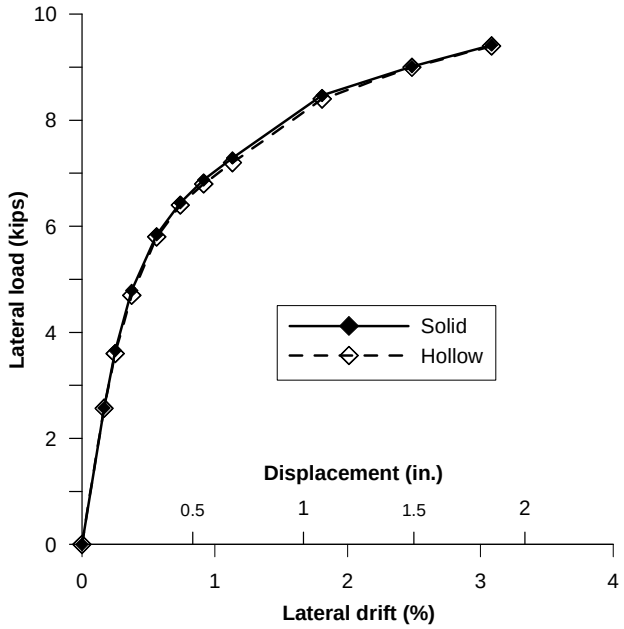

Figure 4.30 Calculated force displacement responses for UHPC-C3a.

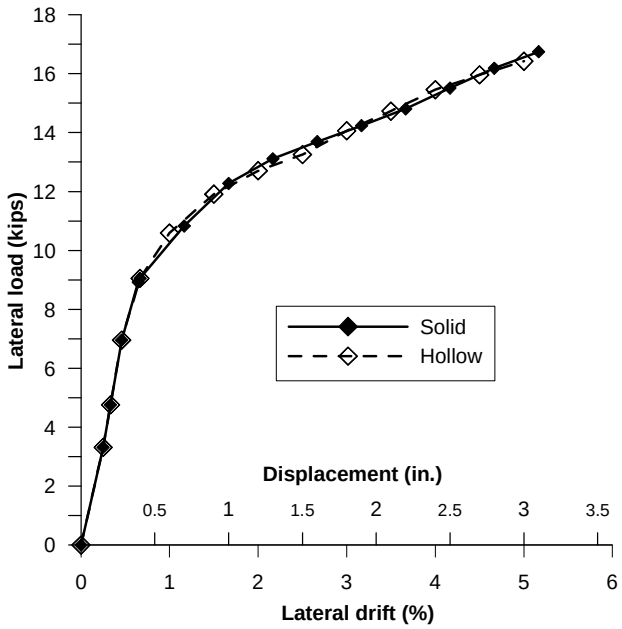

Figure 4.31 Calculated force displacement responses for UHPC-C3b.

CHAPTER - 5 SUMMARY AND CONCLUSION

5.1 Summary

UHPC columns performed better than expected as no major damage was observed to the column at the end of all three tests. It can prove to be a one of the best suitable material for precast seismic applications if appropriate connections are established. With added benefits like easy embedment of steel plates for attaching external steel connections and unbonded post-tensioning a connection capable of resisting large earthquake lateral loads with minor repairable damage to the system can be designed. The primary limitation of using UHPC is its limited compressive strain capacity, which cannot be increased to value that is comparable to that used in current seismic design practice as an acceptable strain limit. A soft interface material was thus introduced to overcome this limitation and improved the performance. Three UHPC columns were tested with three different interface materials along with steel angles as external energy dissipators. Hydrostone was used for column UHPC-C1 and later steel fiber epoxy and glass fiber epoxy was chosen for columns UHPC-C2 and UHPC-C2 based on the performance of Hydrostone and Steel fiber grout respectively. To study the effect of interface pad material in Test-2 and 3 the columns were first tested for few cycles without angles. The limitation of using precast concrete with non-emulative connections for seismic design is to satisfy the code provisions, which require analytical investigation and verification of connections along with experimental investigation. In order to overcome this limitation and to utilize the benefit of precast concrete, a finite element model was developed, which was used to successfully calculate the experimental results.

5.2 Conclusions

The following conclusions have been drawn from the experimental and analytical investigation of UHPC columns presented in this report.

Experimental study

- The hydrostone interface material prematurely failed in compression during the test. The steel fiber grout interface pad failed at the edges when the column was subjected to large displacements but performed better than hydrostone. Steel fiber grout also showed reduction in stiffness when it was re-tested with angles.
- Fiber glass epoxy performed better then Hydrostone and Steel fiber grout. There was no damage observed to the pad at the end of the test and it did not show any reduction in the stiffness when it was retested with angles.
- At the end of all three tests, there was no major damage observed to the UHPC column. There were, however, hair line cracks visible at the end of test on UHPC-C2b surface. This may be due the high compression force developed at the base resulting from non-flexible steel grout pad. Hence, it can be concluded that the fiber glass epoxy overcome the strain limitation of UHPC.
- During both the angle tests UHPC-C2b and UHPC-C3b the weld on the angle connecting the foundation plate failed frequently at cycles of large displacements. This may be due to high stresses developed at the end of the connection when the angle was pulled up. However, upon re-welding the steel angles performed adequately in UHPC-C2b and failed only after 5 percent lateral drift of column.

Analytical study

- Analytically calculated force versus displacement responses closely matched with the responses of all the experimental results.
- At large lateral displacements, the analytical model over-estimated the post-tension force for the tests, which had no steel angle. The calculated post-tensioned force matched well with the experimental results for UHPC-C3b.
- The analytical model under-estimated the compressive strains measured using strain gauges at the base of the column.
- The analytical model was used to study the behavior of the hollow section. After reduction in the cross section area at the center of the column by 15% no reduction in the lateral load was observed.

REFERENCES

[1] Acker,P., and Behoul. 2004. Ductal® Technology: A Large Spectrum of Properties, *Ultra High Performance Concrete, Kassel, Germany, Sept. 13-15: 11-23.*,

[2] Bierwagen, D., and A. Abu-Hawash. 2005. Ultra High Performance Highway Bridge. *Proceedings of the 2005 Mid-Continent Transportation Research Symposium, Ames, IA, August*.

[3] ACI Committee 318: Building Code Requirement for Structural Concrete (ACI 318-02), American Concrete Institute, Farmington Hills MI.

[4] Celik, O. "Analysis and Validation of Design Guidelines Proposed For Precast Concrete Hybrid Frame System" *M.S. thesis, Department of Civil, Construction and Environmental Engineering, Iowa State University*, 2004.

[5] Rossi, P. 2005. Development New Cement Concrete Materials for Construction. *Proceedings of the Institution of Mechanical Engineering, Part L : Journal of Materials: Design and Applications*, Feb., Vol. 219. No. L1 : 67-74.

[6] Gao, R., Liu, Z.-M., Zhang, L.-Q., and P. Stroeven. 2006. Static Properties of Reactive Powder Concrete beams. *Key Engineering Materials*, Jan., Vol. 302-303: 521-527.

[7] Thomas, L. V. " Design and Field Testing of Tapered H-Shaped Ultra High Performance Concrete Piles" *M.S. thesis, Department of Civil, Construction and Environmental Engineering, Iowa State University*, 2008.

[8] Walraven, J.C 2002. From Design of Structures to Design of Materials. Innovations and Developments in Concrete Materials and Construction: Proceedings of International Conference Held at the University of Dandee, Scotland, UK on 9-11 Sept. London: 805-818.

[9] Ma, J., and H Schneider.2002. Properties of Ultra High performance Concrete. *Leipzig Annual Civil Engineering Report* (*LACER*), No.7:25-32.

[10] Richard, P., and M Cheyrezy. 1995. Composition of Reactive Powder Concretes. *Cement and Concrete research*, Oct., Vol.25, No. 7: 1501-1511.

[11] Perry, V. 2001. Reactive Powder Concrete. *PCI Journal*, July/Aug., Vol. 46, No. 4:118.

[12] Vernet, C.P. 2004 Ultra-Durable Concretes: Structure at the Micro- and Nanoscale. MRS Bulletin, May, Vol.29, No.5: 324-327.

[13] Graybeal, B.A. 2006. Material Property Characterization of Ultra-high Performance Concrete. FHWA-HRT-06-103, Aug.

[14] Sritharan, S., Bristow, B., and V. Perry. 2003. Characterizing an Ultra-High Performance Material for Bridge Applications under Extreme Loads. *Proceedings of the 3rd International Symposium on High Performance Concrete, Orlando, Florida*.

[15] Dugat, J., Roux, N., and G. Bernier. 1996.Mechanical Properties of Reactive Powder Concretes. *Materials and Structures*, May, Vol. 29: 233-240.

[16] Schmidt, M., Fehling, E., Teichmann, T., Bunje, K., and R. Bornemann. 2003. Ultra High Performance Concrete: Perspective for the Precast Concrete Industry. *Concrete Precasting Plant and Technology*, Vol.69, No. 3: 16-29.

[17] Yahya C. Kurama, Qiang Shen. "Posttensioned hybrid Coupled Walls under Lateral loads". *ASCE Journal of structural engineering*, February 2004.

[18] Yahya C. Kurama, Brad D. Weldon, Qiang Shen. "Experimental Evaluation of Posttensioned hybrid Coupled Wall Subassemblages". *ASCE Journal of structural engineering*, july 2006.

[19] Qiang Shen, Yahya C. Kurama, Brad D. Weldon. "Seismic Design and Analytical modeling of Posttensioned hybrid Coupled Wall Subassemblages". *ASCE Journal of structural engineering*, july 2006.

[20] Chung-Che Chou, Yu-Chih Chen. “Cyclic tests of post-tensioned precast CFT segments bridge columns with unbonded strands”. *John wiley & sons*, 2005.

[21] ANSYS® Academic Research, v, 11.0.

[22] ANSYS® Academic Research, Release 11.0, Help System, ANSYS, Inc.

[23] Acker, P., and M. Behloul. 2004. Ductal® Technology: A Large Spectrum of Properties, *ultra high performance Concrete, kassel, germany, Sept. 13-15: 11-23.*

[24] Bristow, B. and Sritharan. Uniaxial and Cyclic Behavior of Ultra-High Performance Concrete. *To be submitted to the ACI Materials Journal*.

[25] Charles G. Salmon, E. Johnson, “Steel Structure, Design and Behavior”. *Prentice-Hall*, 1996.

[26] Edward G. Nawy, “Prestress Concrete, A Fundamental Approach”. *Prentice-Hall*, 2003.

[27] Mark, C. C. “Self-Centering bridge pier columns with structural fuses” *M.S. thesis, Department of Civil, Construction and Environmental Engineering, Iowa State University*, 2009.